OUKA
The University of Osaka
Institutional Knowledge Archive

Title	OPTICAL PROPERTIES OF KDP TYPE CRYSTALS IN THE LOW-WAVENUMBER REGION
Author(s)	Kawamura, Tetsuo
Citation	大阪大学, 1974, 博士論文
Version Type	VoR
URL	https://hdl.handle.net/11094/2081
rights	
Note	

The University of Osaka Institutional Knowledge Archive : OUKA

https://ir.library.osaka-u.ac.jp/

The University of Osaka

OPTICAL PROPERTIES OF KDP TYPE CRYSTALS IN THE LOW-WAVENUMBER REGION

Far-Infrared and Raman Spectra of KDP Type Ferroelectrics and Antiferroelectrics

BY

TETSUO KAWAMURA

OPTICAL PROPERTIES OF KDP TYPE CRYSTALS IN THE LOW-WAVENUMBER REGION

Far-Infrared and Raman Spectra of KDP Type Ferroelectrics and Antiferroelectrics

by

Tetsuo KAWAMURA

November 1973

Abstract

The studies on the optical properties of the ferroelectric KH_2PO_4 and KD_2PO_4 and the antiferroelectric $NH_4H_2PO_4$ have been done using far-infrared and Raman spectroscopies. The problem of a lattice dynamical theory of the ferroelectric transition of KH_2PO_4 type crystal has recieved wide attention in recent years. Several experimental techniques have been used to study the dynamical properties of these crystals, but it has not been completely understood.

In the present work the polarized far-infrared and Raman spectra of KH_2PO_4 and KD_2PO_4 have been measured in both paraelectric and ferroelectric phases as a function of temperature. The results have been analyzed by the use of the group theory. The detailed temperature dependence of the spectra has been observed and discussed comparing with the recent dynamical theory. The study on the deuterated substance is very important because in these hydrogen bonded crystals the hydrogen motion is thought to play an important role in the process of phase transition. The results of KD_2PO_4 have been discussed refering to those of KH_2PO_4. $NH_4H_2PO_4$ is the isomorphous to KH_2PO_4 in the paraelectric phase but is antiferroelectric below the transition temperature and the mechanism of the antiferroelectric transition is quite different from that of KH_2PO_4. Only a few experimental works have been reported.

The present works on KH_2PO_4, KD_2PO_4 and $NH_4H_2PO_4$ will be shown as follows: In Chap. 1 the author will introduce the lattice dynamical aspects of ferroelectric transition and review the experimental works on the ferroelectrics by the use of far-infrared and Raman spectroscopies

to point out the problem of the present work. In Chap. 2 the results of the group theoretical analysis are given. These results will be used in the following chapters to analyze the experimental data. The results of far-infrared reflection measurements are given in Chap. 3. In that chapter the main attention has been paid to its low-frequency dielectric behavior and the ferroelectric mode. In Chap. 4 the results of reflection measurements by HCN laser are shown. The reflectivity at 29.7 cm^{-1} has been measured as a function of temperature. The polarized Raman spectra of these crystals are given in Chap. 5. The measurements have been made in wider region. The results of the determination of the mode symmetries and the establishment of the correlation of the modes from one phase to the other are shown. Finally in Chap. 6 the discussion about the results obtained by three methods are given. The conclusion of the present work is also given in Chap. 6.

Acknowledgments

The author wishes to express his sincere gratitude to Professor Dr. A. Mitsuishi for his constant guidance, advice, encouragement, and support throughout the course of this work. The author is also grateful to Professor Dr. H. Yoshinaga, and Professor Dr. K. Kawabe for many enlightening suggestions.

A special acknowledgment is due to As. Professor Dr. S. Nakashima and Dr. A. Manabe for suggestion and discussion. The experimental support of Dr. K. Sakai and Dr. M. Yamanaka, and the supply of DKDP crystal by Professor Dr. N. Furuya and Dr. O. Shimomura of Yamanashi University are also gratefully acknowledged.

The author would also like to express his gratitude to the other members of the Mitsuishi Laboratory and the Yoshinaga Laboratory who assisted in various phases of the investigations, particularly to Dr. T. Hattori, Mr. M. Hineno and Mr. T. Fukumoto.

Finally author's wife deserves special thanks for her support and encouragement.

Contents

Chapter 1 Introduction

1. Lattice Dynamics of Ferroelectrics

The phenomenon of ferroelectricity is observed in a large number of crystals. They can be divided into two groups. One group is characterized by the existence of permanent dipole moments in the paraelectric phase, which become ordered below Curie temperature.[1, 2] The transition to the ferroelectric phase is then an order-disorder type. In the second group there is no permanent dipole moment in the paraelectric phase, and the lattice spontaneously deforms to the ferroelectric state. The displacive type ferroelectrics have recieved considerable interest due to the relationship between the onset of ferroelectricity and the lattice instability. Cochran[3] has proposed a theory of ferroelectricity in which the ferroelectric transition in displacive type crystals is associated with an instability of one of the normal modes of the lattice. In this theory the frequency of the relevant mode lowers on approaching the Curie temperature and the restoring force of the atomic displacement tends to be zero. This mode becomes unstable at the Curie temperature T_c. The atomic displacement below T_c represents the frozen-out displacement of the unstable mode. This unstable mode is called a soft mode. As the ferroelectric state is characterized by a macroscopic spontaneous polarization, the soft mode must be polar and of long wavelength ($k = 0$).

The antiferroelectric state is characterized by the appearance of two opposite sublattice polarizations. Therefore there is no macroscopic polarization and an increase in the unit cell size, so that the antiferroelectric soft mode has a finite wavelength. It can be said that the ferroelectric transition involves the instability of a lattice vibrational

mode at Brillouin zone center, k = 0, whereas antiferroelectric ordering involves the instability of one at the Brillouin zone boundary. The lattice instability theory was at first proposed only for displacive type ferroelectrics, such as perovskite crystal $BaTiO_3$, where the potential in which atom moves is slightly anharmonic. It was later suggested that essentially the same idea can be applied to the order-disorder type ferroelectric like KH_2PO_4(KDP). In KDP the potential for the hydrogen atom is anharmonic or of double minima[4,5] and so KDP type ferroelectrics are also an attractive subject concerning the relationship between the onset of ferroelectricity and the lattice vibration.[6,7] In the present work the author will be concerned with the investigation of optical spectra of KDP type ferroelectrics and antiferroelectrics.[8]

A characteristic of KDP type ferroelectrics is the existence of short hydrogen bonds.[9] The deuteration effects the reduction of Curie temperature[1,2] and so the hydrogen bond is thought to play an important role in the phase transition mechanism. Recent theoretical [6,7] and experimental works[9, 10] have suggested the existence of unstable optic mode as that of perovskite crystal. Further discussion will be made in the section 3.

2. Infrared and Raman Spectra of Ferroelectrics

The infrared and the Raman spectroscopies are the powerful tools for the study of the lattice vibration and the phase transition in ferroelectrics. The selection rules for these spectra are different from each other and these two measurements generally give the complementary data. Measurements with these two techniques give more perfect information about the lattice vibrational modes.

2-1 Infrared Absorption

The infrared behavior of the crystal can be conveniently described in terms of the dielectric function $\varepsilon(\omega)$. The connection between the static dielectric constant and the lattice dispersion is provided by one of the Kramers-Kronig dispersion relations.[10]

$$\varepsilon'(0, T) - \varepsilon_\infty = \frac{2}{\pi} \int_0^\infty \frac{\varepsilon''(\omega', T)}{\omega'} d\omega' \qquad (1\text{-}1)$$

Here $\varepsilon'(\omega, T)$ and $\varepsilon''(\omega, T)$ are the real and imaginary parts of complex dielectric constant and ε_∞ is the high frequency dielectric constant in the region where phonon effects are unimportant. Eq. 1-1 shows that large temperature dependent low-frequency dielectric constant $\varepsilon'(0,T)$, which is characterized by Curie-Weiss law behavior in the ferroelectrics, can occur only if the spectrum $\varepsilon''(\omega)$ contains the contributions from a strong and very temperature-dependent soft mode.

Experimentally complex dielectric constant can be obtained from the far-infrared reflectivity spectrum using Kramers-Kronig dispersion relation.[11] If the oscillator model is valid, the complex dielectric constant can be represented as follows:

$$\varepsilon(\omega) = \varepsilon_\infty + \sum_j \frac{S_j \omega_{TOj}^2}{\omega_{TOj}^2 - \omega^2 + i\omega\gamma_j} \qquad (1\text{-}2)$$

The high frequency dielectric constant ε_∞, characteristic frequency ω_{TOj}, oscillator strength S_j and damping constant γ_j can be obtained from optimum fitting of eq. 1-2 to the experimental result.

For the case of an ionic crystal with a single infrared active mode with no damping, transverse optic mode frequency ω_{TO} and longitudinal optic mode frequency ω_{LO} are split by the crystal polarization.[12]

The relation between ω_{TO} and ω_{LO} is;

$$\frac{\varepsilon_o}{\varepsilon_\infty} = \frac{\omega_{LO}^2}{\omega_{TO}^2} \quad . \tag{1-3}$$

This equation is called as Lyddane-Sachs-Teller relation.[13] In the ferroelectrics the importance of this relation arises from the Curie-Weiss law behavior of the low-frequency dielectric constant:

$$\varepsilon_o \simeq \frac{C}{T - T_c}, \quad (T>T_c).$$

ω_{LO} and ε_∞ are thought to be temperature insensitive and then the L. S. T. relation together with the Curie-Weiss law for the low-frequency dielectric constant predicts a soft mode behavior of the infrared active transverse optical mode;

$$\omega_{TO}^2 = A(T - T_c) \tag{1-4}$$

where A is a constant.

Since the lattice instability theory[3] of the displacive type ferroelectrics have been proposed, many experimental works on the problem of soft mode have been done. The first observation of the temperature dependence of a low frequency transverse optic mode was made by Barker et al.[14] They measured the far-infrared reflectivity of $SrTiO_3$ and derived complex dielectric constant by means of Kramers-Kronig analysis. The lowest frequency mode was found to be overdamped and its mode frequency had the temperature dependence such that given in eq. 1-4. The same type measurements were made by Spitzer et al.[15] on $SrTiO_3$, $BaTiO_3$ and TiO_2 at room temperature. Their results of $BaTiO_3$ show the existence of a soft mode. A more detailed study of low-frequency mode in $BaTiO_3$ was made by Ballentyne,[16] who measured the reflectivity at several temperatures. The results indicated that lowest frequency over-

damped mode does not shift in accordance with the L. S. T. relation, i.e. eq. 1-3, if the peak frequency in ε'' is considered. This is because of the large damping. In a case of large damping the peak of ε'' does not coincide with the characteristic frequency ω_{TO}[18] and then the best fit of ε'' using an eq. 1-2 is necessary to obtain the characteristic frequency. The measurements on $KTaO_3$ were made by Perry et al.[18] The results indicated the presence of a low-frequency soft mode which is in accordance with the temperature dependence of the dielectric constant as the manner given by eqs. 1-3 and 1-4.

These data for perovskite crystal show the presence of a soft mode, but the dielectric function cannot be represented by a sum of non-interacting classical oscillator function.[19] The importance of optical mode coupling has been suggested by Barker and Hopfield.[20] They have shown that the reflectivity of $BaTiO_3$, $SrTiO_3$ and $KTaO_3$ could be fitted by a coupled oscillator function.

2-2 Raman Effect

Raman scattering experiments have become a powerful tool recently for the study of ferroelectric phase transition in ferroelectrics. This is partly due to the fact that Raman scattering is complementary in nature to infrared absorption. The Raman data together with infrared data give more complete information about the vibrational spectra.

Recently the laser has been developed and has become to be used for the Raman scattering as an exciting source. It gives a coherent and linearly polarized light. This enables us to measure the low frequency Raman scattering and polarized spectra more accurately. Thus the Raman scattering is useful in studying the optical property of crystal, for

example, the soft mode and the line shape anomaly in the spectra. In addition, because of symmetry information available from polarized scattering spectra, the Raman scattering technique has been useful in studying the change of the crystal structure at the phase transition.

The intensity of the Raman scattering is given by the equation[12, 21]

$$J(\omega) \propto I_L \left| \frac{\partial \alpha_{ij}}{\partial Q} \right|^2 \times \langle (\delta p(\omega))^2 \rangle \qquad (1\text{-}5)$$

where I_L stands for the intensity of incident light, α_{ij} stands for the polarizability tensor components, Q stands for the displacement in the normal coordinate and $\delta p(\omega)$ is the Fourier component of the polarization fluctuation due to the lattice vibration. $\langle (\delta p(\omega))^2 \rangle$ is directly related to the imaginary part of complex dielectric susceptibility $\chi''(\omega)$ by the fluctuation dissipation theorem[21-23] and we obtain

$$J(\omega) = K(n(\omega) + 1)\, \chi''(\omega) \qquad (1\text{-}6)$$

for Stokes line, where $n(\omega)$ stands for the Bose factor and K is the constant. $\chi''(\omega)$ obtained by the Raman scattering measurements can be compared with the imaginary part of complex dielectric constant $\varepsilon''(\omega)$ which is obtained by the far-infrared measurements. If the oscillator model is valid $\chi''(\omega)$ can be represented by such a classical oscillator function as eq. 1-2.

The relation in eq. 1-6 was applied in the classical limit $\hbar\omega \ll k_B T$ by DiDomenico, Porto and Wemple in their Raman scattering observation of soft mode in $BaTiO_3$.[23] It is noted that when the lattice vibrational mode is underdamped its Raman line should be very sharp which is the case of $PbTiO_3$ measured by G. Burns and B. A. Scott.[24] The

results show that the spectra consist of underdamped modes including a soft mode. In $BaTiO_3$,[23] however, the situation is somewhat different. The soft mode is of low-frequency and so broad that the Bose factor is extremely important. The observed spectra do not show a peak but a broad Rayleigh wing. In this case the Bose factor correction is needed to extract the actual mode shape $\chi''(\omega)$ from the Raman signal. This is also the case of KDP[25] and will be shown later. DiDomenico et al.[23] applied the relation in eq. 1-6 and the classical oscillator function to their Raman scattering spectra in the observation of a soft mode in $BaTiO_3$.

Many works have been done on the ferroelectrics in recent years. The results are reviewed by Worlock[26] and others.[27, 28] Much attention has been paid also to the soft mode behavior. Of special interest is the field-induced Raman scattering employed in $SrTiO_3$ and $KTaO_3$ by Fleury and Worlock.[29] These crystals have the perovskite structure and have a center of inversion above the transition temperature. So the soft mode observed by infrared measurements is Raman inactive. The applied field distorts the crystal slightly lowering the crystal symmetry from O_h to C_{4v} and causes the infrared active mode to become Raman active. They observed a field-induced soft mode[29] and measured its temperature dependence.[30] The results indicated that the temperature dependence of a soft mode is in good agreement with the expected one such as given by eq. 1-4. They also discussed about the electric-field-induced scattering cross sections and the temperature dependence of the soft mode linewidth.[31] Balkanski et al.[32] studied the Raman spectra and the far-infrared spectra of SbSI. They measured these spectra of SbSI above and below the transition temperature and analyzed

their data by means of group theory. The mode symmetries in the different phases were determined and their correlations from one phase to the other were established. Since the structual phase transition is associated with displacements of certain atoms, the lattice vibrational modes involving these atomic motions are more affected by the crystalline change from one phase to the other. Therefore such an investigation made by Balkanski et al.[32] is very important to get information about the structual phase transtition involving the ferroelectric phase transition. The same type measurements and analysis of the spectra for SbSI were also done by Agrawal et al.[33] They reported the existence of a strongly temperature-dependent soft mode. Harbeke et al.[34] also studied the Raman spectra of SbSI and analyzed the soft mode behavior in terms of two coupled anharmonic oscillators. The soft mode changes its frequency with temperature and crosses a temperature independent mode. This fact offers the possibility of observing mode interactions.[35] In SbSI such a coupled oscillator was found to be in good agreement with the observed spectra.

In some perovskite crystals the instability of zone boundary mode occurs at the structual phase transition. This is the antiferroelectric transition because it causes a doubling of the unit cell. Well known example is the cubic to tetragonal transition of $SrTiO_3$ at 110 K. In the Raman spectra of $SrTiO_3$[36] the new lines were observed below 110 K. This fact is thought to be due to the structual change which doubles the unit cell and shifts the modes from the zone boundary to its center.

3. KDP Type Ferroelectrics and Antiferroelectrics

KDP type ferroelectrics are known to be the hydrogen bonded

ferroelectrics and the order-disorder type. These crystals are charaterized by the short hydrogen bond which is thought to play a significant role in the process of phase transition. In the low-temeprature phase they become ferroelectric which is considered to result from an ordering of the protons. Whereas considerable progress has been made recently in the understanding of the ferroelectric phenomenon in KDP type ferroelectrics, the vibrational spectra of these crystal contain several interesting features which are still not completely understood. The dynamical aspect of the phase transition of KDP and the related works are reviewed below.

3-1 Lattice Dynamical Aspects

The crystal structure of KDP has been investigated in detail by X ray[9] and neutron diffraction techniques[10] and is shown in Fig. 1-1. A characteristic of the crystal structure is the existence of short hydrogen bond which connects two PO_4 groups perpendicularly to the polarization axis (c-axis). This hydrogen bond plays a significant role in its ferroelectricity. For example the dueteration increases the Curie temperature[1,2] from 120 K to 220 K in KDP as shown in Table 1-1.

Neutron diffraction experiments[10] on KDP showed that the intensity profile of hydrogen atoms corresponds to the structure elongated along the bond axis in the paraelectric phase. In the ferroelectric phase, however, the hydrogens are observed to be in ordered off-center position. This is believed to occur from the fact that every hydrogen atom vibrates along the bond axis or is statistically distributed over two equilibrium positions along the bond axis in the paraelectric phase.

Slater[37] and Takagi[38] proposed a statistical order-disorder model of KDP, but could not explain the large deuteration effect on the Curie temperature. Blinc et al.[39] interpreted their infrared data introducing the tunneling character, in which proton tunnels in a double well potential through a low-intermediate barrier, in order to explain the large isotope shift of the Curie temperature. A pseudo-spin-Ising type model was employed by de Gennes[4] to describe the tunneling process. Tokunaga et al.[6] modified Slater's model introducing the tunneling character. Their results show that the tunneling mode becomes soft in the same manner as the soft mode of displacive type ferroelectrics. They assumed the order-disorder mechanism for $[K\text{-}(PO_4)]$ sublattice as such that the motion of $[K\text{-}(PO_4)]$ dipole instantaneously follows these tunneling protons due to the change of electrostatic field.[9] The order-disorder mechanism of $[K\text{-}(PO_4)]$ sublattice may not be reasonable, but the lattice is thought to play an important role in a sense it carries the spontaneous polarization along the c axis. Because the principal component of hydrogen motion is perpendicular to the polarization axis, it appears that neglect of the $[K\text{-}(PO_4)]$ sublattice cannot give a quantitative description of the spontaneous polarization. The X ray[9] and the neutron scattering[10] data both showed that in the ferroelectric phase K and P atoms have the opposite displacements along the c axis. When all ionic displacements are considered, the spontaneous polarization can be accounted for in a reasonable manner.[40] With respect to this point, Kobayashi[7] extended the pseudospin tunneling model and proposed the coupling between the tunneling mode and the optical mode of $[K\text{-}(PO_4)]$ sublattice. This yields a coupled mode of which frequency becomes soft in the same

manner as in Cochran's description[3] for the perovskite crystal.

Cochran[3] proposed that the lattice instability occurs in KDP as the similar manner to the displacive type ferroelectrics. He described the ferroelectric mode as in Fig. 1-2; hydrogen atoms moving in the ab plane and K and P atoms moving oppositely along the c axis. Below Curie temperature this mode motion is frozen out and the spontaneous polarization occurs due to the displacements of K and P atoms.

It is thought that essential mechanism which causes the ferroelectric transition in KDP type crystal is the proton tunneling mode. The dipole system may be the order-disorder mechanism of other ions or the coupled proton-phonon mode. These theories[6, 7] suggest the existence of a polar mode whose characteristic frequency tends to be zero and vanishes when the temperature is lowered through the Curie temperature. Such a mode is both infrared and Raman active in KDP.

The effect of deuteration is an attractive subject in KDP type ferroelectrics, as the existence of the proton tunneling mode[4] has been proposed theoretically. The tunneling frequency should be reduced drastically by deuteration.

The crystal of $NH_4H_2PO_4$(ADP) is isomorphous to KDP but is antiferroelectric below the transition temperature.[8] Cochran[3] also argued that the antiferroelectric transition is caused by the instability of the temperature dependent zone boundary mode. He inferred that the antiferroelectric mode in ADP should occur at the Z point; $k = (0, 0, \frac{2\pi}{c})$. This mode is optically inactive. However, ADP is also the hydrogen bonded crystal and so the proton tunneling mode is probable. And that the low-frequency dielectric constant[41] is very large and varies with temperature, so the temperature dependent mode

may exist as predicted by eqs. 1-3 and 1-4.

3-2 Infrared and Raman Spectra of KDP Type Ferroelectrics

The vibrational spectra of KDP may be separated into three regions: i) the lower-frequency region below 300 cm^{-1} corresponding to the external vibrations of the lattice, ii) the mid-frequency region from 300 cm^{-1} to 1100 cm^{-1} corresponding to the internal vibrations of the molecule contained in the crystal and iii) the high-frequency region above 1100 cm^{-1} corresponding to the vibrations of light-weight protons of hydrogen bonds.

Several works[5, 42] have been done in the high-frequency region to get information for the hydrogen motions. Blinc et al.[5] investigated the infrared absorption spectra of KDP type crystals in the region from 700 cm^{-1} to 3100 cm^{-1}. They interpreted their data as due to the proton tunneling between two minima of potential energy. This model, the tunneling mode model, is the fundamentals of the recent lattice dynamical model of KDP.

Wiener[43-45] and his co-workers have measured the infrared spectra of KDP type crystals in the mid-region. The spectra show the existence of broad bands above T_c and the occurence of sharpening of these bands below T_c. They theorized that these bands are attributed to the internal vibration of PO_4 ions and are broadened above T_c because they are coupled to the low-frequency hydrogen tunneling mode. Below T_c the tunneling modes disappear as the protons become ordered. Thus these results revealed several details on the role of the hydrogen atoms in the process of ferroelectric phase transition of these crystals. Further the deuteration may cause the reduction of tunneling

frequency and so the significant change in the spectra also.

The low-frequency spectra of KDP type crystal have been investigated by use of the far-infrared and Raman scattering techniques. Barker et al.[46] measured the far-infrared reflection spectrum of KDP at room temperature. The results indicate the existence of a broad band near 50 cm^{-1}, though the data below 100 cm^{-1} are not sufficient. This mode contributes largely to the low-frequency dielectric constant and so they concluded that the broad band near 50 cm^{-1} is a ferroelectric mode. Kawamura et al.[47-49] have also measured the far-infrared reflection spectra of KDP in wider region from 20 cm^{-1} to 550 cm^{-1} at several temperatures above and below T_c. The results showed that the ferroelectric mode strongly depends on the temperature in its peak frequency and intensity. The peak frequency decreases and the intensity increases as the temperature is lowered to T_c. Below T_c this mode disappears. The same type measurements were made by Sugawara et al.[50] and the similar results were obtained.

The Raman spectrum of the ferroelectric mode of KDP was studied by several groups.[51-53] The work by Kaminow[51] showed that the line shape of this mode, which is observed as a Rayleigh wing, could be fitted by a simple-damped-harmonic oscillator function. The damping factor is temperature independent and the characteristic frequency exhibits a soft mode behavior

$$\omega_o^2 = K\,(T - T_c)/T. \qquad (1\text{-}7)$$

Such a temperature dependence of the ferroelectric mode is consistent with either the coupled proton-phonon mode[7] or the collective proton tunneling mode[6] model of KDP. The deuteration causes the reduction of tunneling frequency and therefore the effect of deuteration on the

low-frequency spectra is an attractive subject. Kawamura et al.[54] measured the far-infrared reflection spectra of DKDP in the region from 20 cm^{-1} to 550 cm^{-1} at several temperatures above and below T_c. Comparison of the obtained data with the zero-frequency reflectivity* indicates that the ferroelectric mode must exist below 20 cm^{-1}, if any. The Raman spectra of DKDP were measured by the several groups.[51, 54-57] The results by Reese et al.[56, 57] showed the ferroelectric mode in very low-frequency region. In these works of Raman scattering on KDP type crystals, the investigation was made on the lowest frequency mode. Scott et al.[58] observed the evidence of strong anharmonic coupling between the ferroelectric mode and the other lattice vibrational mode in the spectra of CsH_2AsO_4 and KH_2AsO_4. The Raman spectra of these crystals show the ferroelectric mode and the overdamped mode above T_c and the observed data are accurately described by a coupled mode equation. Recently the same type analysis was made on KDP and ADP by She and Broberg.[60, 61] Such an anharmonic interaction is also manifested in the far-infrared spectra of KDP, in which two noninteracting oscillator function could not successfully be fitted to the observed spectra.[47]

The ferroelectric mode was observed both in the far-infrared and the Raman spectra. These results are consistent with the recent model of KDP proposed theoretically but its origin is unknown yet. It may be the polarization fluctuation due to the ion displacement induced by the proton tunneling mode[6] or the coupled proton-phonon mode.[7]

In the series of Raman and far-infrared works mentioned above,

---

*Note: Zero-frequency reflectivity was calculated from the low-frequency dielectric constant in the microwave region.

much attention has been paid to the ferroelectric mode behavior or the spectra in the partial region. But so far determination of the mode symmetries in both phases, the mode assignments and their correlation from one phase to the other have not been done completely. The determination of the mode symmetries, the mode assignments and the establishment of the correlation are possible by the aid of group analysis and such investigations lead us to clarify the correct origin of the ferroelectric mode.

Agrawal et al.[53] observed the Raman spectra of several KDP type ferroelectrics up to 2800 cm^{-1} both above and below T_c and determined the mode symmetries though insufficient.

The antiferroelectric ADP, which is isomorphic with KDP, has received rather little attention. Kawamura et al.[47, 49] reported the observation of the overdamped E symmetry mode in the far-infrared spectra.* Such a mode is also observed by Broberg et al.[61] and Ryan et al.[62] in their Raman scattering spectra.

4. Summary

As stated in the preceeding section, considerable progress has been made recently in the understanding of the phenomena in KDP type ferroelectrics though, the vibrational spectra of these crystals have not still been completely understood. The present work is concerned with the investigation of the phase transition in KDP type ferroelectrics using far-infrared spectroscopy and Raman scattering technique.

---

*Note: The ferroelectric mode of KDP belongs to B_2 symmetry species.

The present investigations are as follows; i) the measurements of detailed temperature dependence of the vibrational spectra of KDP using a polarized radiation, ii) the determination of the mode symmetries in both phases, the establishment of the correlation from one phase to the other and of the mode assignments comparing with the group theoretical analysis, iii) the studies of the anomalous temperature dependence of the spectra such as ferroelectric mode behavior and the proton tunneling mode, iv) the same type investigations on the deuterated substance DKDP, and v) the same type investigations on the antiferroelectric ADP. These experimental works will lead us to the better understanding of the ferroelectric phase transition in KDP type crystals.

References

1) 川辺和夫、強誘電体、共立出版.

2) 三井利夫、達崎達、中村英二、強誘電体、槇書店.

3) W. Cochran, Advan. Phys. 9 (1960) 387, ibid, 10 (1961) 401.

4) P. G. de Gennes, Solid State Commun. 1 (1963) 132.

5) R. Blinc and D. Hadzi, Mol. Phys. 1 (1958) 391, and J. Chem. Solids 13 (1960) 204.

6) M. Tokunaga, Prog. Theor. Phys. (Japan) 36 (1966) 857, and Ferroelectrics 1 (1970) 195.

7) K. K. Kobayashi, J. Phys. Soc. Japan 24 (1968) 497.

8) W. Känzig, Ferroelectrics and Antiferroelectrics, ed. F. Seits and D. Turnbull, Solid State Phys. (Academic, New York, 1957).

9) B. C. Frazer and R. Pepinski, Acta Cryst. 6 (1953) 273.

10) G. E. Bacon and R. S. Pease, Proc. Roy. Soc. (London) A 230 (1955) 359.

11) For example, M. Cardona, Optical Properties of Solids, ed. S. Nudelman and S. S. Mitra (Plenum, New York, 1969) Chap. 6.

12) M. Born and K. Huang, Dynamical Theory of Crystal Lattices (Oxford Univ., London, 1954).

13) For example, C. Kittel, Introduction to Solid State Physics, 3rd. ed. (John Wiley & Sons, New York, 1967) p. 151.

14) A. S. Barker, Jr. and M. Tinkham, Phys. Rev. 125 (1962) 1527.

15) W. Spitzer, R. C. Miller, D. A. Kleiman and L. E. Hawarth, Phys. Rev. 126 (1962) 1710.

16) J. M. Ballentyne, Phys. Rev. 136 (1964) A 429.

17) T. Nakamura, J. Phys. Soc. Japan 21 (1966) 491.

18) C. H. Perry and T. F. McNelly, Phys. Rev. 154 (1967) 456.

19) A. S. Barker, Jr., Ferroelectricity, ed. E. F. Weller (Elsevier, Amsterdam, 1967) p. 213, and Far-Infrared Properties of Solids, ed. S. S. Mitra and S. Nudelman (Plenum, New York, 1970) p. 247.

20) A. S. Barker, Jr. and J. J. Hopfield, Phys. Rev. 135 (1964) A 1732.

21) R. Loudon, Advan. Phys. 13 (1964) 423.

22) A. S. Barker, Jr. and R. Loudon, Rev. Mod. Phys. 44 (1972) 18.

23) M. DiDomenico, Jr., S. H. Wemple, S. P. S. Porto and R. P. Bauman, Phys. Rev. 174 (1968) 522.

24) G. Burns and B. A. Scott, Phys. Rev. Letters 25 (1970) 167.

25) I. P. Kaminow and T. C. Damen, Phys. Rev. Letters 20 (1968) 1105.

26) J. M. Worlock, Structural Phase Transitions and Soft Modes, ed. E. J. Samuelsen, E. Anderson and J. Feder (Universitetsforlaget, Oslo, 1971) p. 397.

27) R. E. Nettleton, Ferroelectrics, 1 (1970) 111.

28) E. F. Steigmeier, J. Phys. 33 Suppl. C 2 (1972) 15.

29) P. A. Fleury and J. M. Worlock, Phys. Rev. Letters 18 (1967) 665.

30) J. M. Worlock and P. A. Fleury, Phys. Rev. Letters 19 (1967) 1176.

31) J. M. Worlock, Proc. 1st Intern. Conf. Light Scattering Spectra of Solids, ed. G. B. Wright (Springer, 1969) p. 411.

32) M. Balkanski, K. K. Teng, S. M. Shapiro and M. K. Ziolkiewicz, Phys. Stat. Sol. 44 (1971) 355.

33) D. K. Agrawal and C. H. Perry, Phys. Rev. B 4 (1971) 1893.

34) G. Harbeke, E. F. Steigmeir and R. K. Whener, Solid State Commun. 8 (1970) 1765.

35) J. F. Scott, Proc. 2nd Intern. Conf. Light Scattering in Solids, ed. M. Balkanski (Flammarion, Paris, 1971) p.387.

36) P. A. Fleury, J. F. Scott and J. M. Worlock, Phys. Rev. Letters 21 (1968) 16.

37) J. C. Slater, J. Chem. Phys. 9 (1941) 16.

38) Y. Takagi, J. Phys. Soc. Japan 3 (1948) 271.

39) R. Blinc and D. Hadzi, Mol. Phys. 1 (1958) 391.

40) F. Jona and G. Shirane, Ferroelectric Crystals (Pergamon, New York, 1962).

41) I. P. Kaminow, Phys. Rev. 138 (1965) A 1539.

42) R. M. Hill and S. K. Ichiki, J. Chem. Phys. 48 (1968) 838, and Y. Sato and Y. Machida, Solid State Commun. 7 (1969) 327.

43) Y. Imry, I. Pelah and E. Wiener, J. Chem. Phys. 43 (1965) 2332.

44) E. Wiener, S. Levin and I. Pelah, J. Chem. Phys. 52 (1970) 2881.

45) S. Levin, I. Pelah and E. Wiener, Phys. Stat. Sol. (b) 58 (1973) 61.

46) A. S. Barker, Jr. and M. Tinkham, J. Chem. Phys. 38 (1963) 2257.

47) T. Kawamura, A. Mitsuishi and H. Yoshinaga, Japan J. Appl. Phys. 7 (1968) 1303, and J. Phys. Soc. Japan 28 (1970) 227.

48) M. Yamanaka, T. Kawamura and M. Hineno, J. Phys. D: Appl. Phys. 5 (1972) 743.

49) T. Kawamura, and A. Mitsuishi, Technology Reports of Osaka Univ. 23 (1973) 365.

50) F. Sugawara and T. Nakamura, J. Phys. Soc. Japan 28 (1970) 165.

51) I. P. Kaminow and T. C. Damen, Phys. Rev. Letters 20 (1968) 1105, and Light Scattering Spectra of Solids, ed. G. B. Wright (Springer, New York, 1969) p. 675.

52) C. M. Wilson and H. Z. Cummins, Light Scattering in Solids, ed. M. Balkanski (Flammarion, Paris, 1971) p. 420.

53) D. K. Agrawal and C. H. Perry, ibid p. 429.

54) T. Kawamura and A. Mitsuishi, To be submitted to Optics Commun.

55) K. I. White, W. Taylor, R. S. Katiyar and S. M. Kay, Phys. Letters 33 A (1970) 175.

56) R. L. Reese, I. J. Fritz and H. Z. Cummins, Solid State Commun. 9 (1971) 327.

57) I. J. Fritz, R. L. Reese, E. M. Brody, C. M. Wilson and H. Z. Cummins, Light Scattering in Solids, ed. M. Balkanski (Flammarion, Paris, 1971) p. 415.

58) R. S. Katiyar, J. F. Ryan and J. F. Scott, Phys. Rev. B 4 (1971) 2635, and Light Scattering in Solids, ed. M. Balkanski (Flammarion, Paris, 1971) p. 436.

59) J. F. Scott and C. M. Wilson, Solid State Commun. 10 (1972) 597.

60) C. Y. She, T. W. Broberg and L. S. Wall, Phys. Rev. B 6 (1972) 1847.

61) T. W. Broberg, C. Y. She, L. S. Wall and D. F. Edwards, Phys. Rev. B 6 (1972) 3332.

62) J. F. Ryan, R. S. Katiyar and W. Taylor, J. Phys. Suppl. 33 C 2 (1972) 49.

Table 1-1

	$T_{c(H)}$ K	$T_{c(D)}$ K
KH_2PO_4	123	213
KH_2AsO_4	97	162
RbH_2PO_4	147	218
RbH_2AsO_4	110	178
CsH_2AsO_4	143	212
$NH_4H_2PO_4$	148	232

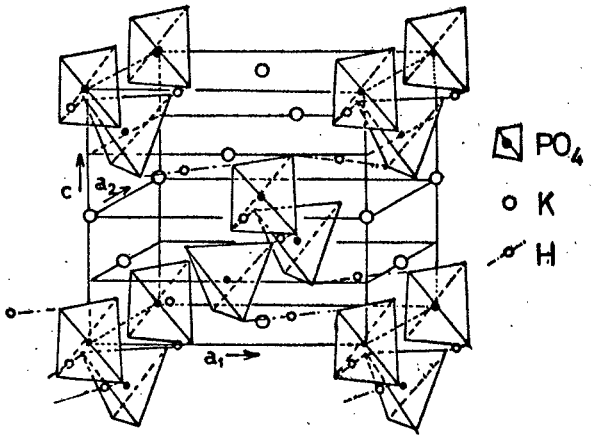

Fig. 1-1 Structure of KH_2PO_4 (Slater[37]).

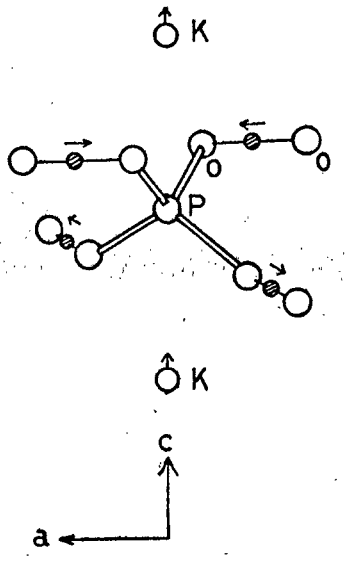

Fig. 1-2 Ferroelectric mode (Cochran[3])

Chapter 2 Group Character

In this chapter the results of group theoretical analysis are given for both paraelectric and ferroelectric structures. The group analysis gives us the information about the number of normal modes, their mode symmetry and the selection rule. Comparison of the observed spectra with the results of group theoretical analysis leads us to the correct mode assignments.

KDP and its isomorphous crystals are the paraelectrics and have a tetragonal structure above Curie temperature T_c, and below T_c they become ferroelectric and have an orthorhomic structure.[1] We can get more accurate information about the ferroelectric transition by the following procedures: making the precise mode assignment of observed bands in both phases, and examining the relation between the normal modes when the crystal goes from one structure to the other.

The KDP type crystals are composed of ions and molecules, and interatomic force in the PO_4 group is thought to be much stronger than the forces between the ions. If this is the case the more appropriate classification of the normal modes is possible. The further discussion will be made also about this point.

1. Structure

The paraelectric structure of KDP type crystal was examined by X ray[2] and neutron diffraction[3] measurements. The space group is D_{2d}^{12} ($I\bar{4}2d$) with four molecules in the body centered tetragonal unit cell. The structure of KDP[4] is shown in Fig. 2-1. The orthogonal axes x, y and z are taken to be parallel to its crystallographic axes a_1, a_2 and

c, respectively. The symmetry elements of this group are a four-fold rotation reflection axis S_4 and two-fold rotation axis C_2 parallel to the z axis, two-fold rotation axis C_2 parallel to the x and y axes and glide plane σ_d.[5] The potassium ions and phosphate ions locate on the points with S_4 symmetry.

In the ferroelectric phase the crystal symmetry is reduced. The space group is C_{2v}^{19} (Fdd2) with eight molecules in an enlarged orthorhomic unit cell. The transformation of the unit cell from body-centered to face-centered is accompanied by doubling of the cell size with crystallographic axes rotating 45° in the xy plane. The structure of KDP below T_c is shown in Fig. 2-2, where each (H_2PO_4) ion is represented as a closed circle.[5] The spontaneous polarization occurs along z axis below T_c.

The hydrogen bonded antiferroelectric ADP[6] is isomorphous with KDP in the paraelectric phase. The paraelectric structure is the same with that of KDP, namely D_{2d}^{12}.[7, 8] Below the transition point, i.e. in the antiferroelectric phase, the structure of ADP is D_2^4 $(P2_12_12_1)$.[7] This is in contrast to KDP, of which structure is C_{2v}^{19} in the ferroelectric phase. The transition in ADP results in an only slight orthorhomic distortion of original unit cell. The structure of $ND_4D_2PO_4$ (DADP) in the projection on ac plane is shown in Fig. 2-3 as a reference.[9] The significant difference between the structure of KDP and that of ADP is as follows. In ADP each NH_4group is tetrahedrally connected to four PO_4 groups by N-H---O hydrogen bonds.

The characteristics of these crystals KDP and ADP are the O-H---O hydrogen bonds. Each PO_4 group is linked by hydrogen bonds to a tetrahedral arrangement of PO_4 group neighbours. The ordering of O-H---O

bonds in KDP has been observed by neutron diffraction experiment[3] as shown in Fig. 2-4 (a). For the antiferroelectric ADP the ordering is assumed to be as shown in Fig. 2-4 (b) which is depicted by Nagamiya.[10]

2. Group Theoretical Consideration and Selection Rules

2-1 Factor Group Analysis

The space group of KDP in the paraelectric phase is D_{2d}^{12}, and one crystallographic unit cell contains four molecules.[4] As the primitive lattice vector, it is more convenient to introduce following vectors; $\mathbf{t}_1$, $\mathbf{t}_2$, and $\mathbf{t}_3$.[11] The components of these vectors are given in the rectangular coordinates by $(-\frac{a}{2}, \frac{a}{2}, \frac{c}{2})$, $(\frac{a}{2}, -\frac{a}{2}, \frac{c}{2})$ and $(\frac{a}{2}, \frac{a}{2}, \frac{c}{2})$, respectively. These vectors are shown in Fig. 2-5 (a) schematically. The primitive unit cell now has the volume $a^2 \cdot c/2$ and contains two molecules.

The atoms P_3, P_4, K_3, K_4, $H_{1'}$, $H_{2'}$, $H_{3'}$, $H_{4'}$, O_i-P_3 and O_j-P_4 (i, j = 1, 2, 3, 4) are contained in the primitive unit cell (see Fig. 2-1). The other atoms are equivalent to them simply by the translational operations.

In the ferroelectric phase the crystal structure is face-centered orthorhomic C_{2v}^{19}. One crystallographic unit cell contains eight molecules as shown in Fig. 2-2. In this case the primitive vectors $\mathbf{t}_1'$, $\mathbf{t}_2'$ and $\mathbf{t}_3'$ can be chosen as shown in Fig. 2-5 (b) and one primitive cell contains also two molecules.

The KDP crystal may be regarded as consisting of K and (H_2PO_4) ions.[1] In this case the normal mode vibrations of the crystal can be classified in two categories.[12] i) The lattice mode or external mode

correspond to the translational and rotational vibrations of ion groups where (H_2PO_4) ion vibrates or rotates as a whole; and ii) The internal mode corresponding to the molecular vibrations of (H_2PO_4) ions. In general the former lies in the low-frequency region and the latter lies in the high-frequency region.

The character tables for D_{2d} and C_{2v} symmetry are shown in Table 2-1 (a) and (b) respectively.[13] The irreducible representations and the symmetry operations are listed in the table. The distributions of normal mode vibrations among the irreducible representation can be obtained by the factor group analysis.[13] The results are shown in Table 2-2. This result is in good agreement with that of Shur.[14] In the factor group analysis only the atoms in the primitive unit cell were taken into consideration and all other atoms were assumed to have identical displacements. So these are the normal modes in the long-wavelength limit (k=0). The selection rules for all these normal modes with regard to Raman scattering and infrared absorption are determined by the representation of the polarizability tensor and the dipole moment. In Table 2-2 the representations of non-vanishing polarizability tensor components and dipole moment components are also listed.[12,15]

According to the results shown in Table 2-2 there are 28 Raman active modes $4A_1+6B_1+6B_2+12E$,* of which $6B_2+12E$ are also infrared active in the paraelectric phase. In the infrared B_2 modes are polarized parallel to the z axis and the doubly degenerate E modes are polarized perpendicular to the z axis.

In the ferroelectric phase after the transition at T_c, the space group symmetry changes from D_{2d}^{12} to C_{2v}^{19}.[*] The correlation between the

*Note: A doubly degenerate E mode is accounted as one mode.

irreducible representation of the space group D_{2d}^{12} and C_{2v}^{19} is shown in Table 2-3,[13] and it results in that $4A_1+6B_2$ modes in the paraelectric phase transform into $10A_1$ modes in the ferroelectric phase. $5A_2+6B_1$ modes above T_c transform to $11A_2$ modes below T_c. The doubly degenerate 12E modes above T_c split into $12B_1+12B_2$ modes below T_c. These modes are all Raman active and of which $10A_1+12B_1+12B_2$ are also infrared active.

The antiferroelectric ADP is isomorphous with KDP in the paraelectric phase.[6] The similar procedure used to the analysis of KDP is also applicable to ADP. The primitive unit cell now contains 24 atoms and the crystal can be regarded as composed of NH_4 and (H_2PO_4) ions. The group theoretical analysis has been given by Shur[14] and his results are reproduced in Table 2-4. The number of the translational oscillation is the same with that of KDP, while those of rotational oscillations and internal oscillation of the ion increase due to the presence of NH_4 ions. The rotational oscillations are now distributed as $2A_1+2A_2+4E$, while in KDP they are A_1+A_2+2E.

2-2 Vibrational Modes

In the preceeding section the results of factor group analysis are given, where the KDP crystal was regarded as composed of K and (H_2PO_4) ions.[1] In this section the more detailed discussion will be given for the external vibrational mode, the internal vibrational mode of PO_4 ion and hydrogen vibrational mode.

2-2-1 External Modes

The external motions of $[K-(H_2PO_4)]$ sublattice consist of

translational and rotational vibrations and the number of these vibrational modes are given in Table 2-2. In the paraelectric phase A_1+A_2+2E modes are rotational vibrations and $2B_1+2B_2+4E$ are translational vibrations. The schematic representation of the translational vibrational modes are shown in Fig. 2-6 (a). The external vibrations are purely ionic vibrations, and the B_2 modes and E modes transform as P_z and (P_x, P_y) dipole moment except acoustical ones. The translational modes in the ferroelectric phase are given by Shur[14] and results are reproduced in Fig. 2-6 (b). It is worth noticing that the ferroelectric mode depicted by Cochran (Fig. 1-2) corresponds to the B_2 mode in which K ion and (H_2PO_4) ion displace oppositely as shown in Fig. 2-6 (a).

2-2-2 Internal Modes

It is well known that the free PO_4 ion has a tetrahedral point group T_d and has four distinct frequencies:[17] a totally symmetric vibration $\nu_1(A_1)$, a doubly degenerate vibration $\nu_2(E)$, and two triply degenerate vibrations $\nu_3(F_2)$ and $\nu_4(F_2)$. These vibrational modes are all Raman active and of which two F_2 modes are also infrared active. In the case of free ion, these absorptions occur at ν_1=980 cm^{-1}, ν_2= 363 cm^{-1}, ν_3=1083 cm^{-1} and ν_4=515 cm^{-1}.[17] In the crystal it seems that the tetrahedral PO_4 ion is deformed by the crystalline field under the crystal point group D_{2d}. In the paraelectric phase PO_4 ions lie on the site of S_4 symmetry which is the site group of point group T_d.[5] Murphy et al.[18] have interpreted their data assuming that the PO_4 ion has approximately T_d symmetry and occupying S_4 site. If this is the case, the E type modes of free PO_4 ions transform into A+B type modes of S_4 symmetry and the F_2 type modes transform into B+E type modes. And that molecular vibrations are expected to be almost

unchanged. On the other hand, if each atom of PO_4 ion strongly binds with the lattice, the original molecular vibrations disappear and new lattice modes with species under the crystal point group D_{2d} are formed. The corresponding correlation among the molecular group T_d, the site group S_4 and the crystal point group D_{2d} are shown in Table 2-5. Such a correlation diagram is well known from group theory.[13)]

In the ferroelectric phase deformation lowers the crystal symmetry to C_{2v}, and then S_4 symmetry can no longer be the site group of C_{2v}. C_2 symmetry is the subgroup of C_{2v} and also that of T_d symmetry. Thus C_2 symmetry is the only possible site of PO_4 molecule. The correlations among T_d symmetry, C_2 site symmetry and C_{2v} symmetry are shown in Table 2-6.[13)]

2-2-3 Proton Modes

The vibrations of light-weight hydrogen atom are in the high-frequency region above 1000 cm^{-1}. Many works have been done on KDP type crystals using a near-infrared[18-21)] and Raman spectroscopy[22)] and have given information about the hydrogen motions.

Neutron diffraction experiments[3)] on KDP have shown that the hydrogen motions are largely elongated along OHO bond axis. Blinc et al.[19)] have interpreted their near-infrared data as due to a double minima potential where proton tunnels quantum mechanically.

Here we consider the proton tunneling mode in the crystal symmetry D_{2d}. The primitive unit cell of KDP contains four non-equivalent hydrogen atoms as shown in Fig. 2-1. A set of four symmetry arrangements of the displacements of these hydrogen atoms are shown in Fig. 2-7 (a)$\sim$(d). In these modes protons tunnel collectively. As k=0 tunneling mode is of interest here, all equivalent atoms have identical displacements. These

four proton modes transform according to the irreducible representation of D_{2d} symmetry: the mode shown in Fig. 2-7 (a) transforms as A_2 symmetry species, the mode (b) transforms as B_2, the modes (c) and (d) transforms as E respectively. It is noticeable that the mode (b) transforms as B_2 symmetry species which gives P_z dipole moment. This mode corresponds to the ferroelectric mode motion depicted by Cochran[16] (Fig. 1-2) and may form an important component of the ferroelectric mode. The deuteration should reduce the tunneling frequency. So the comparison of the spectrum of KDP with that of DKDP should give the information about the proton tunneling modes and the phase transition.

The similar analysis was made by Kaminow[23] and Lavrencic et al.[42] But the results of Lavrencic et al. indicate that the mode given in Fig. 2-7 (a) transforms as B_1 symmetry species. This mode is symmetric with S_4 operation along z axis and asymmetric with C_2 operation along x axis. So it must transform as A_2 symmetry species. The present results is also in good agreement with Kaminow et al.[25]

In this section the vibrational modes due to $[K-(H_2PO_4)]$ sublattice, PO_4 molecule and four non-equivalent protons in KDP are considered independently. The intra-molecular vibrations of PO_4 ion are expected to lie in the region from 300 cm^{-1} to 1100 cm^{-1} because PO_4 ion perhaps behaves as an independent molecule in KDP and so its natural frequencies are expected to be almost unchanged. The vibrational modes of $[K-(H_2PO_4)]$ sublattice are expected to lie in the low-frequency region. The collective proton tunneling modes transform as A_2, B_2 and E representations and they are interesting in connection with the ferroelectric mode. The results obtained here will be discussed comparing with the experimental data in the following chapters.

Recerences

1) F. Jona and G. Shirane, Ferroelectric Crystals (Pergamon, Oxford, 1962).

2) B. C. Frazer and R. Pepinski, Acta Cryst. 6 (1953) 273.

3) G. E. Bacon and R. S. Pease, Proc. Roy. Soc. (London) A 220 (1953) 397, and ibid A 230 (1955) 359.

4) J. West, Z. Krist. 74 (1930) 306.

5) International Table for X Ray Crstallography, ed. N. F. Henry and K. Lonsdale (Kynoch, New York, 1963) vol. 1.

6) W. Känzig, Solid State Physics, ed. Seitz and Turnbull (Academic, New York, 1957) vol. 4.

7) R. O. Keeling and R. Pepinski, Z. Krist. 106 (1955) 236.

8) R. Ueda, J. Phys. Soc. Japan 3 (1948) 328.

9) E. A. Wallace and W. Cochran, J. Phys. Suppl. 33 C2 (1972) 61.

10) T. Nagamiya, Prog. Theor. Phys. (Japan) 7 (1952) 275.

11) T. Fujiwara, J. Phys. Soc. Japan 29 (1970) 1282.

12) M. Balkanski, M. K. Teng, and M. Nusimovici, Phys. Rev. 176 (1968) 1098.

13) For example, G. Turrell, Infrared and Raman Spectra of Crystals (Academic, London, 1972), and R. McWeeny and D. Dhil, Symmetry: An Introduction to Group Theory and Its Applications (Pergamon, Oxford, 1963).

14) M. S. Shur, Sov. Physics-Solid State, 8 (1966) 1008; ibid 8 (1967) 2007; Sov. Physics-Crystallography, 11 (1966) 394; and ibid 12 (1967) 175.

15) R. Loudon, Advan. Phys. 13 (1964) 423.

16) W. Cochran, Advan. in Phys. 9 (1960) 387, and ibid 10 (1961) 401.

17) For example, G. Herzberg, Infrared and Raman Spectra of Polyatomic Molecules (van Nostrand, New York, 1945).

18) G. M. Murphy and G. Weiner, J. Chem. Phys. 22 (1954) 1322.

19) R. Blinc and D. Hadzi, Mol. Phys. 1 (1958) 391.

20) Y. Imry, I. Pelah and E. Wiener, J. Chem. Phys. 43 (1965) 2332.

21) R. M. Hill and S. K. Ichiki, J. Chem. Phys. 48 (1968) 838.

22) I. P. Kaminow, R. C. C. Leite and S. P. S. Porto, J. Phys. Chem. Solids, 26 (1965) 2088.

23) I. P. Kaminow, Phys. Rev. 138 (1965) A 1539.

24) B. Lavrencic, I. Levstek, B. Zeks, R. Blinc and D. Handzi, Chem. Phys. Letters 5 (1970) 441.

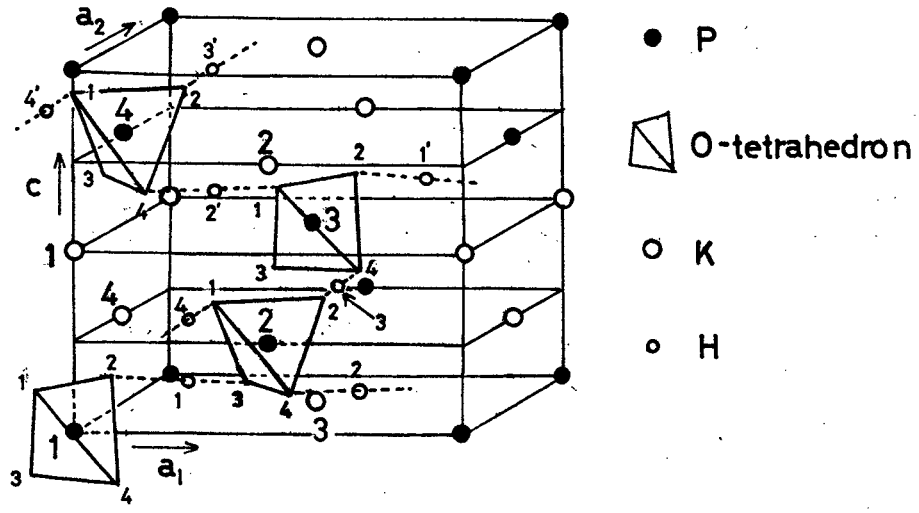

Fig. 2-1 Crystal structure of KH_2PO_4 in the paraelectric phase.

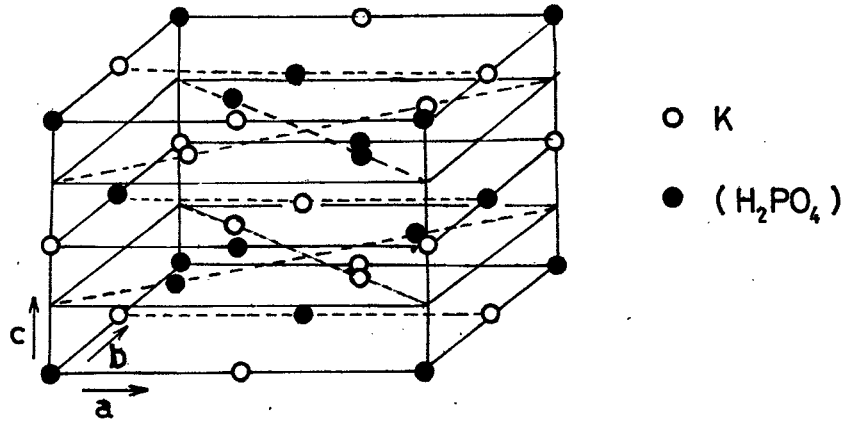

Fig. 2-2 Crystal structure of KH_2PO_4 in the ferroelectric phase.

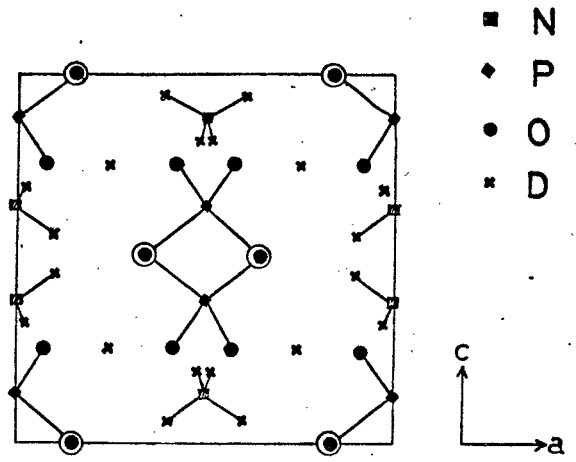

Fig. 2-3 The structure of $ND_4D_2PO_4$ in projection on ac plane. (E. A. Wallace et al.[9])

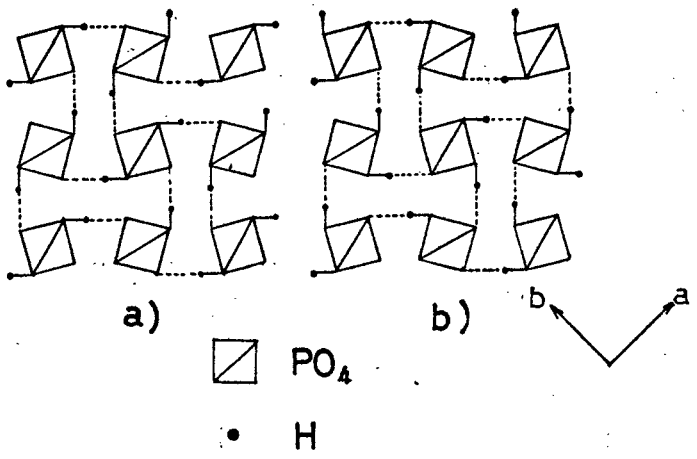

Fig. 2-4 a) Hydrogen ordering in the ferroelectric structure of KH_2PO_4 in projection on ab plane. (Frazer[2])

b) Hydrogen ordering in the antiferroelectric strucutre of $NH_4H_2PO_4$. (Nagamiya[10])

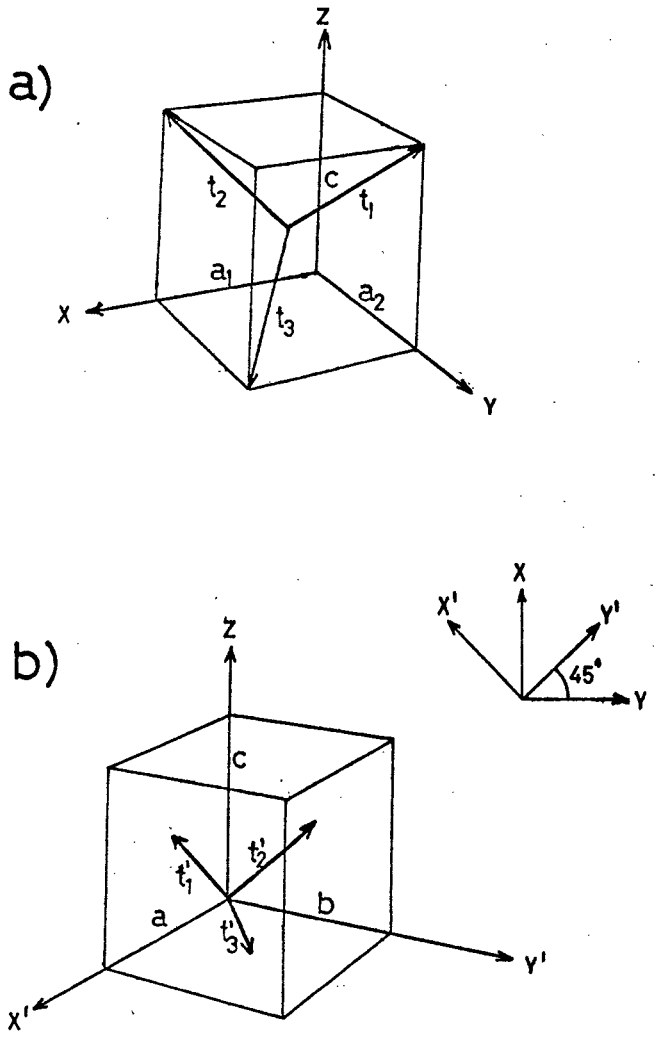

Fig. 2-5 a) Unit cell of body-centered tetragonal lattice showing primitive vectors.

b) Unit cell of face-centered orthorhomic lattice showing primitive vectors.

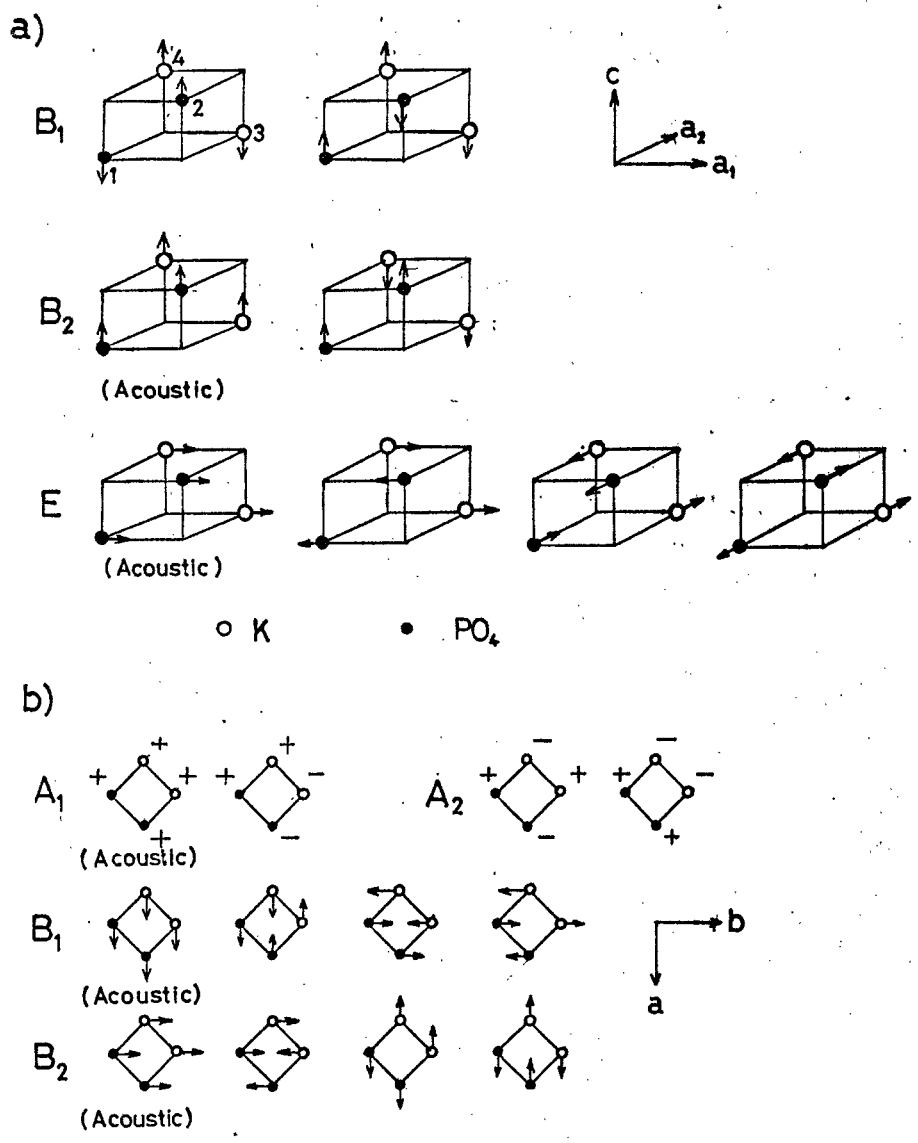

Fig. 2-6 a) Translational vibrations of [K-(H_2PO_4)] sublattice in D_{2d} symmetry.

b) Translational vibrations of [K-(H_2PO_4)] sublattice in C_{2v} symmetry (Shur[14]).

(H_2PO_4) groups are represented as open circles.

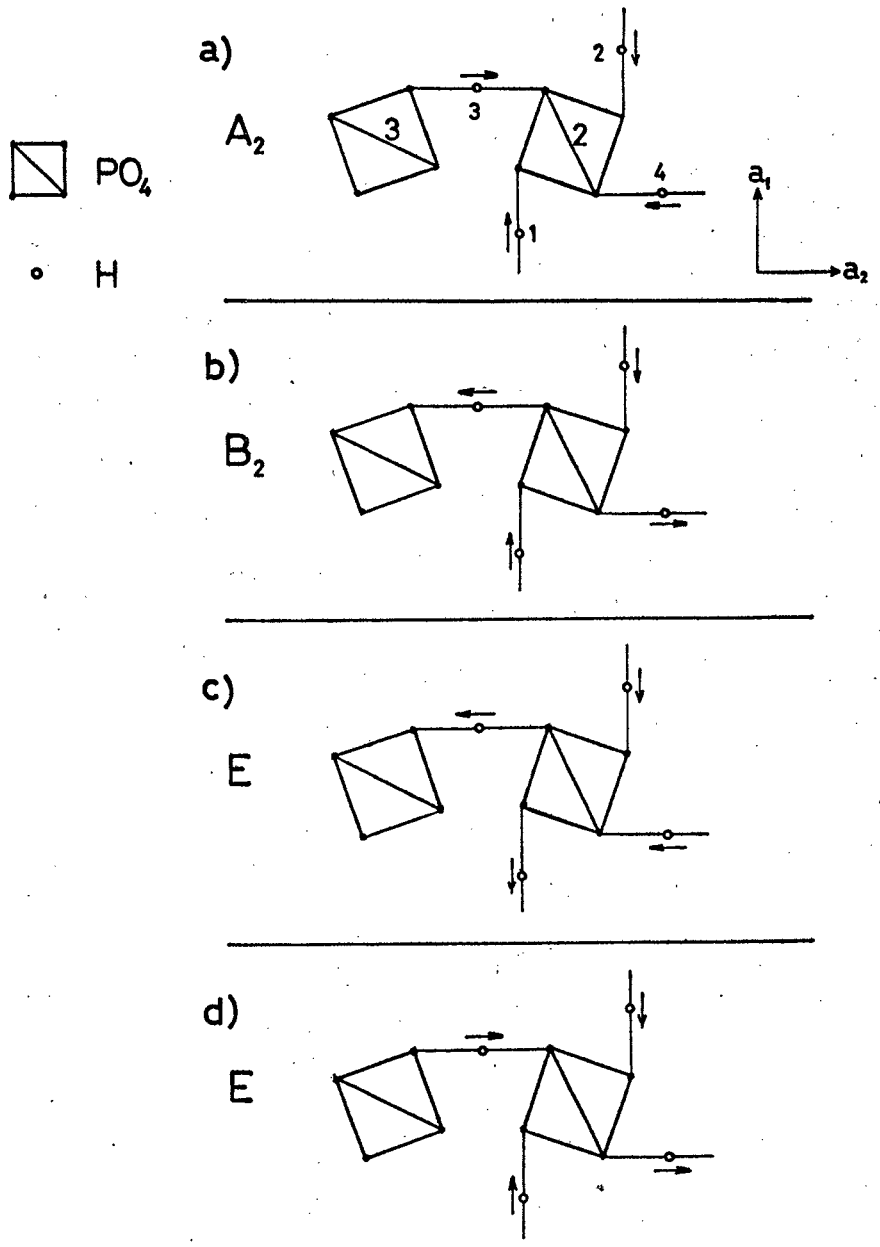

Fig. 2-7 Schematic representations of the four proton tunneling modes in KH_2PO_4.

Table 2-1

a) Character table for D_{2d} symmetry

D_{2d}	E	$2S_4$	C_2	$2C_2^{x,y}$	$2\sigma_d$	
A_1	1	1	1	1	1	
A_2	1	1	1	-1	-1	R_z
B_1	1	-1	1	1	-1	
B_2	1	-1	1	-1	1	T_z
E	2	0	-2	0	0	$(T_x, T_y), (R_x, R_y)$

b) Character table for C_{2v} symmetry

C_{2v}	E	C_2	$\sigma_v(x'z)$	$\sigma_v(y'z)$	
A_1	1	1	1	1	T_z
A_2	1	1	-1	-1	R_z
B_1	1	-1	1	-1	T_x, R_y
B_2	1	-1	-1	1	T_y, R_x

Table 2-2

Total number of normal mode (N_{tot}) transforming as an irreducible representation for D_{2d}^{12} and C_{2v} symmetries in KH_2PO_4

D_{2d}^{12}		N_{tot}	N_{acous}	N_{opt}	N_{rot}	N_i	Raman tensor component	Dipole moment
	A_1	4	0	0	1	3	$\alpha_{xx}+\alpha_{yy}, \alpha_{zz}$	
$(T>T_c)$	A_2	5	0	0	1	4		
	B_1	6	0	2	0	4	$\alpha_{xx}-\alpha_{yy}$	
	B_2	7	1	1	0	5	α_{xy}	P_z
	E	13	1	3	2	7	α_{yx}, α_{xz}	P_x, P_y
C_{2v}^{19}								
	A_1	11	1	1	1	8	$\alpha_{x'x'}, \alpha_{y'y'}, \alpha_{zz}$	P_z
$(T<T_c)$	A_2	11	0	2	1	8	$\alpha_{x'y'}$	
	B_1	13	1	3	2	7	$\alpha_{zx'}$	$P_{x'}$
	B_2	13	1	3	2	7	$\alpha_{y'z}$	$P_{y'}$

Note: N_{acous}, N_{opt}, N_{rot} and N_i refer to acoustical and optical translations, rotational oscilations and internal vibrations of $(H_2PO_4)^{-1}$ ions respectively.

Table 2-3

Compatibility ralations between irreducible representation of space group D_{2d}^{12} and C_{2v}^{19} in the two phases

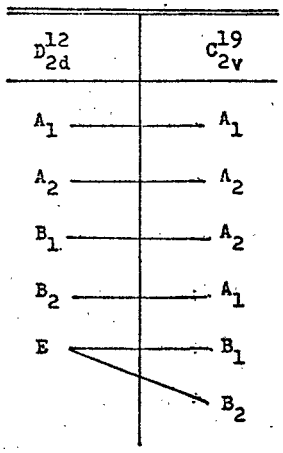

Table 2-4

Total number of normal mode (N_{tot}) transforming as an irreducible representation for D_{2d}^{12} symmetry in $NH_4H_2PO_4$

D_{2d}^{12}		N_{tot}	N_{acous}	N_{opt}	N_{rot}	N_i
$T > T_t$	A_1	7	0	0	2	5
	A_2	7	0	0	2	5
	B_1	9	0	2	0	7
	B_2	9	1	1	0	7
	E	20	1	3	4	12

Note: N_{acous}, N_{opt}, N_{rot} and N_i refer to acoustical and optical translations, rotational osscilations and internal vibrations of $(H_2PO_4)^{-1}$ ions respectively.

Table 2-5

Correlation Table for the PO_4 ion in the Crystal Field of D_{2d} Symmetry

Isolated $(PO_4)^{-3}$	$(PO_4)^{-3}$	KH_2PO_4
Symmetry	Site symmetry	Group symmetry
T_d	S_4	D_{2d}
A_1	A	A_1
		A_2
E	B	B_1
		B_2
F_2		
F_2	E	E

Table 2-6

Correlation Table for the PO_4 ion in the Crystal Field of C_{2v} Symmetry

Isolated $(PO_4)^{-3}$	$(PO_4)^{-3}$	KH_2PO_4
Symmetry	Site symmetry	Group symmetry
T_d	C_2	C_{2v}
A_1	A	A_1
		A_2
E		
F_2	B	B_1
		B_2
F_2		

Chapter 3 Far-Infrared Spectra

The polarized reflection measurements were made on single crystals of KDP and DKDP in the far-infrared region from 20 cm^{-1} to 550 cm^{-1} at several temperatures above and below T_c.[1-3] The mode assignments were made in both phases compared with the group theoretical analysis. A strongly temperature dependent B_2 mode was observed in KDP. This mode accounts for the large part of temperature dependence of the low-frequency dielectric constant. In DKDP the corresponding band is expected to lie below 20 cm^{-1}. The results are discussed compared with the recent dynamical model of KDP. For the antiferroelectric ADP the same type measurements were made only in the paraelectric phase.[1, 2] The results are discussed comparing with those of KDP.

1. Introduction

Recent dynamical theories[4] of KDP suggest the existence of a polar vibrational mode of which characteristic frequency tends to be zero as the temperature approaches T_c from above. This polar mode must be infrared active. For the study of such a mode, it is necessary to measure the polarized spectrum as a function of temperature, to establish the correlations of the modes from one phase to the other, and to make mode assignments. Such measurements and analysis on KDP were made by the present author.[1, 2]

The same type measurements of the far-infrared spectra of DKDP and ADP were also done by the author.[1-3] The deuteration effect on the spectra is an attractive subject, because the hydrogen bond is thought to play an important role in the process of phase transition in

KDP type ferroelectrics. For the antiferroelectric ADP, its antiferroelectric phenomenon and the process of phase transition are rather unknown. The zone boundary phonon which is infrared inactive may become unstable as the Cochran's theory.[5] However, the proton tunneling mode is also probable in ADP and the low-frequency dielectric constant ε_a' along the a axis exhibits the temperature variation. The measurements of the far-infrared spectra may give the information in connection with these points.

The infrared spectrum in the high-frequency region shows the broad and very weak bands, some bands being observed as a shoulder and so it is difficult to identify the bands in the infrared spectrum. On the other hand the Raman spectrum in the high-frequency region shows rather isolated bands. So the Raman scattering technique is more suitable to study the high-frequency spectra. Therefore in the present work, main attention for the use of far-infrared technique is paid to the investigation of the low-frequency dielectric behavior. The complex dielectric constant can be derived from the reflectivity with the Kramers-Kronig analysis and the contribution of the mode to the low-frequency dielectric constant can be calculated using eq. 1-1. It is impossible to derive absolute value of the dielectric constant from the Raman spectra.

2. Experiments

2-1 Sample Preparation

The oriented single crystals of KDP and ADP were bought from Nippon Denpa Kogyo Co. The crystal dimension is 2×18×20 mm ~~for~~ along its x, y and z axis respectively. The far-infrared measurements for P_z polarization

(E∥C) and P_y polarization (E⊥C) were done on the yz surface. The final polishing was done with ethanol and 0.1μ alumina. The single crystals of DKDP were supplied by Prof. Dr. N. Furuya and Dr. O. Shimomura in Yamanashi University. The Curie temperature of the DKDP crystal used here is about 218.4 K and the degree of deuteration is about 90 %.[6] The crystal was cut parallel to the crystallographic axes with dimension about 2.5×16×20 mm. The sample was polished with saturated heavy water (D_2O). It was done every time just before every measurement to eliminate the effect of rehydrogenation.

2-2 Far-Infrared Spectrometer

The far-infrared reflection spectrum was obtained by use of two spectrometers. The one is the far-infrared grating spectrometer,[7] which has been constructed in Prof. Yoshinaga's laboratory. This was used in the region from 30 cm^{-1} to 550 cm^{-1}. In the low-frequency region from 20 cm^{-1} to 110 cm^{-1}, a Michelson type Fourier spectrometer[8] was used which has been developed also in the same laboratory. The detectors used were a Golay cell and a Ge-bolometer.[9] The Ge-bolometer was used in the low-frequency region below 200 cm^{-1} to improve the signal to noise ratio.

2-3 Measurements

In the infrared region KDP type crystals are expected to exhibit a low-frequency band which strongly depends on temperature and shows the strong absorption. The KDP type crystals are anisotropic and the modes expected to be observed are polarized parallel or perpendicular to the c axis. Therefore in the study of KDP type ferroelectrics, it is necessary to measure the infrared spectrum using polarized radiation

and reflection method, as a function of temperature.

2-3-1 Polarized Measurements

Several kinds of polarizers have been developed for the use in the far-infrared region. In this experiment the wire grid polarizer was produced and used for the measurements.

A wire grid polarizer was produced by evapolation of a metal conductor on one side of the groove of a film of diffraction grating. When the wavelength of the radiation is much larger than the spacing of the wires, radiation with the electric vector perpendicular to the wires is largely transmitted. The details are reported by Bird et al.[10] and M. Hass et al.[11]

In this study, the film of echelette grating with lattice constant d=1.6 μm was made with polyethylen sheet with 300 μm thickness which is transparent in the infrared region. Aluminium was evaporated on the film at an angle of 80°. The degree of polarization was more than 97 % and the polarized transmittance is about 60 % in the region from 20 cm^{-1} to 550 cm^{-1}. In the latter half of the experiments, the wire grid polarizer produced by Perkin Elmer Co. was also used.

In the polarized measurements using a grating spectrometer, the direction of the electric vector of polarized radiation was carefully selected, because the diffraction efficiency of the grating depends strongly on the direction of polarized radiation. The direction of polarized radiation was selected so as to give the better diffraction efficiency.

2-3-2 Reflection Measurements

The reflection measurements were made by setting an attachment[12] into the spectrometer and using a cryostat. The sample was replaced by

an aluminized mirror for a reference. The reflectivity could be obtained by comparing the signal reflected by the sample with the one by the reference mirror. The reflectivity measurements were made at an angle of incidence about 12° both for the grating spectrometer and Fourier spectrometer. The optical system for reflection measurements was carefully adjusted because the miss-alignment of reflecting angle and the position of the sample and the mirror led to a large experimental error.

The accuracy of the reflectivity measurements were ±1 % in the region from 120 cm^{-1} to 550 cm^{-1} and ±2 % in the low-frequency region below 120 cm^{-1}.

2-3-3 Low Temperature Works

i) The low temperature measurements were made using cryostat. The cryostats for the grating spectrometer and the Fourier spectrometer were specially constructed. The structure of the cryostat for the Fourier spectrometer is shown in Fig. 3-1. The other one for the grating spectrometer is the same structure except its dimension. The temperature of the sample was determined by equiribrium between the power dissipated in a heater and the cooling rate. The main tank was filled with liquid-nitrogen and the subtank was kept empty.

The sample holder temperature was stabilized by controlling the heater current using an electronic temperature controller. A chromel-alumel thermocouple with diameter of 0.3 mm was used as a temperature sensor. It was recalibrated with ice, dryice with ethanol and liquid-nitrogen temperature. The minimum temperature obtained was 84 K when the subtank was filled with liquid-nitrogen. The estimated accuracy of the temperature control is ±0.5 K, and stability about ±0.1 degree in the temperature range from 84 K to 300 K.

ii) The sample holder was made of copper for the good thermal conduction. The sample was attached to the sample holder with silver paste which gives good thermal contact. The temperature sensor was pressed on the sample holder very close to the sample.

3. Analysis of Reflection Spectrum

In this study the reflection measurements were made. The analysis of the reflectivity was made to extract available information, such as characteristic frequency, oscillator strength and so on. Usually two kinds of the analyses are used. One method is an optimum fit of the data by means of classical dispersion formula and the other is the Kramers-Kronig analysis.[13-16)]

3-1 Classical Dispersion Analysis

The classical dispersion formula given in the eq. 1-2 is rewritten here;

$$\varepsilon(\omega) = \varepsilon_\infty + \sum_j \frac{S_j \omega_j^2}{\omega_j^2 - \omega^2 + i\gamma_j \omega} \tag{3-1}$$

$$= \varepsilon' - i\varepsilon''$$

$$\varepsilon' = n^2 - \kappa^2 \tag{3-2}$$

$$\varepsilon'' = 2n\kappa, \tag{3-3}$$

where the complex refractive index is written in the form $N=n-i\kappa$. The reflectivity for the normal incidence is given as follows

$$R = \frac{(n-1)^2 + \kappa^2}{(n+1)^2 + \kappa^2}. \tag{3-4}$$

The parameters are determined by the optimum fit of the data by eqs. 3-1, 3-2, 3-3 and 3-4.

3-2 Kramers-Kronig Analysis

The analysis mentioned before is applicable only when the oscillator model is valid. When the spectrum has complex feature, it is very difficult to analyze. The analysis by Kramers-Kronig dispersion relation has no such restrictions. But the parameters S_j, γ_j and ω_j cannot be obtained by the latter method.

From the measurements of the reflectivity R, the optical parameters n and κ are determined from following relationships;[13-16)]

$$n = \frac{1 - R}{1 + R - 2\sqrt{R}\cos\theta} \tag{3-5}$$

$$\kappa = \frac{-2\sqrt{R}\sin\theta}{1 + R - 2\sqrt{R}\cos\theta} \tag{3-6}$$

for the normal incidence, where θ is the phase angle.

The complex dielectric constant $\varepsilon(\omega) = \varepsilon' - i\varepsilon''$ is given also by eqs. 3-2 and 3-3. The phase angle θ at a particular frequency ω_m is expressed by the Kramers-Kronig dispersion relation;

$$\theta(\omega_m) = \frac{2\omega_m}{\pi} \int_0^\infty \frac{\ln\sqrt{R(\omega)} - \ln\sqrt{R(\omega_m)}}{\omega^2 - \omega_m^2} d\omega. \tag{3-7}$$

Compute the phase angle θ and one can obtain n, κ, ε' and ε''. The characteristic frequency of the mode is given by the peak of $\varepsilon''\times\omega$ vs ω curve.

3-3 Practical Analysis

In the series of these experiments the far-infrared spectra were analyzed using a Kramers-Kronig dispersion relation. The integration in eq. 3-7 was performed on a high speed digital computer using a measured reflection spectrum.

It is clear from eq. 3-7 that the whole reflection spectrum from zero to infinite frequency region contributes to the value of phase $\theta(\omega_m)$. However reflection spectrum is measured in some finite region. Examination of eq. 3-7 shows that the major contribution comes from the neighbourhood of ω_m and from the region where the reflectivity is changing rapidly. In these series of experiments, the spectra were measured from 20 cm^{-1} to 550 cm^{-1}. The reflectivity above 550 cm^{-1} was taken to be constant with a value obtained from high-frequency dielectric constant ε_∞ in the visible region. This assumption is valid since the spectra above 550 cm^{-1} show relatively small reflectivity which hardly exceeds 25 % and changes gradually with frequency increase.

The reflectivity below 20 cm^{-1} was estimated as follows. The low-frequency reflectivity near 0 cm^{-1} was calculated using an equation $R = |\sqrt{\varepsilon} - 1|^2/|\sqrt{\varepsilon} + 1|^2$. The low-frequency dielectric constant used was measured at 9.2 GHz (about 0.03 cm^{-1}) by Kaminow et al.[18, 19] in the microwave measurements on KDP, ADP and DKDP. The results are listed in Table 3-1. The reflectivity from 0 to 20 cm^{-1} was extrapolated with a straight line. KDP type crystals are the piezoelectric in both phases. The static dielectric constant represents the "free" crystal response, i.e. the contribution of the piezoelectrically coupled, mechanical resonance is present. The low-frequency dielectric constant for analysis of the far-infrared data must be the "clamped" crystal response in the region above mechanical resonance. The dielectric constant at 9.2 GHz represents the clamped crystal response as shown by Baumgartner[20] and Hill et al.[21] Thus the use of the dielectric constant at 9.2 GHz for this analysis is valid.

The eqs. 3-5 and 3-6 are obtained from the Fresnel equations at

normal incidence.[14] The reflectivity measurements, however, were made at an angle of incidence about 12°. The reflectivity for the oblique incidence was calculated using Fresnel equation[14] for n=2.0 and κ=1.0. The relfectivity for normal incidence is 20 %. $R_\perp$ and $R_\parallel$ are 20.7 % and 19.3 % respectively for the oblique incidence at 12°, where $R_\parallel$ is the reflectivity for the electric vector parallel to the plane of incidence and $R_\perp$ is the one for the electric vector perpendicular to the plane of incidence. The error due to the assumption of normal incidence is within the experimental error. Therefore the assumption of normal incidence is thought to be valid.

The main factor which determines the accuracy of the computed optical constant depends on the accuracy of measured reflectivity. In these experiments the uncertainty of reflectivity was ±2 % below 120 cm^{-1}. This uncertainty resulted in the peak frequency 60±2 cm^{-1} and the peak intensity 9.9±1.4 for the band observed in ε'' spectrum of KDP for E∥C at 295 K. It was found that the uncertainty of the reflectivity did not show significant error in ε''.

The typical results of Kramers-Kronig analysis are shown in Figs. 3-2, 3-3 and 3-4. The dispersion relations are clearly shown in terms of reflectivity, phase angle and other optical constant versus frequency. The results of KDP will be shown and discussed again in the next section.

4. Results and Discussion

4-1 Results

KDP

The far-infrared reflection spectra of KDP were measured in the

region from 20 cm^{-1} to 550 cm^{-1} at 295 K, 200 K, 150 K, 130 K and 84 K for the electric vector E of radiation parallel to the c axis, and the results are shown in Fig. 3-5. The zero-frequency reflectivities are shown in the figure with open circles. It is to be noticed that the marked change occurs in the low-frequency reflectivity when the temperature is lowered, together with the reflectivity near 200 cm^{-1}. Figure 3-6 shows the reflection spectra for E⊥C at 295 K and 200 K. The spectra for E⊥C are quite different from those for E∥C and do not change so much with temperature.

The complex dielectric constant was derived from the reflection spectrum using Kramers-Kronig dispersion relation. The method of derivation was discussed in the preceeding section. The results are shown in Figs. 3-7 and 3-8.

According to the group character shown in Table 2-2, the B_2 symmetry species above T_c transforms as P_z dipole moment and the A_1 symmetry species below T_c also transforms as P_z dipole moment. Therefore the bands in the spectrum taken by E∥C measurement belong to B_2 symmetry above T_c and A_1 symmetry below T_c. Similarly the E symmetry species transforms as P_x or P_y dipole moment and so the bands observed in E⊥C spectrum belong to E symmetry.

In Fig. 3-7 the broad low-frequency band is clearly observed. This band strongly depends on temperature; the peak intensity increases and its peak frequency decreases as the temperature is lowered to T_c from above. The peak frequency is 60 cm^{-1} at 295 K and shifts to 12 cm^{-1} at 150 K. Below T_c this band disappears in the spectrum. The band near 200 cm^{-1} is also very broad and strongly depends on temperature as seen in Fig. 3-7. This band has a 295 K peak at 178 cm^{-1} and shifts

to higher frequency as temperature approaches T_c. When the temperature is lowered through T_c this band becomes intense and has a 84 K peak at 208 cm^{-1}. According to the group theoretical analysis, the external modes of [K-(H_2PO_4)] sublattice are expected to be observed in the low-frequency region; one translational vibrational mode of B_2 symmetry above T_c and one translational and one rotational vibrational mode of A_1 symmetry below T_c. In the spectrum two bands are observed above T_c while group theory predicts only one mode. The appearance of the low-frequency band which has a 295 K peak at 60 cm^{-1} is thought to relate to the ferroelectric transition mechanism and will be discussed later. The band which has a 295 K peak at 178 cm^{-1} must be a translational mode. This translational mode remains near 208 cm^{-1} below T_c. The rotational mode of A_1 symmetry is not found below T_c because it may be very weak. The rotational mode of A_1 symmetry is originally A_1 mode above T_c* and is infrared inactive. So the oscillator strength of this mode is thought to be very small.

The spectra above 300 cm^{-1} show the existence of several bands. These bands above T_c are very weak; a weak band near 380 cm^{-1} and a broad band extending from 400 cm^{-1} to 480 cm^{-1}. Below T_c new sharp bands appear and have 84 K peak at 344 cm^{-1} and 514 cm^{-1}. These bands in the region from 300 cm^{-1} to 550 cm^{-1} can be assigned to the PO_4 internal mode. The detailed mode assignment of PO_4 internal vibrational mode will be discussed in the following section.

As seen in Fig. 3-8 several bands are observed in the spectra of E

---

*Note: According to the correlation table given in Table 2-3, the B_2 and A_1 modes above T_c transform to A_1 modes below T_c. The A_1 mode is the rotational external mode and the B_2 mode is the translational one above T_c as shown in Table 2-2.

symmetry; these bands have 295 K peaks at 86 cm^{-1}, 104 cm^{-1}, 122 cm^{-1}, 152 cm^{-1}, 206 cm^{-1} and 526 cm^{-1}. The 526 cm^{-1} band is PO_4 internal vibration. Group theoretical analysis predicts five external vibrational modes. Three of them are translational vibrations of $[K-(H_2PO_4)]$ sublattice and the remainders are rotational vibrations. They are in close agreement with the five observed bands in the region below 300 cm^{-1}. In the reflection spectrum for E⊥C (E symmetry) shown in Fig. 3-6 the background continuum extending from 20 cm^{-1} to 100 cm^{-1} is observed. This background continuum is thought to relate to the proton tunneling mode. The similar phenomenon is also observed in the Raman spectrum of E symmetry and the discussion will be made in Chap. 5.

DKDP

Figure 3-9 shows the reflection spectra of DKDP for E∥C at several temperatures above and below T_c. The spectrum in the region below 100 cm^{-1} is quite different from that of KDP. In DKDP the 295 K reflectivity is about 20 % at 100 cm^{-1} and increases gradually as the frequency lowers. Reflectivity below 100 cm^{-1} decreases slightly as the temperature is lowered. The zero-frequency reflectivities are shown in the figure with open circle and two of them above T_c are fairly high compared with the reflectivity at 20 cm^{-1} as shown in the figure. The reflectivity measurements below 20 cm^{-1} were also done. Unfortunately signal to noise ratio was not good enough for quantitative analysis, but the results indicate that the reflectivity above T_c has an inclination to rise as the frequency decreases.

Figure 3-10 shows the reflection spectra of DKDP for E⊥C at 295 K and 220 K. The spectrum below 250 cm^{-1} is very similar to that of KDP

but reflectivity is relatively low. The spectrum above 300 cm^{-1} shows several broad bands.

The complex dielectric constant was derived from the reflection spectrum by the Kramers-Kronig analysis. As mentioned before the zero-frequency reflectivity is fairly high compared with that at 20 cm^{-1} for E∥C. So it is not a good approximation to extrapolate linearly from 0 cm^{-1} to 20 cm^{-1}. There is such uncertainty for the approximation though, the local nature of Kramers-Kronig dispersion relation gives rise to only small error in the dielectric constant except in the low-frequency region below several tens wavenumber. The obtained imaginary parts ε'' of complex dielectric constant are shown in Figs. 3-11 and 3-12.

As seen in Fig. 3-9, which shows the reflectivity of DKDP for E∥C, there is no band in the low-frequency region below 100 cm^{-1}, while in KDP the reflectivity rises rapidly below 100 cm^{-1}. As stated before the zero-frequency reflectivity above T_c is fairly high compared to that at 20 cm^{-1} and the reflectivity below 20 cm^{-1} has an inclination to rise. Therefore it can be concluded that the low-frequency mode must be below 20 cm^{-1} in the paraelectric phase. Microwave measurements by Hill and Ichiki[21] on KDP show that ε'' has a Debye form with a peak near 1 cm^{-1} at room temperature. Recent light scattering experiments on DKDP by Reese et al.[22] also support this fact. Below T_c the zero-frequency reflectivity is nearly equal to that at 20 cm^{-1} and the low-frequency mode must disappear after the phase transition.

Figure 3-11 shows the existence of two bands near 200 cm^{-1}. These bands form a composite broad peak above T_c, and below T_c split into two isolated peaks. They become sharp and intense below T_c and have 84 K

peaks at 166 cm^{-1} and 228 cm^{-1}. In KDP only one band corresponding to 228 cm^{-1} band of DKDP is observed at 208 cm^{-1}. These bands of KDP and DKDP can be assigned to the translational vibrational mode of [K-(PO_4)] sublattice. The band which has a 84 K peak at 166 cm^{-1} in DKDP is not found in KDP.

The spectrum in the region above 300 cm^{-1} shown in Fig. 3-11 has, on the whole, similar feature and similar temperature dependence to those of KDP, except some additional weak bands. These bands observed in the region above 300 cm^{-1} can be also assigned to the PO_4 internal modes and will be discussed in the next section.

As seen in Fig. 3-12 the bands of E symmetry are observed at 96 cm^{-1}, 108 cm^{-1}, 122 cm^{-1}, 170 cm^{-1} and 206 cm^{-1} at 295 K in the low-frequency region. These bands have almost the same frequency and the same line shape as those of KDP. These bands can also be assigned to the external mode of [K-(PO_4)] sublattice. The spectrum in the region above 300 cm^{-1} is more complex than that of KDP and shows the existence of some additional bands.

The effect of deuteration on KDP is clearly seen in the spectra.

i) In the low-frequency region below 300 cm^{-1}: The broad low-frequency B_2 mode is found around 50 cm^{-1} in KDP above T_c, while in DKDP no band is observed in the region from 20 cm^{-1} to 100 cm^{-1}. The corresponding band must lie below 20 cm^{-1}. In DKDP two bands are observed near 200 cm^{-1} both above and below T_c. They have 84 K peaks at 166 cm^{-1} and 228 cm^{-1}. Whereas in KDP only one band corresponding to 228 cm^{-1} band of DKDP is observed and it has 84 K peak at 208 cm^{-1}. But the band corresponding to 166 cm^{-1} band of DKDP is absent in KDP. It is worth noticing that there are some differences between the spectrum of B_2

symmetry for DKDP and that for KDP, while there are no such difference between the spectrum of E symmetry for DKDP and that for KDP.

ii) In the region from 300 cm^{-1} to 550 cm^{-1}: The additional bands are observed in both spectra of B_2 and E symmetries for deuterated substance. These additional bands can be also assigned to the PO_4 internal mode. The effect of deuteration will be discussed later.

ADP

Figures 3-13 and 3-14 show the reflection spectra of ADP for E∥C and E⊥C respectively. Measurements were done at 295 K, 200 K and 152K, i.e. only in the paraelectric phase, because the single crystal of ADP shatters at the transition temperature T_t (T_t=148 K). The overall feature of the spectrum for E∥C is alike with that of KDP. But the reflectivity below 100 cm^{-1} is relatively low compared with that of KDP and no remarkable change occurs on approaching T_t from above. On the other hand the spectrum for E⊥C is quite different from that of KDP, as seen in Fig. 3-14. The reflectivity shows a minimum near 130 cm^{-1} and increases rapidly as the frequency lowers and reaches finally almost 60 %. The shoulders are observed near 80 cm^{-1} and 150 cm^{-1}. Whereas in KDP three sharp bands are observed around 100 cm^{-1}.

In Figs. 3-15 and 3-16 the imaginary parts of complex dielectric constants are shown. As seen in Fig. 3-15, the low-frequency band is observed in the spectrum of B_2 symmetry. This band is broad but weak compared with that of KDP. This band has a 295 K peak at 76 cm^{-1} and slightly shifts to the lower frequency as the temperature lowers. The second band near 200 cm^{-1} shows very similar line shape and similar temperature dependecne to those of the band observed near 200 cm^{-1} in

the B_2 spectrum for KDP. This band has a 295 K peak at 198 cm^{-1}. In KDP the corresponding band has a 295 K peak at 178 cm^{-1}. The difference in the frequency is reasonably attributed to the harmonic shift due to the substitution of K ion by NH_4 ion.

Figure 3-16 shows the existence of the broad low-frequency band which has 295 K peak at 50 cm^{-1}. The corresponding band is found neither in KDP nor in DKDP. This band decreases in its frequency as the temperature approaches to T_t from above and has 152 K peak at 34 cm^{-1}. While, the ferroelectric mode of KDP has a peak below 10 cm^{-1} at 130 K and disappears below T_c. This fact indicate that the characteristic frequency of this mode becomes zero at the transition point in KDP. However, in ADP it seems that the characteristic frequency does not become zero at the transition point. The other bands below 300 cm^{-1} in the spectrum of E symmetry are found at 80 cm^{-1}, 155 cm^{-1} and 164 cm^{-1}, of which 80 cm^{-1} and 155 cm^{-1} bands are observed as shoulders. The corresponding bands of KDP are at 86 cm^{-1}, 104 cm^{-1}, 122 cm^{-1}, 152 cm^{-1} and 206 cm^{-1}. The spectral line shape of ADP is quite different from that of KDP.

The spectra of B_2 and E symmetries in the region from 300 cm^{-1} to 550 cm^{-1} are very similar to that of KDP. This is in contrast with the case of DKDP in which the additional bands are observed.

The results of the far-infrared measurements on KDP, DKDP and ADP have been shown above. The results are listed in Tables 3-2, 3-3 and 3-4 together with the mode symmetries and possible mode assignments. The anomalous temperature dependence of the spectra and the change in the spectra at the phase transition are observed. And the difference

among the spectra of KDP, DKDP and ADP have become clear. Further discussion will be made in the following section.

4-2 Internal Mode of Phosphate Group

The far-infrared spectra of KDP, DKDP and ADP show the existence of several bands in the region from 300 cm^{-1} to 550 cm^{-1}. These bands must be due to the PO_4 internal vibrations. The selection rules for PO_4 ion have been discussed by Murphy et al.[23] They interpreted that PO_4 ion behaves approximately as the isolated ion in the crystal and have T_d symmetry and occupy S_4 site.

In the far-infrared spectra from 300 cm^{-1} to 550 cm^{-1}, the bands observed are very weak and some are observed as the shoulders of strong bands. Therefore it is difficult to identify the bands in detail. Further discussion will be done in Chap. 5 where the well defined bands are observed in the Raman scattering spectra. Here the author will state the possible interpretation of the infrared active mode on the basis of the Murphy's interpretation; the PO_4 ion does approximately behave as an isolated molecule in the crystal.* This interpretation leads us that the frequency of the internal vibration is not largely changed even in the crystal. In the far-infrared spectrum of B_2 symmetry for KDP a weak band is observed near 390 cm^{-1} and a broad one extending from 400 cm^{-1} to 480 cm^{-1}. The 390 cm^{-1} band is very weak and is assigned to the $\nu_2(E)$ vibrations of PO_4 ion. The absorption due to the $\nu_2(E)$ vibrations of free PO_4 ion is 363 cm^{-1}.[24] In the Raman spectrum of B_2 symmetry for KDP the corresponding band is observed at 394 cm^{-1} as an intense band. The $\nu_2(E)$ vibration of free PO_4 ion is Raman active

*Note: This interpretation is also confirmed in the present work as discussed in Chap. 5.

but infrared inactive. In the crystal lattice it seems that the PO_4 ion is slightly deformed by the crystalline field and $\nu_2(E)$ vibration becomes infrared active. As this vibrational mode has originally no dipole moment, its oscillator strength is thought to be very small even in the crystal.

In the spectrum of B_2 symmetry the broad band extending from 400 cm^{-1} to 480 cm^{-1} are also observed. This band is also observed in DKDP. Y. Imry et al.[25] measured the infrared absorption spectra of powdered KDP and DKDP. They observed a broad band around 400 cm^{-1} in KDP and interpreted it to be due to the absorption of low-energy protonic level. If this is the case the deuteration causes the reduction of the frequency. But the present results show that the broad bands exist near 400 cm^{-1} to 480 cm^{-1} both in KDP and DKDP. Therefore the band near 400 cm^{-1} is not due to the protonic level but is thought to be the $\nu_4(E)$ vibration of PO_4 ion. Below T_c new bands appear at 344 cm^{-1} and 514 cm^{-1} in the spectrum of A_1 symmetry for KDP. These bands are assigned to $\nu_2(E)$ and $\nu_4(F_2)$ of PO_4 ions. The appearance of these bands below T_c can be explained by the change of the mode symmetry. According to the correlation table (Table 2-3) A_1 and B_2 mode for $T>T_c$ transform to A_1 mode for $T<T_c$. The 344 cm^{-1} and 514 cm^{-1} bands are A_1 modes above T_c, and below T_c they transform into A_1 modes and become infrared active.

The spectra of these crystal in the region above 300 cm^{-1} are very similar to each other except some additional bands appearing in DKDP. This fact indicates that the PO_4 ion behaves as an individual molecule in these crystal. The bands observed are well assigned to the PO_4 internal mode and are listed in Tables 3-2, 3-3 and 3-4.

4-3 Phase Transition: Ferroelectric Mode

In KDP the broad low-frequency band is observed in the spectrum of B_2 symmetry. The peak frequency decreases and, at the same time, the peak intensity increases when the temperature is lowered to T_c from above. The peak frequency and the half-width are shown in Table 3-5. The contribution of this band to the low-frequency dielectric constant was examined by eq. 1-1. The results are as follows; $\Delta\varepsilon \simeq 12$ where $\varepsilon_c'(0) \simeq 21$ at 295 K, $\Delta\varepsilon \simeq 32$ where $\varepsilon_c'(0) \simeq 40$ at 200 K, and $\Delta\varepsilon \simeq 80$ where $\varepsilon_c'(0) \simeq 96$ at 150 K respectively. It is found that this band accounts for the large part of low-frequency dielectric constant $\varepsilon_c'(0)$ which has anomalous temperature dependence such as Curie-Weiss law.[18] The temperature dependence and the contribution to $\varepsilon_c'(0)$ of this band indicate that this band is a ferroelectric mode. The similar results were obtained by Kaminow[26] in his Raman scattering measurements and by Sugawara et al.[27] in the far-infrared measurements.

The half-width of this mode is very large and this fact indicates that the ferroelectric mode is highly overdamped. In the case of overdamped mode neither the peak frequency of ε'' nor that of conductivity $\sigma=\varepsilon''\cdot\omega/2$ give the characteristic frequency of the mode.[28, 29] Kaminow et al.[26] have analyzed their Raman data with a simple-damped-harmonic oscillator function and obtained the characteristic frequency and other parameters. But the reflection spectrum obtained here suggests that it is necessary to analyze it including higher frequency band near 200 cm^{-1}. The classical oscillator fit to the reflectivity was tried. The eq. 3-1, which includes two oscillators in this case, was used. But it was found impossible because no choice of parameters gave the dip observed near 120 cm^{-1}. The study of similar non-classical oscillator model has been

made on $KTaO_3$.[30] It is thought that the mode coupling in terms of anharmonic interaction must be taken into consideration. This theory has been stated in classical form by Barker et al. and found to give a reasonable description of $BaTiO_3$ and $SrTiO_3$.[31]

Figure 3-17 shows the imaginary part ε'' of complex dielectric constant in the low-frequency region. As seen in the figure the high-frequency tail drops more steeply than ω^{-3}. In the case of oscillator function, the high-frequency tail drops as ω^{-3} and in the case of Debye type relaxation, it drops as ω^{-1}. Thus results obtained here are far from the characteristics of Debye type relaxation and are rather resonance type. This result is in good agreement with that of Kaminow et al.[26]

In DKDP the spectrum of B_2 symmetry shows no bands in the region from 20 cm^{-1} to 100 cm^{-1}. The low-frequency band must lie in the region below 20 cm^{-1} in the paraelectric phase as mentioned before. This is the region beyond the present measurement. In KDP the contribution of the bands above 140 cm^{-1} to the low-frequency dielectric constant is as follows; $(\varepsilon'(0)-\Delta\varepsilon) \simeq 9$ at 295 K, $\simeq 12$ at 200 K and $\simeq 16$ at 150 K respectively. In DKDP the contribution of the band above 140 cm^{-1} is thought to be almost the same with that of KDP, and the low-frequency dielectric constant of DKDP shows also Curie-Weiss law behavior and very large near T_c in the paraelectric phase. Therefore the large contribution must arise from the low-frequency band below 20 cm^{-1}.

The ferroelectric mode is observed in KDP which belongs to B_2 symmetry and is polarized parallel to the c axis. This mode is rather resonance type. In DKDP the corresponding mode must lie below 20 cm^{-1}. Thus the deuteration causes a large reduction of the mode frequency.

Such a result is consistent with the collective tunneling mode[32] or the coupled proton-phonon mode model.[33, 34] It is to be noticed that group theory predicts only one optically active lattice mode of B_2 symmetry, while two bands are observed experimentally in the region from 20 cm^{-1} to 300 cm^{-1} above T_c; the ferroelectric mode and the 178 cm^{-1} band in KDP. In DKDP two bands are observed in the same region. The striking difference can be seen between the spectrum of B_2 symmetry for KDP and that for DKDP, whereas the spectrum of E symmetry for DKDP is very similar to that of KDP. Therefore the author concludes that not only the hydrogen motion but also the lattice vibrational mode of B_2 symmetry plays a significant role in the process of ferroelectric phase transition. Further discussion will be done in Chap. 6.

4-4 Antiferroelectric ADP

In ADP the overdamped low-frequency bands are observed in both spectra for B_2 and E symmetries. The B_2 band is weak compared with that of KDP. The band observed in E symmetry spectra has a 295 K peak at 50 cm^{-1} and a 152 K peak at 34 cm^{-1}. The band grows in intensity as the temperature approaches T_t. The contribution of this band to the low-frequency dielectric constant is very large. The present result is consistent with the measurement of low-frequency dielectric constant along the a axis ε_a' which is larger than that along the c axis ε_c' and is more temperature dependent.[19]

ADP is antiferroelectric below T_t unlike the other crystals. Cochran[5] and others[33] have discussed that in ADP the only mode at the corner of Brillouin zone becomes unstable which is infrared inactive. Such an antiferroelectric transition is discussed in $SrTiO_3$.[35]

The unstable zone boundary mode has been reported by Meister et al.[36] in their neutron scattering experiments on $ND_4D_2PO_4$. So it is probable that the zone boundary phonon becomes unstable and the transition occurs before the observed low-frequency E mode becomes unstable. The origin of the low-frequency E mode is unknown. It is noted that the lattice modes of E symmetry are at 80 cm^{-1}, 155 cm^{-1} and 164 cm^{-1}. The peak frequency and the line shapes of these bands are quite different from those of KDP. Further discussion will be made in Chap. 6.

5. Summary

The polarized far-infrared reflection spectra of KDP and DKDP were measured at several temperatures above and below T_c. The frequencies and the symmetries of the observed bands were determined in both phases. The number of the bands in the spectrum of E symmetry below 300 cm^{-1} were in good agreement with the group theoretical prediction. While two B_2 modes were observed in the region below 300 cm^{-1}, the group theoretical prediction allows only one band. The bands above 300 cm^{-1} observed in the spectra of these crystals were well assigned to the internal modes of PO_4 ion. The ferroelectric mode was found in the spectrum of B_2 symmetry for KDP in the paraelectric phase. In DKDP the corresponding band must lie below 20 cm^{-1}. The large deuteration effect on the ferroelectric mode is consistent with the recent dynamical model of KDP proposed theoretically.[32-34] For ADP the spectra were measured only in the paraelectric phase. The frequencies and the symmetries of the observed bands were also determined. In ADP the broad low-frequency band was observed in the spectrum of E symmetry. The contribution of this band to the low-frequency dielectric constant is

very large and strongly temperature dependent. This phenomenon is consistent with the results of measurements of low-frequency dielectric constant.[19)]

Reference

1) T. Kawamura, A. Mitsuishi and H. Yoshinaga, Japan J. Appl. Phys. 7 (1968) 1303, and J. Phys. Soc. Japan 28 (1970) 227.

2) T. Kawamura and A. Mitsuishi, Technology Reports of Osaka Univ. 23 (1973) 365.

3) T. Kawamura and A. Mitsuishi, to be submitted to Optic Commun.

4) M. Tokunaga, Ferroelectrics 1 (1970) 195.

5) W. Cochran, Advan. Phys. 10 (1961) 401.

6) O. Shimomura and N. Furuya, Private communication.

7) H. Yoshinaga, S. Fujita, S. Minami, A. Mitsuishi, R. A. Oetjen and Y. Yamada, J. Opt. Soc. Amer. 48 (1958) 315.

8) K. Sakai, Appl. Opt. 11 (1972) 2894.

9) Y. Nakagawa and H. Yoshinaga, Japan J. Appl. Phys. 9 (1970) 125.

10) G. R. Bird and M. Parrish, J. Opt. Soc. Amer. 50 (1960) 886.

11) M. Hass and M. O'Hara, Appl. Opt. 4 (1965) 1027.

12) A. Mitsuishi, J. Phys. Soc. Japan 16 (1961) 533.

13) T. S. Robinson, Proc. Phys. Soc. (London) B 65 (1952) 910.

14) D. M. Roessler, Brit. J. Appl. Phys. 16 (1965) 1119.

15) G. R. Wilkinson, Laboratory Methods in Infrared Spectroscopy, ed. R. G. J. Miller (Heyden, London, 1965) p. 150.

16) R. M. Roessler, Brit. J. Appl. Phys. 16 (1965) 1359.

17) G. M. Murphy and G. Weiner, J. Chem. Phys. 22 (1954) 1322.

18) I. P. Kaminow and G. O. Harding, Phys. Rev. 129 (1963) 1522.

19) I. P. Kaminow and G. O. Harding, Phys. Rev. 138 A (1965) 1539.

20) H. Baumgartner, Helv. Phys. Acta 24 (1951) 326.

21) R. M. Hill and S. K. Ichiki, Phys. Rev. 130 (1963) 150.

22) R. L. Reese, I. J. Fritz and H. Z. Cummins, Solid State Commun. 9 (1971) 327.

23) G. M. Murphy, G. Meier and J. J. Oberly, J. Chem. Phys. 22 (1954) 1322.

24) G. Hertzberg, Infrared and Raman Spectra of Polyatomic Molecules (van Nostrand, New York, 1954).

25) Y. Imry, I. Pelah and E. Wiener, J. Chem. Phys. 43 (1965) 2332.

26) I. P. Kaminow and T. C. Damen, Phys. Rev. Letters 20 (1968) 1105.

27) F. Sugawara and T. Nakamura, J. Phys. Soc. Japan 28 (1969) 158.

28) A. S. Barker, Jr., Far-Infrared Properties of Solids, ed. S. S. Mitra and S. Nudelman (Plenum, New York, 1970) p. 247.

29) T. Nakamura, J. Phys. Soc. Japan 21 (1966) 491.

30) R. C. Miller and W. G. Spitzer, Phys. Rev. 129 (1963) 94.

31) A. S. Barker, Jr. and J. J. Hopfield, Phys. Rev. 135 (1964) A 1732.

32) M. Tokunaga, Prog. Theor. Phys. (Japan) 36 (1966) 875.

33) K. K. Kobayashi, J. Phys. Soc. Japan 24 (1968) 497.

34) R. Blinc and B. Zeks, Advan. Phys. 21 (1972) 693.

35) J. M. Worlock, J. F. Scott and P. A. Fleury, Light Scattering Spectra of Solids, ed. G. B. Wright (Springer, New York, 1969) p. 689.

36) H. Meister, J. Skalyo, Jr., B. C. Frazer, and G. Shirane, Phys. Rev. 184 (1969) 550.

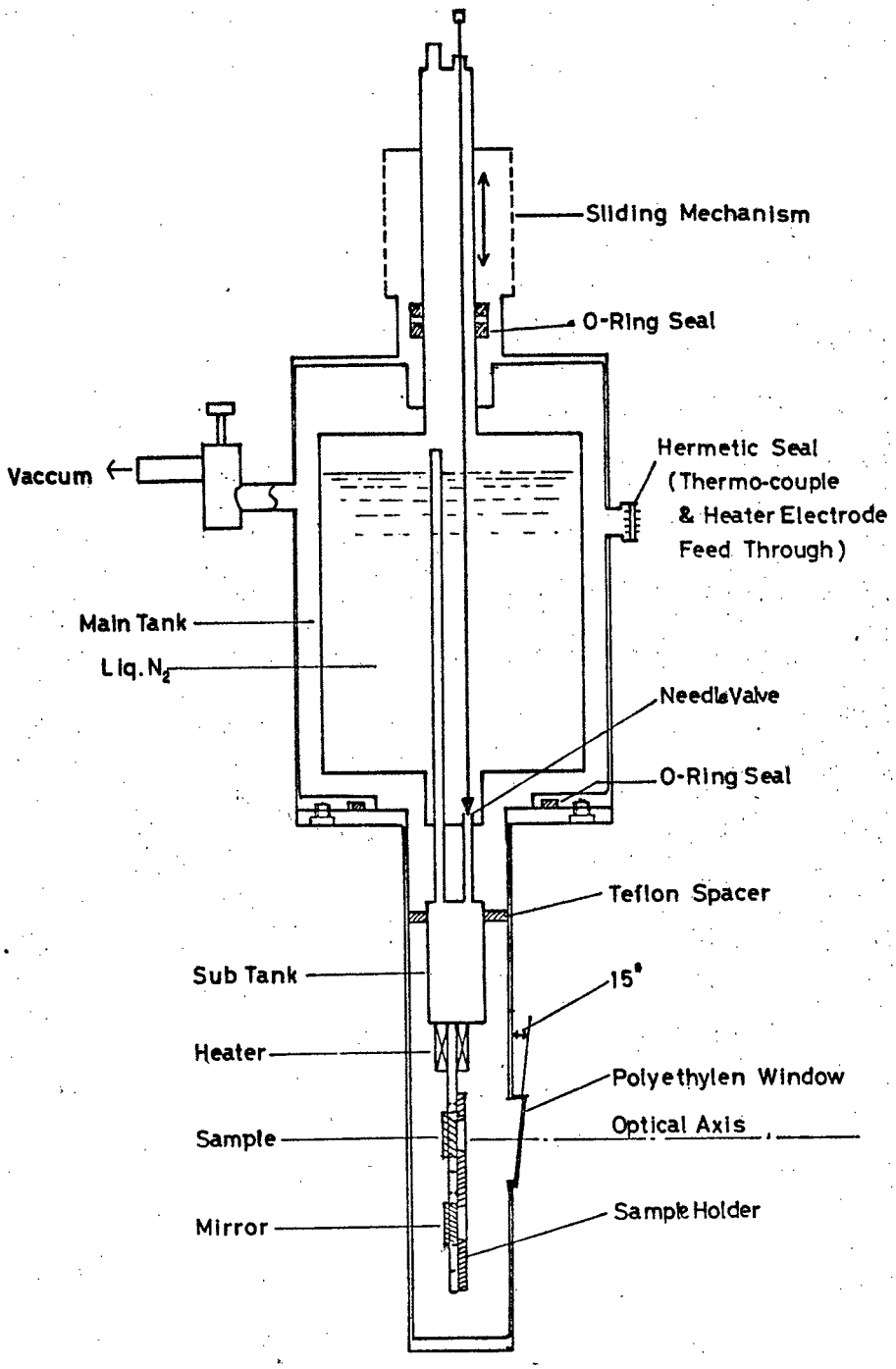

Fig. 3-1 Cryostat for reflection measurements.

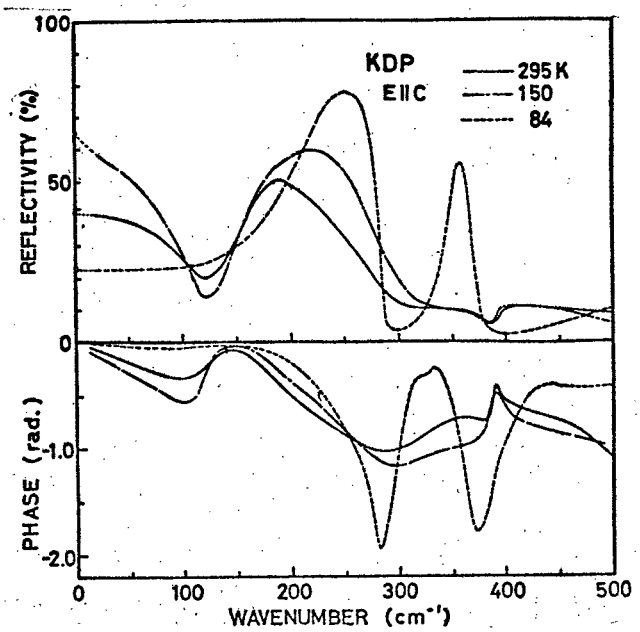

Fig. 3-2 Reflectivity and phase of KDP.

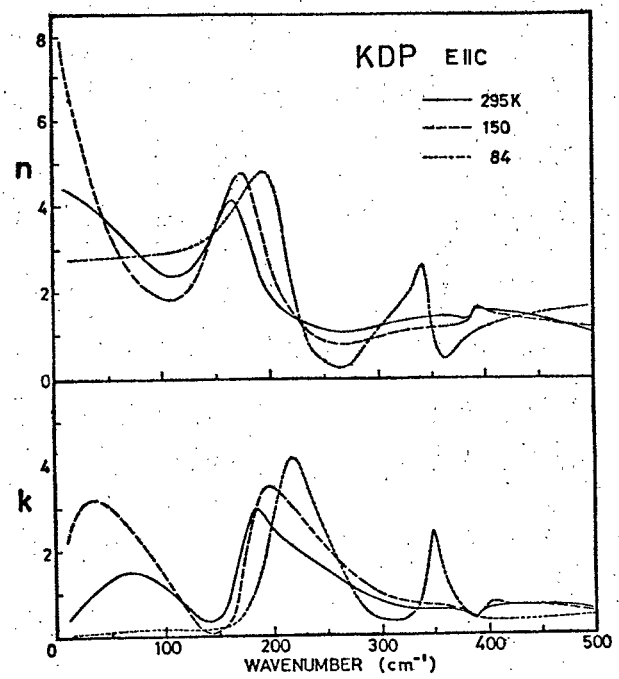

Fig. 3-3 Real and imaginary parts of complex refraction coefficient ($N=n-ik$).

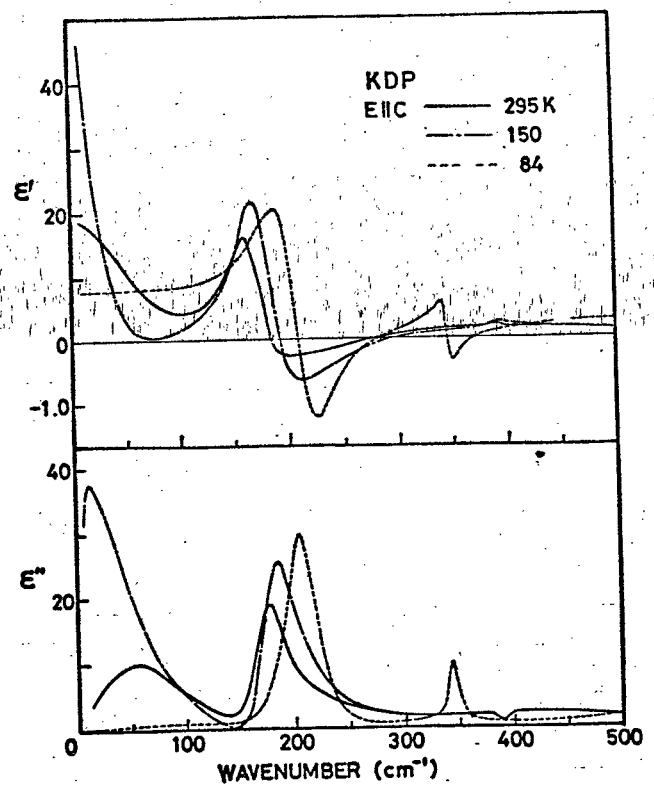

Fig. 3-4 Real and imaginary parts of complex dielectric constant ($\varepsilon=\varepsilon'-i\varepsilon''$).

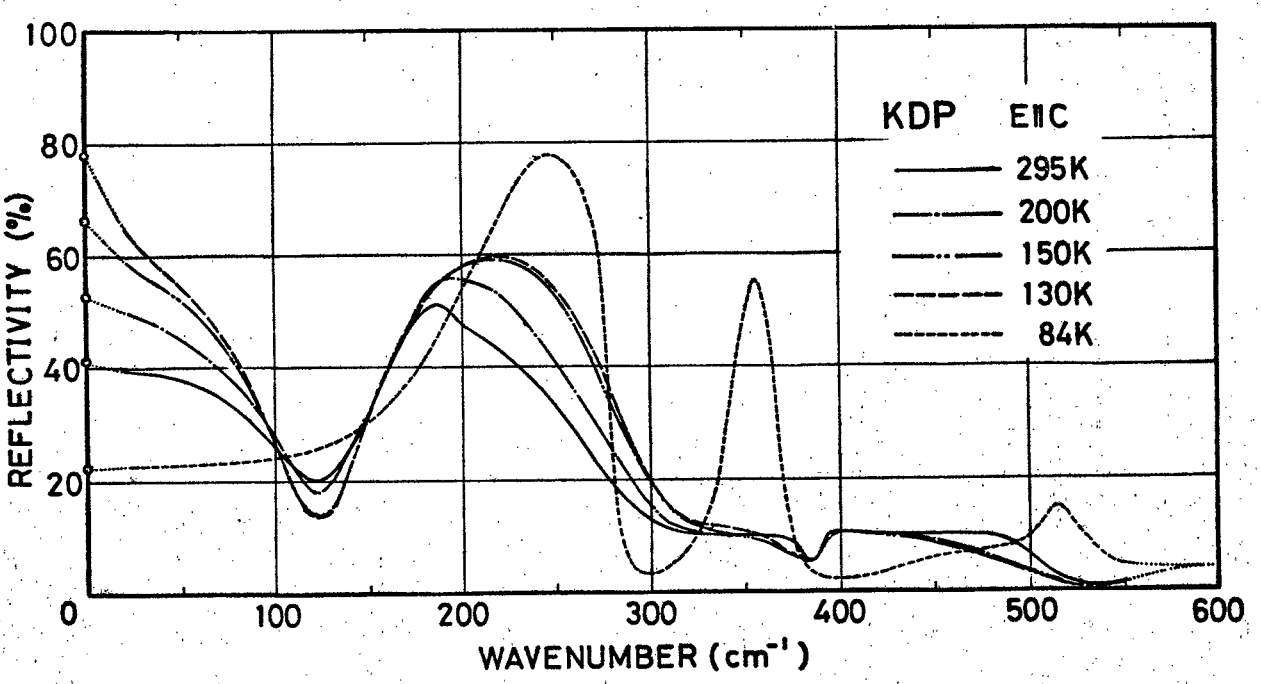

Fig. 3-5 Reflectivity of KDP taken by E∥C measurement at several temperatures. Zero frequency reflectivities are shown with open circles.

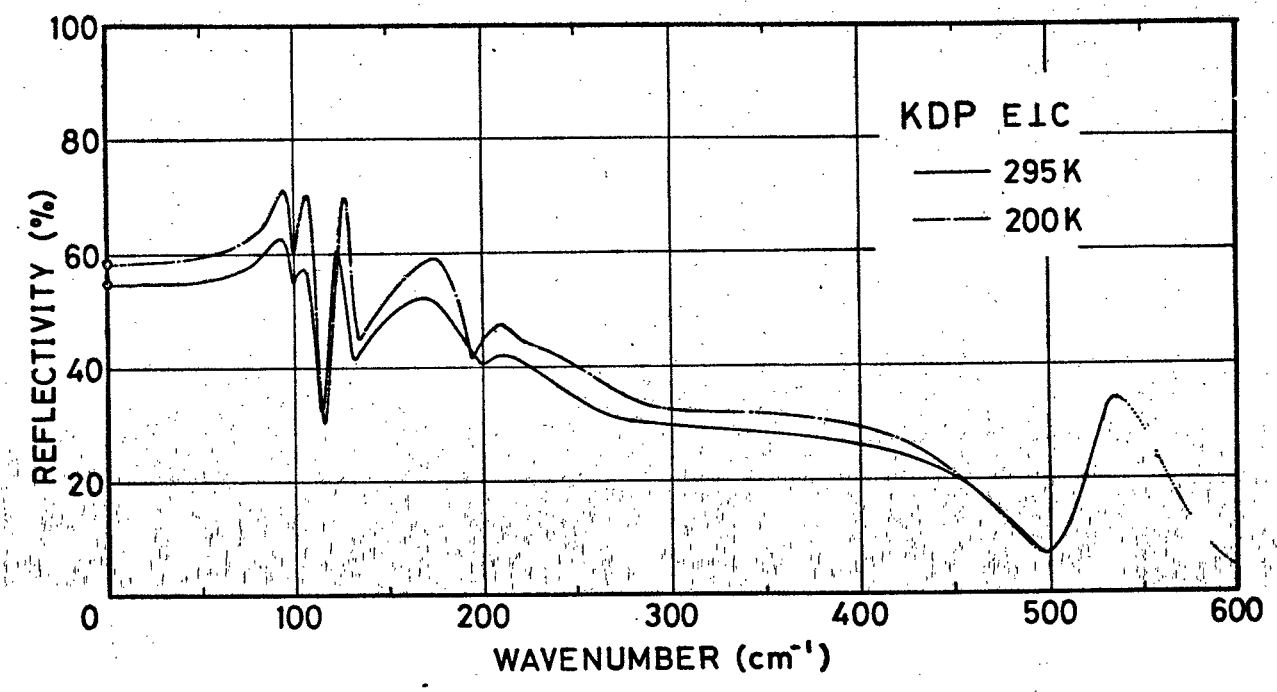

Fig. 3-6 Reflectivity of KDP taken by E⊥C measurement. Zero-frequency reflectivities are shown with open circles.

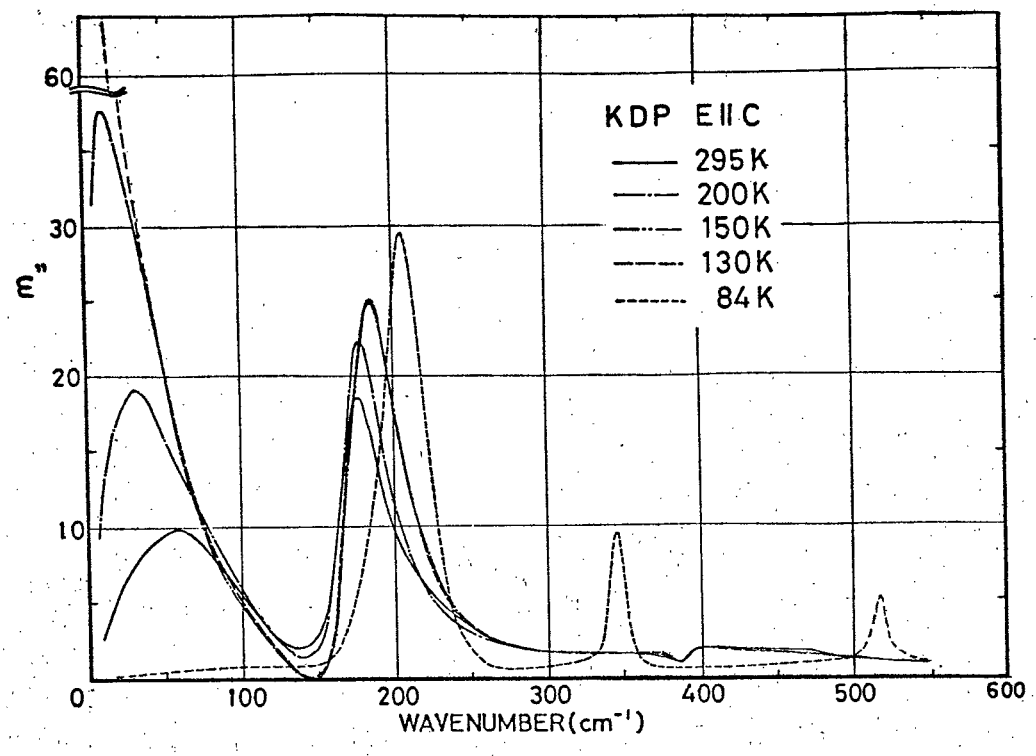

Fig. 3-7 Imaginary part of complex dielectric constant for KDP in the direction E∥C.

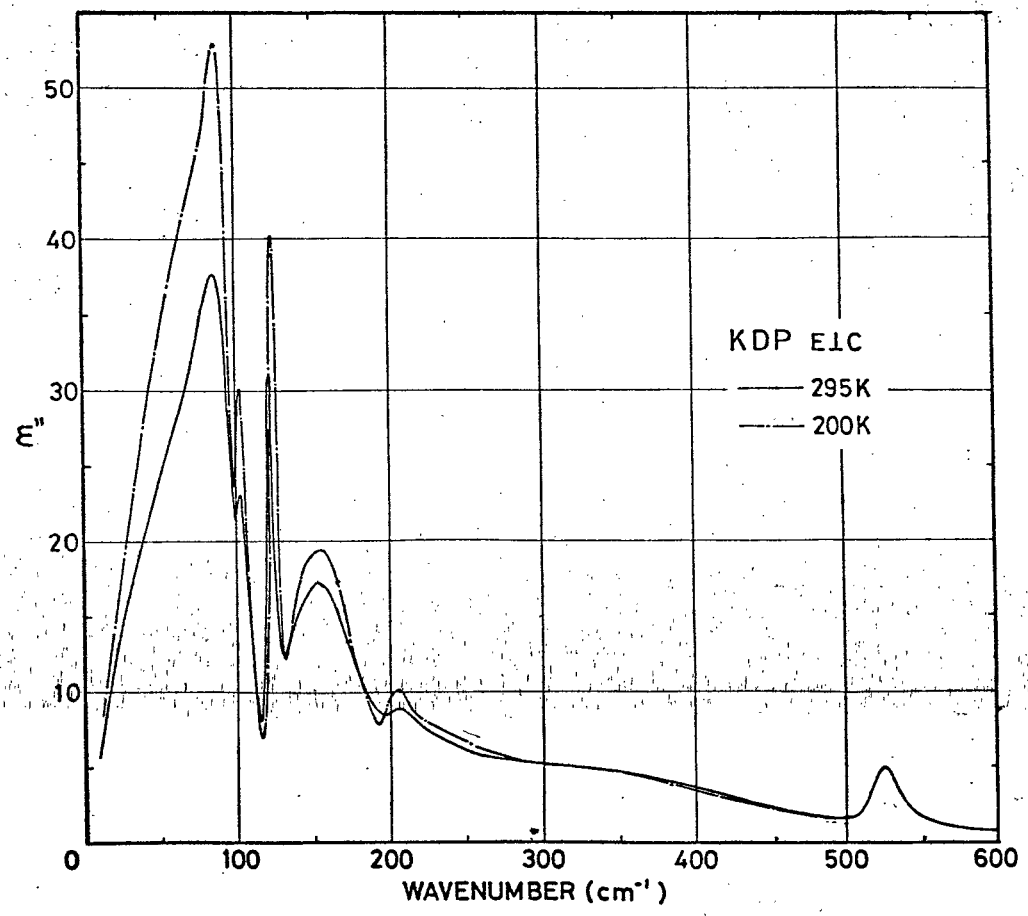

Fig. 3-8 Imaginary part of complex dielectric constant for KDP in the direction E⊥C.

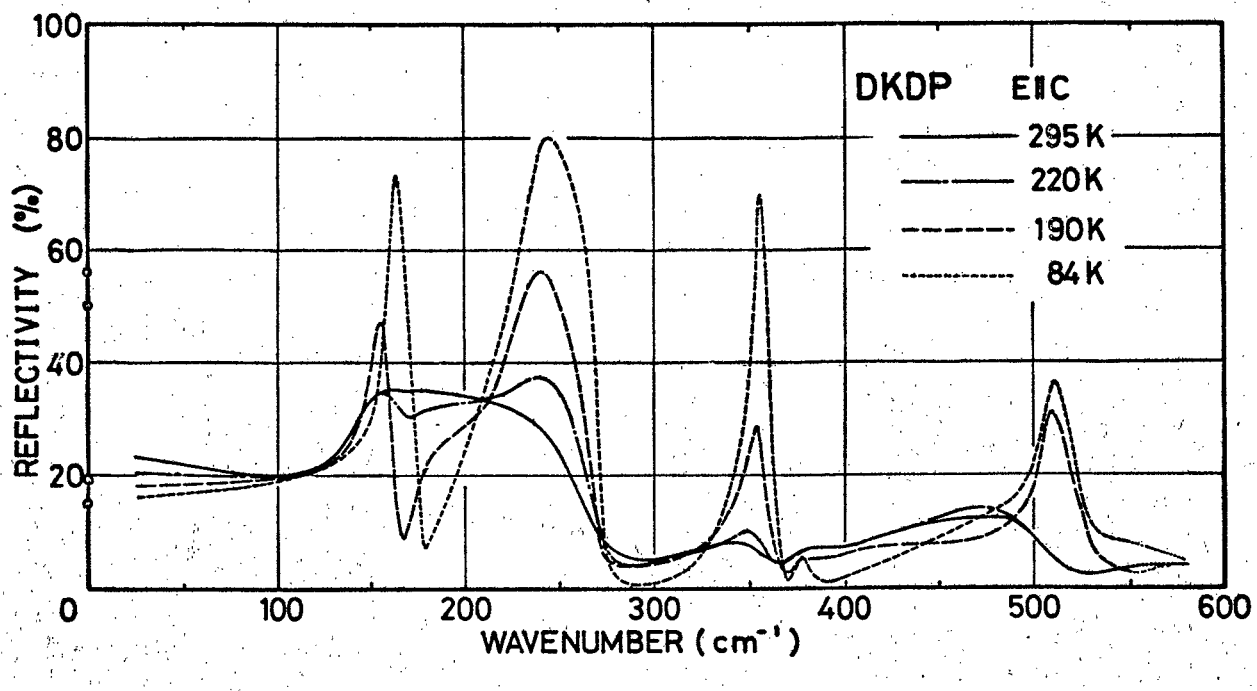

Fig. 3-9 Reflectivity of DKDP taken by E∥C measurement at several temperatures. Zero-frequency reflectivities are shown with open circles.

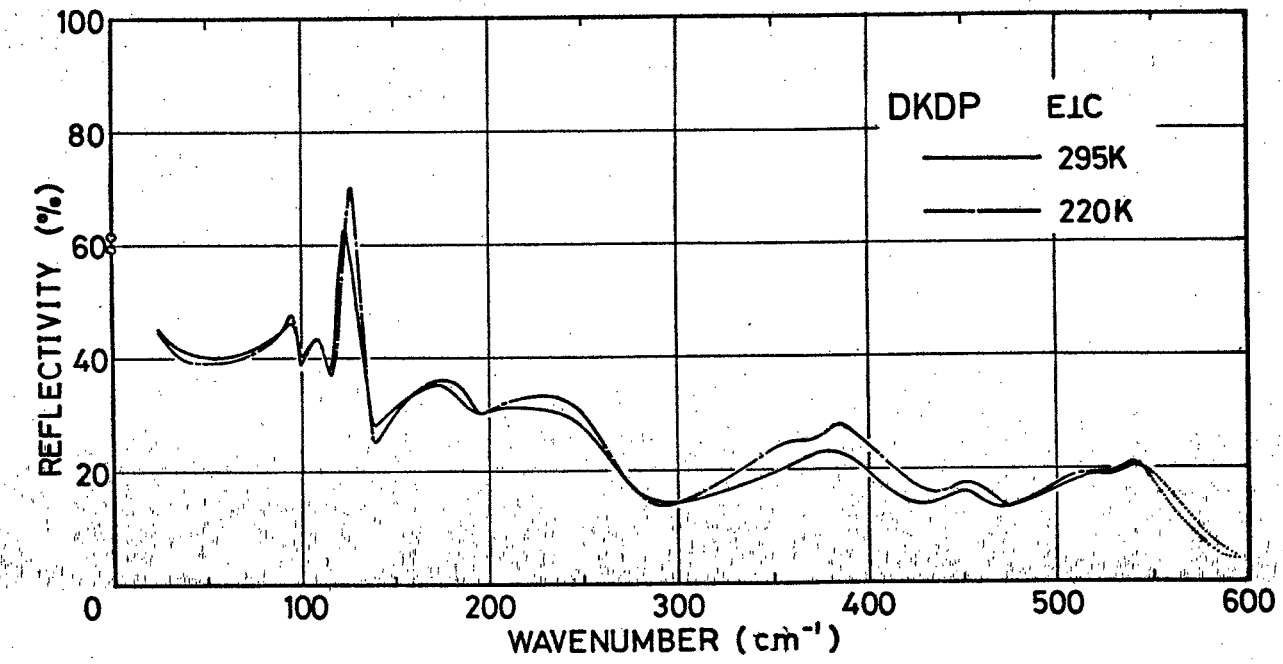

Fig. 3-10 Reflectivity of DKDP taken by E⊥C measurement. Zero-frequency reflectivities are shown with open circles.

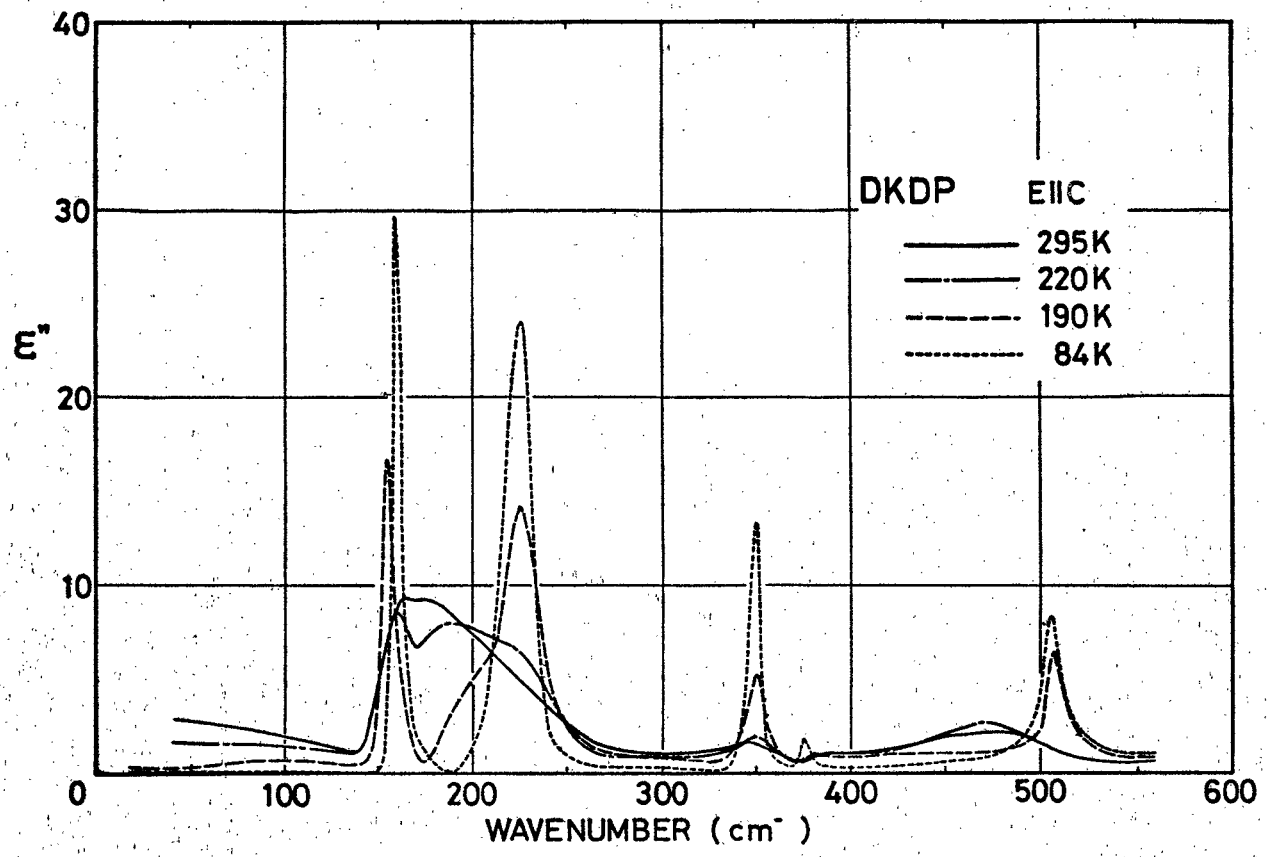

Fig. 3-11 Imaginary part of complex dielectric constant for DKDP in the direction E∥C.

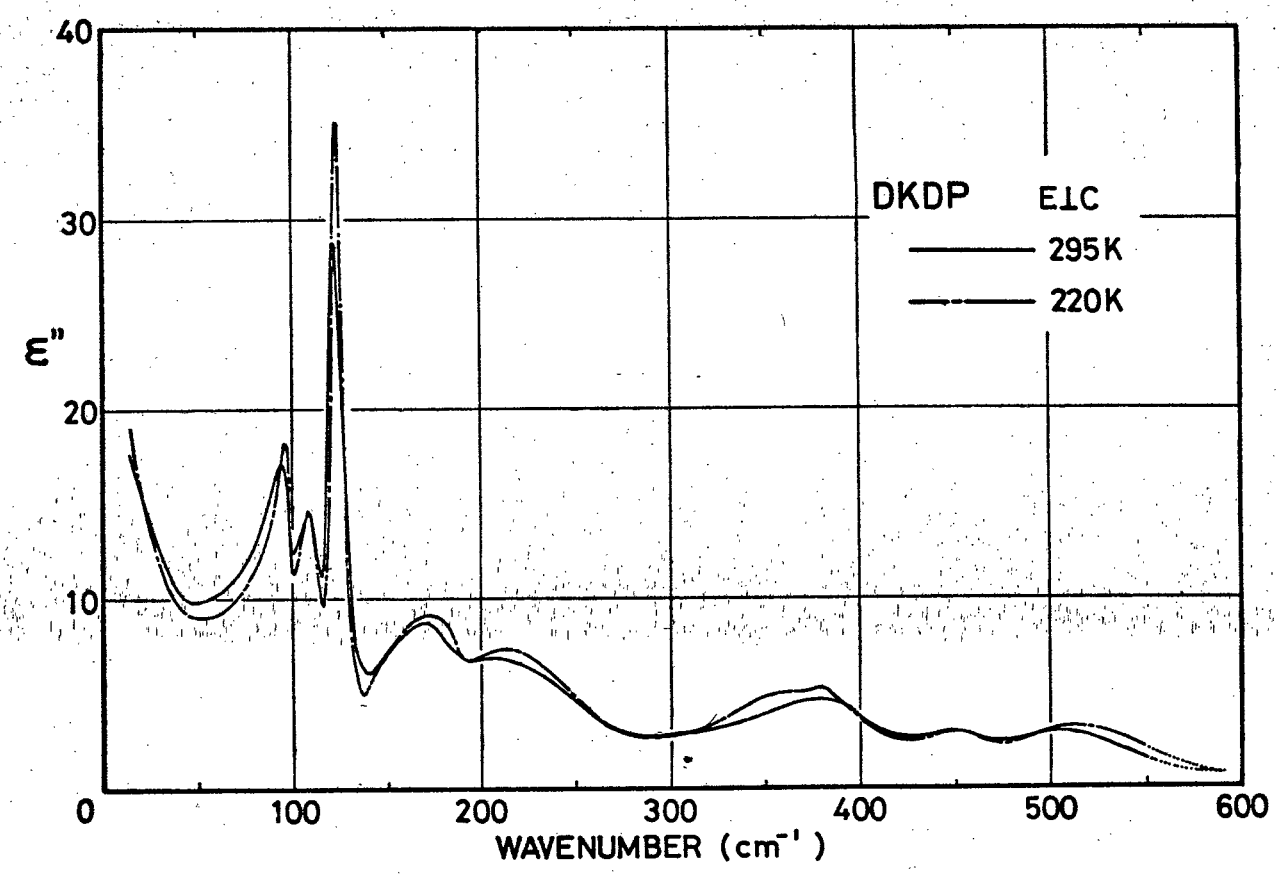

Fig. 3-12 Imaginary part of complex dielectric constant for DKDP in the direction E⊥C.

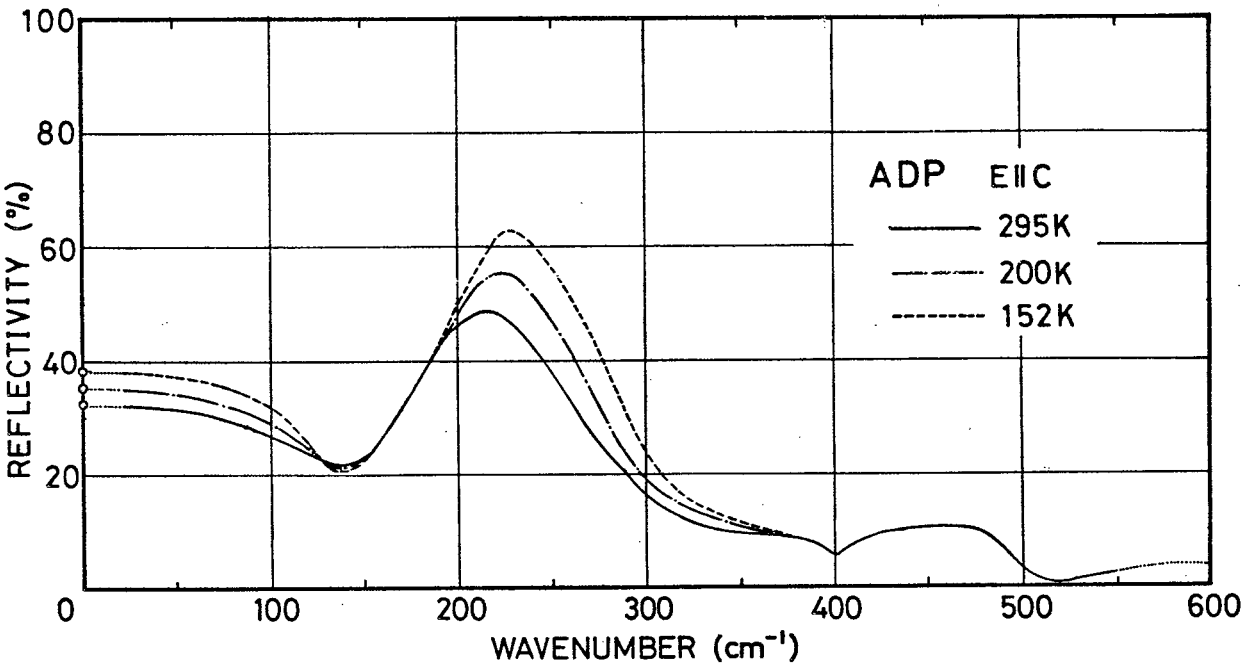

Fig. 3-13 Reflectivity of ADP taken by E∥C measurement at several temperatures. Zero-frequency reflectivities are shown with open circles.

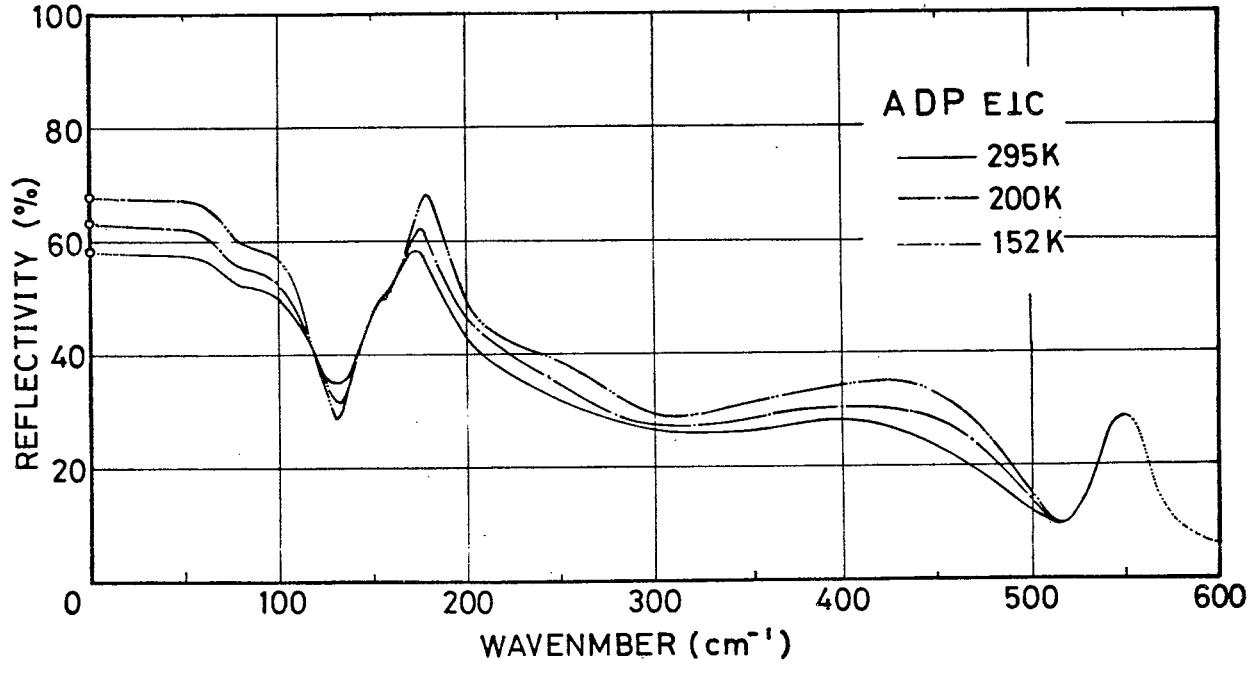

Fig. 3-14 Reflectivity of ADP taken by E⊥C measurement. Zero-frequency reflectivities are shown with open circles.

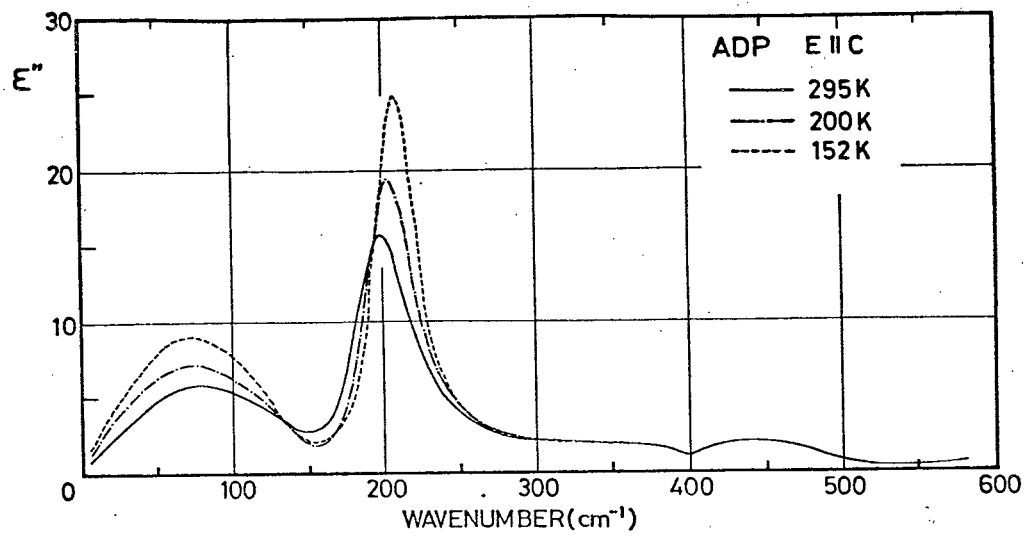

Fig. 3-15 Imaginary part of complex dielectric constant for ADP in the directon E∥C.

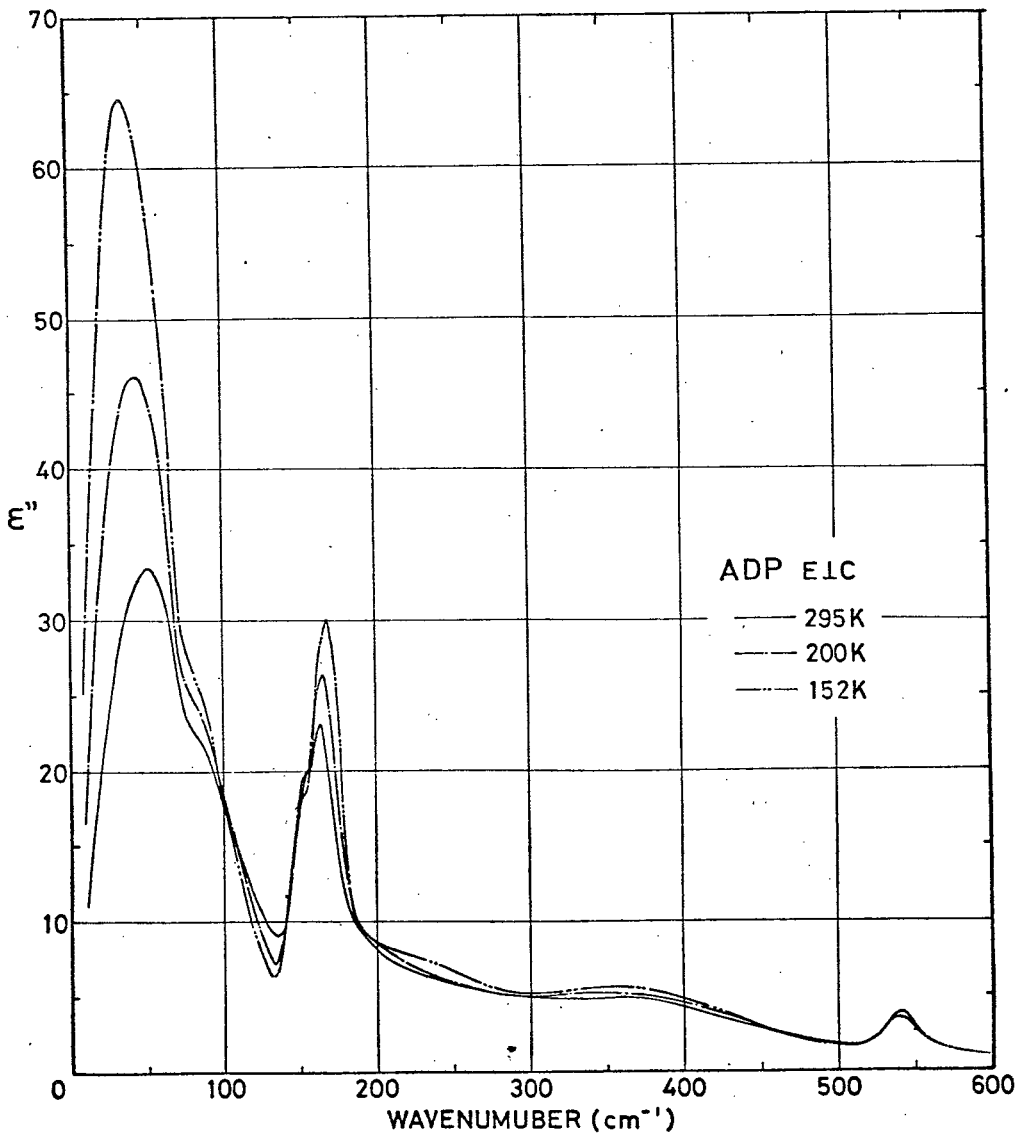

Fig. 3-16 Imaginary part of complex dielectric constant for ADP in the direction E⊥C.

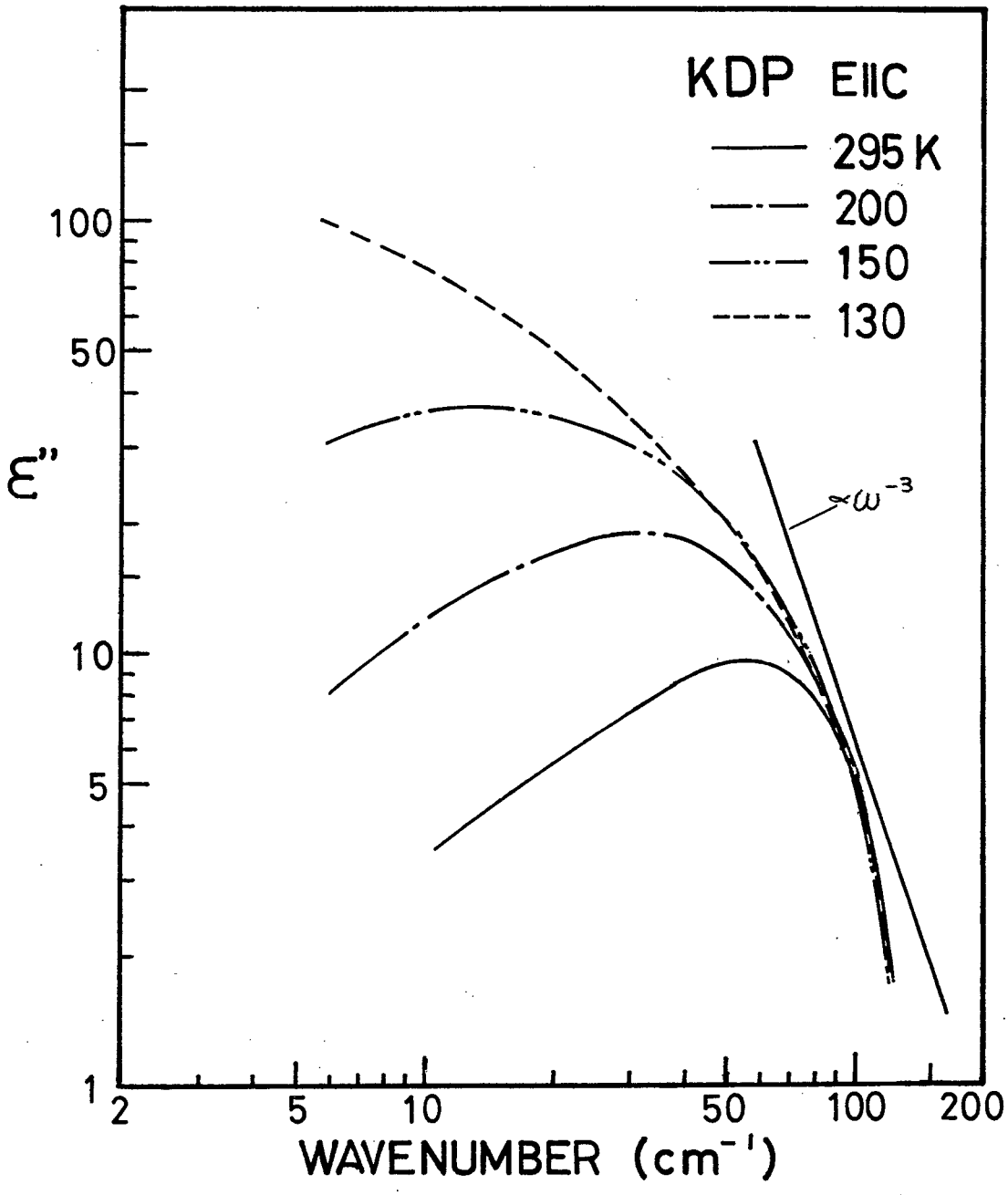

Fig. 3-17 Imaginary part of complex dielectric constant for KDP in the low-frequency region.

Table 3-1

Zero frequency reflectivity R

a) KDP

Temp.	ε_c'	R(E∥C)	ε_a'	R(E⊥C)
295 K	21	41 %	44	55 %
200	40	53	52.4	58
150	96	66		
130	261	78		
84	7.5	22		

b) DKDP

Temp.	ε_c'	R(E∥C)	ε_a'	R(E⊥C)
295 K	50	56 %	58	59 %
220	34	50	62	60
190	6.5	19		
84	5.1	14		

c) ADP

Temp.	ε_c'	R(E∥C)	ε_a'	R(E⊥C)
295 K	14	33 %	56	58 %
200	16	36	82	64
152	18	38	107	68

Note : ε_a' and ε_c' : low frequency dielectric constant at 9.2 GHz measured by Kaminow et al. Reflectivities were derived by the Eq : $R = \left| (\sqrt{\varepsilon} - 1)/(\sqrt{\varepsilon} + 1) \right|^2$.

Table 3-2

Infrared Active Mode Frequencies in KH_2PO_4 (T_c=123K)

Dipolemoment	295K	200K	150K	130K	Mode Assignment	84K	Mode Assignment
$P_z(E \parallel C)$	$60cm^{-1}$	$32cm^{-1}$	$12cm^{-1}$	$< 10cm^{-1}$	B_2,lattice mode?		
	178	180	186	190	B_2,lattice mode	$208cm^{-1}$	A_1,lattice mode
	380w	380w	380w	380w	B_2, $\nu_2(PO_4)$	344	A_1, $\nu_2(PO_4)$
		-- 400	480wb --		B_2, $\nu_4(PO_4)$		
						514	A_1, $\nu_4(PO_4)$
$P_y(E \perp C)$	86	88			E, lattice mode		
	102	104			E, lattice mode		
	122	124			E, lattice mode		
	152	152			E, lattice mode		
	206	204			E, lattice mode		
	526	526			E, $\nu_4(PO_4)$		

Note: The mode frequencies are derived from the imaginary part of dielectric constant ε''. Subscript "w" means a weak band, "s" means a shoulder of strong band and "b" means a broad band.

Table 3-3

Infrared Active Mode Frequencies in KD_2PO_4 (T_c=218K)

Dipolemoment	295K	220K	Mode Assignment	190K	84K	Mode Assignment
$P_z(E \parallel C)$	$< 20cm^{-1}$	$< 20cm^{-1}$	B_2,lattice mode?			
	164	160	B_2, ?	$154cm^{-1}$	$166cm^{-1}$	A_1, ?
	176	190	B_2,lattice mode	226	228	A_1,lattice mode
	345w	350w	B_2, $\nu_2(PO_4)$	350	352	A_1, $\nu_2(PO_4)$
	380ws	380ws	B_2, $\nu_2(PO_4)$		378	A_1, $\nu_2(PO_4)$
	--400	480--	B_2, $\nu_4(PO_4)$			
	(480 peak)			508	508	A_1, $\nu_4(PO_4)$
$P_y(E \perp C)$	96	94	E,lattice mode			
	108	108	E,lattice mode			
	122	124	E,lattice mode			
	170	170	E,lattice mode			
	206	212	E,lattice mode			
	360bs	360bs	E, $\nu_2(PO_4)$			
	390b	380b	E, $\nu_2(PO_4)$			
	450b	446b	E, $\nu_4(PO_4)$			
	512b	502b	E, $\nu_4(PO_4)$			

Note: The mode frequencies are derived from the imaginary part of dielectric constant ε''. Subscript "w" means a weak band, "s" means a shoulder of strong band and "b" means a broad band.

Table 3-4

Infrared Active Mode Frequencies in $NH_4H_2PO_4$ (T_t=148K)

Dipolemoment	295K	200K	152K	Mode Assignment
P_z(E ∥ C)	76cm^{-1}	72cm^{-1}	72cm^{-1}	B_2, lattice mode?
	198	200	208	B_2, lattice mode
	390w	390w	390w	B_2, $\nu_2(PO_4)$
	-- 400	480b --		B_2, $\nu_4(PO_4)$
P_y(E⊥C)	50	40	34	E, lattice mode?
	80s	80s	80s	E, lattice mode
	155s	155s	155s	E, lattice mode
	164	168	168	E, lattice mode
	540	540	540	E, $\nu_4(PO_4)$

Note: The mode frequencies are derived from the imaginary part of dielectric constant ε'' . Subscript "ω" means a weak band, "s" means a shoulder of strong band and "b" means a broad band.

Table 3-5

The mode frequencies and width in KDP and ADP

a) KDP (E ∥ C)

Temp. K	ω_1	$\Delta\omega_1$	ω_2	$\Delta\omega_2$ (cm^{-1})
295	60	89	178	43
200	52	85	180	37
150	12	88	186	30
130	< 10	186	188	31
84	---	---	208	34

b) ADP (E ∥ C)

Temp. K	ω_1	$\Delta\omega_1$	ω_2	$\Delta\omega_2$ (cm^{-1})
295	76	111	200	43
200	72	109	200	38
152	72	101	210	34

c) ADP (E⊥C)

Temp. K	ω_1	$\Delta\omega_1$ (cm^{-1})
295	50	85
200	40	74
152	34	56

Note : The frequencies were derived from peaks in ε''.

Chapter 4 Low-Frequency Reflectivity Measurements by HCN Laser

The polarized reflectivity of KDP and ADP were measured as a function of temperature with a HCN laser in the 29.7 cm^{-1} line.[1] The reflectivity of KDP for E∥C shows a Curie-Weiss law behavior and it can be explained by a strongly damped oscillator model in the paraelectric phase.

1. Introduction

In the preceeding section it is suggested that there exists a ferroelectric mode, of which frequency tends to be zero as the temperature is lowered to T_c from above. If there is such a mode, we can expect the anomaly in the reflectivity in the low frequency when temperature is lowered through T_c.[1]

The measurement in the low-frequency region using a far-infrared spectrometer is troublesome because of the weak spectral power of the radiation source.[2] Recently the far-infrared HCN laser has been developed,[3] which provides relatively high output power and the polarized radiation of 29.7 cm^{-1} line. This enables us to measure the reflectivity more accurately and in good spectral purity at 29.7 cm^{-1}.

The purpose of the study in this chapter is to measure the polarized reflectivities of KDP and ADP as a function of temperature using HCN laser. This method is simple and provides direct evidence of an anomaly in the reflectivity accompanying the ferroelectric transition.

2. Experiments

2-1 Source

The HCN laser used has been developed by Yamanaka et al.[3] The lineary polarized radiation at 29.7 cm^{-1} is obtained by inserting a wire grid into the laser cavity. The output power was of the order of 1 mW. The radiation at 29.7 cm^{-1} is much less absorbed by water vapor, and so the experiments can be done in the air and it makes the measurement easy.

2-2 Optical System

Figure 4-1 shows the optical diagram of the measurements. The laser beam was chopped and led to a beam splitter (Mylar film). Then the beam was split to a cryostat and to a mirror. These two beams reached to a Golay cell by being alternatively interrupted with two shutters.

The polyethylene lenses were set as shown in the figure and the beam was focused to the sample. The diameter of the focused beam was about 4 mm. The angle of incidence was about 11.5°.

2-3 Measurements

The reflectivity of the sample can be obtained by changing a sample to an aluminized mirror as a reference. Such a measurement was tried. But the rigidness of the sliding mechanism of the cryostat is poor and this method results large experimental error. Therefore the low temperature work was done with the sample being kept stationary in the cryostat. Comparing the signal reflected by the sample with the one reflected by the mirror, the relative reflectivity was measured.

It was measured as a function of temperature and normalized by the value at room temperature.

The sample temperature was kept constant within ±1 K by controlling the heater current and the flow rate of liquid-nitrogen from a needle valve. The cryostat used here has the same structure shown in Fig. 3-1. An alignment of the optical system in Fig. 4-1 was made using a parallel visible light beam set at the position of the Golay cell. The lens was aligned with a plane mirror set at the site of the lens. The lock-in detection system was used at a frequency of 10 Hz.

3. Results and Discussion

3-1 KDP

Figure 4-2 shows the temperature dependence of the polarized reflectivity of KDP, normalized by the value at room temperature. Although there is the gradual change of the laser output power, the experimental error due to the laser itself was about ±1 %.

The laser output power reached to the sample was of the order of 0.1 mW and it raised the temperature of the sample about less than 0.2 degree.[4] The experimental error with normalized reflectivity was ±0.02, ±0.05 and ±0.1 at 200 K, 120 K and 90 K respectively, simply depending upon the rigidness of preliminary set up of the optical system.

The reflectivity for E∥C (P_z dipole moment) increases rapidly with decreasing temperature and has a maximum near Curie temperature (T_c= 123K), and then decreases steeply below T_c. Such a change in the reflectivity with temperature reflects the ferroelectric mode observed

in KDP shown in Fig. 3-5.

i) $T > T_c$

We shall consider the optical mode in the single oscillator model. The dielectric constant at a frequency ω can be calculated from the dispersion formula[5)]

$$\varepsilon(\omega, T) = \varepsilon' - i\,\varepsilon'' = \varepsilon_\infty + \frac{S(T)\omega_o(T)^2}{\omega_o(T)^2 - \omega^2 + i\gamma\omega} \qquad (4\text{-}1)$$

where $S(T)$, $\omega_o(T)$ and γ stand for the oscillator strength, characteristic frequency and damping constant respectively. In this case ω is equal to the HCN laser frequency (29.7 cm^{-1}).

The assumption of the single oscillator model is valid, because the far-infrared measurement of KDP shows that the ferroelectric mode for E∥C has a resonant type dielectric dispersion (Chap. 3, Sec. 4-3).

Moreover, according to the Raman scattering,[6)] $S(T)$ and $\omega_o(T)$ of the ferroelectric mode are given as

$$S(T) = C \,/\, (T - T_c) \qquad (4\text{-}2)$$

$$\omega_o(T)^2 = A(T - T_c) \,/\, T \qquad (4\text{-}3)$$

respectively. The reflectivity is obtained by

$$R = \left| \frac{\sqrt{\varepsilon} - 1}{\sqrt{\varepsilon} + 1} \right|^2 . \qquad (4\text{-}4)$$

The parameters A, C, γ, ε_∞ were determined by fitting the calculated reflectivity to the experimental ones. The method of the least squares was used to obtain the best fit to the experimental curve. The following values were obtained; $\gamma \simeq 180$ cm^{-1}, $\varepsilon_\infty \simeq 6.6$, $C \simeq 2500$ K and $A \simeq 7920 (cm^{-1})^2$. The calculated curve with these values is shown by dashed curve in Fig. 4-2. The values obtained are in good agreement with those by Kaminow.[6)]

The obtained value of the high-frequency dielectric constant ε_∞ is larger than the one in the high-frequency limit (ε'_∞=2.3). This discrepancy arises from the assumption of a single oscillator model. From eq. 4-1, the low-frequency limit of the dielectric constant ε_o is given by[5)]

$$\varepsilon_o = \varepsilon_\infty + S(T). \qquad (4\text{-}5)$$

In KDP more than one mode are observed in the far-infrared spectrum, so we rewrite eq. 4-5

$$\varepsilon_o = \varepsilon'_\infty + \sum_j S_j + S(T). \qquad (4\text{-}6)$$

The value of ε_∞ obtained here ($\simeq$6.6) includes the contribution from the modes above 150 cm^{-1}, then

$$\varepsilon_\infty = \varepsilon'_\infty + \sum_{j=2} S_j .$$

Thus ε_∞ is larger than ε'_∞.

ii) $T < T_c$

The reflectivity below T_c decreases drastically with temperature. It may be able to fit the observed reflectivity by an oscillator model, but as mentioned above the experimental error is large. So it can be said that the mode may have very low-frequency peak or disappear below T_c.

The reflectivity for E⊥C increases gradually as the temperature approaches T_c from above and decreases suddenly below T_c. The far-infrared reflection measurement on KDP for E⊥C shows a broad background in the spectrum up to near 100 cm^{-1}. We have no model to analyze this spectrum. The results obtained here seem to indicate that this background in the

spectrum disappears below T_c.

The absolute reflectivities at room temperature were measured by use of the sample holder. The sample was replaced by a reference mirror alternatively and the absolute reflectivity was measured. The results were 36±1 % and 53±1 % for E∥C and E⊥C, respectively, which are in good agreement with the data obtained using a far-infrared spectrometer. The experimental error of this method is smaller than that of spectrometer.

3-2 ADP

Figure 4-3 shows the results of ADP. The crystal shatters below transition temperature (T_t = 148 K) and therefore measurements were made only in the paraelectric phase. The reflectivities both for E∥C and E⊥C increase gradually as temperature is lowered toward T_t. No attempt was made to analyze these results by the oscillator model. The far-infrared measurements show that there are low-frequency modes both for E∥C and E⊥C. Both modes show no drastical change in their frequencies or intensity as seen in KDP. The results obtained here correspond to the temperature dependence of the low-frequency modes.

The absolute reflectivity at room temperature was measured. The results were 29±1 % and 56±1 % for E∥C and E⊥C respectively, which are also in good agreement with those of reflectivity measurements by the spectrometer shown in Chap. 3.

4. Summary

The polarized reflectivities of KDP and ADP at 29.7 cm^{-1} were measured as a function of temperature by use of HCN laser. The

reflectivity for E∥C of KDP showed Curie-Weiss law behavior and the curve above T_c could be explained by a strongly damped-harmonic oscillator, the characteristic frequency of which changes as $\omega_o^2 \propto (T-T_c) / T$. This result supports that the ferroelectric mode in KDP depends upon temperature as the soft mode of perovskite crystals.[7] The other results of KDP and ADP were in good agreement with those of far-infrared measurements shown in Chap. 3.

References

1) T. Kawamura, A. Mitsuishi, and H. Yoshinaga, J. Phys. Soc. Japan 28 Suppl. (1969) 227.

2) 三石明善、河村徹郎、強誘電体相転移合同研究会記録（昭和４６年度）京都　１９７２年１月，P.４３.

3) M. Yamanaka, H. Yoshinaga and S. Kon, Japan J. Appl. Phys. 7 (1968) 250.

4) M. Yamanaka, T. Kawamura and M. Hineno, J. Phys. D: Appl. Phys. 5 (1972) 1743.

5) A. S. Barker, Jr., Ferroelectricity, ed. E. Weller (Elsevier, Amsterdam, 1967) p. 211.

6) I.P. Kaminow and T. C. Damen, Phys. Rev. Letters, 20 (1968) 1105.

7) C. H. Perry, Far-Infrared Spectroscopy, ed. K. D. Möller and W. G. Rothschild (Wiley, New York, 1971) p. 557.

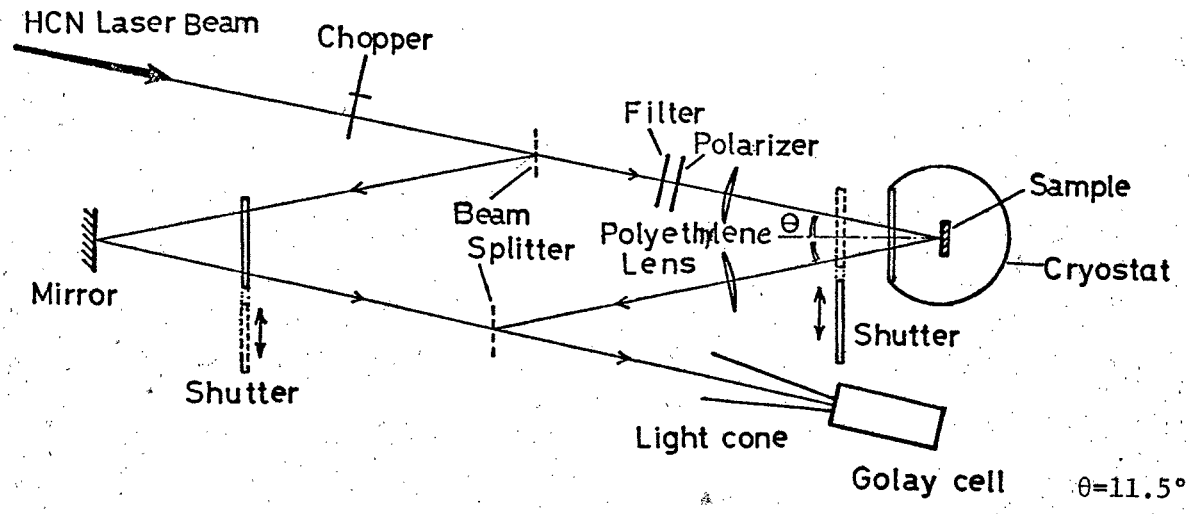

Fig. 4-1 Schematic diagram of experimental system.

Filter ; powder filter (TlCl+TlI+NaF)

Polarizer ; wire grid polarizer

Polyethylen lens ; 32 mm in diameter and 150 mm in focal length

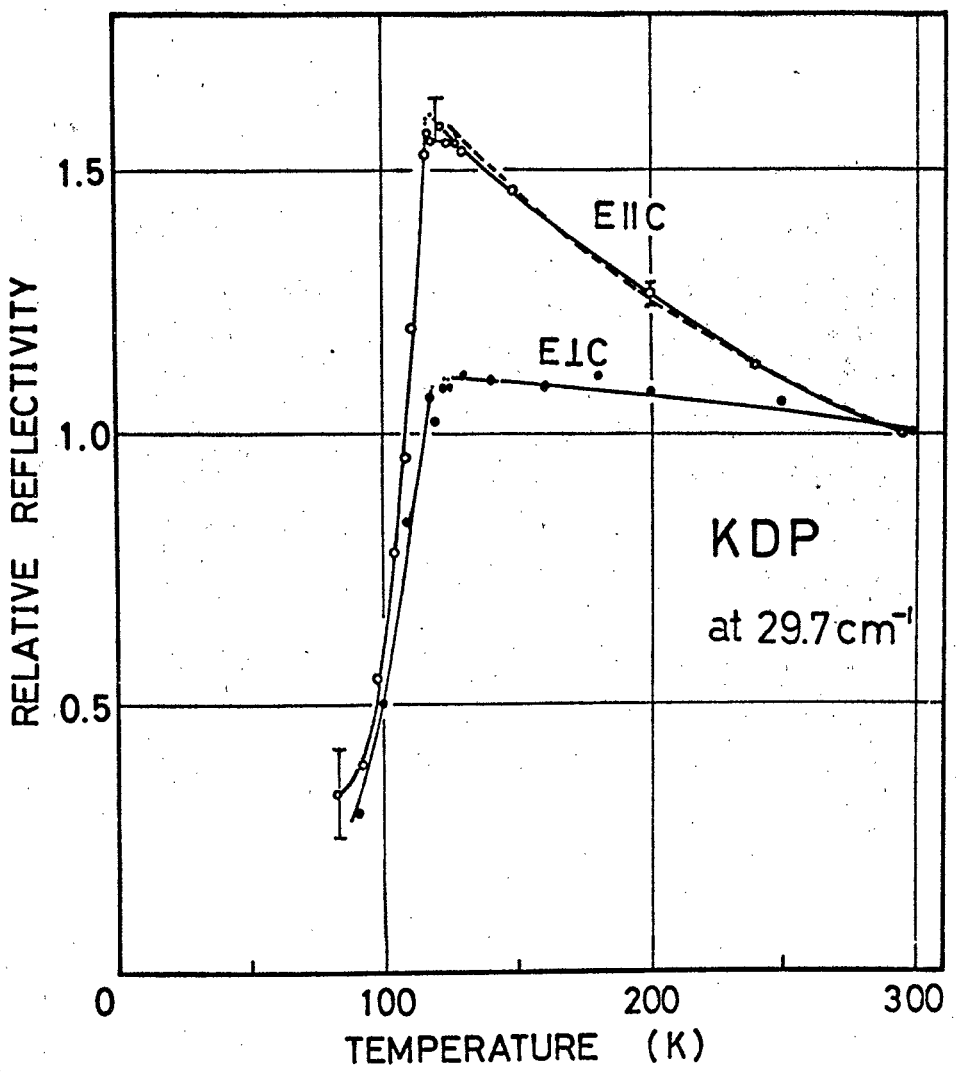

Fig. 4-2 Temperature dependence of polarized reflectivity for KDP at 29.7 cm^{-1}. The reflectivity is normarized at room temperature. The dashed curve shows the calculated reflectivity by single oscillator model.

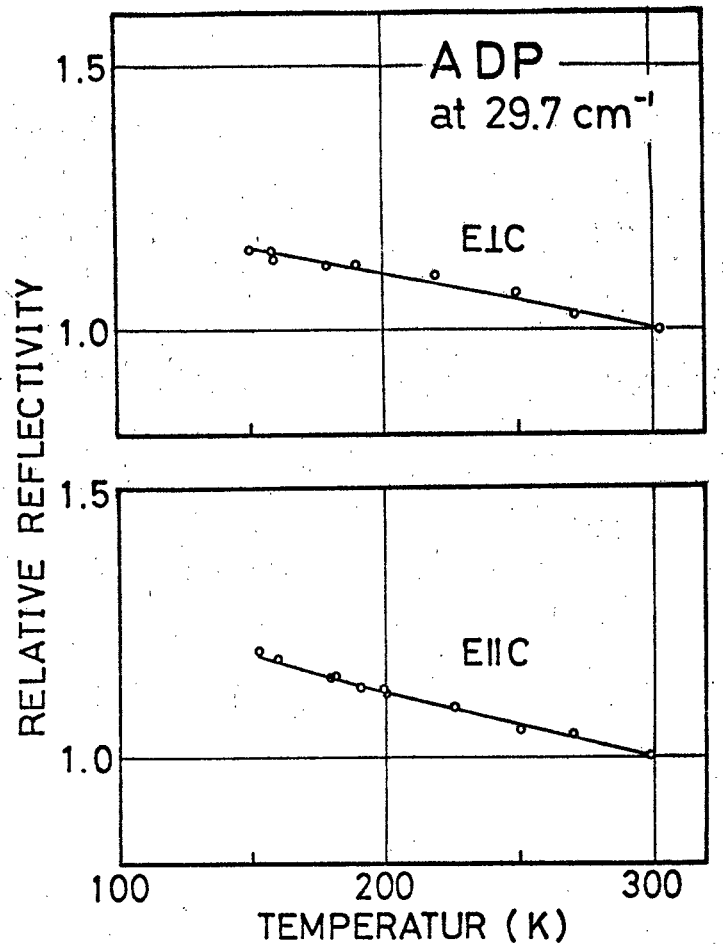

Fig. 4-3 Temperature dependence of polarized reflectivity for ADP at 29.7 cm^{-1}. The reflectivity is normarized at room temperature.

Chapter 5 Raman Spectra

The polarized Raman spectra of KDP and DKDP were measured in the region up to 1100 cm^{-1} in both paraelectric and ferroelectric phases as a fuction of temperature.[1, 2] The frequency and the symmetries of the observed bands were determined in both phases. The correlation relation of the modes in the different phases and the precise mode assignments were also established. The detailed temperature dependence of the low-frequency spectra were also examined in the vicinity of the ferroelectric transition temperature. In KDP the Raman scattering due to the polarization fluctuation of the ferroelectric mode was observed and the present result is in good agreement with the earlier works.[3-5] The effect of deuteration on the spectra are discussed comparing the results of KDP with those of DKDP.[2]

For the antiferroelectric ADP the same type measurements were made only in the paraelectric phase. The Raman scattering due to the polarization fluctuation of the low-frequency mode was observed in the spectra of E symmetry.[1]

1. Introduction

In the preceeding chapters the main attention has been paid to the low-frequency spectra of KDP type crystals and its dielectric behavior. The far-infrared measurements on KDP have revealed a strongly temperature dependent low-frequency band and showed that this band is responsible for much of low-frequency dielectric constant: i.e., this band is the ferroelectric mode. But so far the assignment of the mode and the establishment of the correlation relation of the modes in both

phases have not been done completely.

The infrared spectrum in the high-frequency region shows the broad and weak bands and so it is difficult to identify the bands. The Raman spectrum shows relatively sharp and isolated bands and moreover it shows more detailed polarizing characteristics; for example, the modes of A_1, B_1, B_2 and E symmetry species of D_{2d} group are Raman active of which the modes of B_2 and E symmetries are also infrared active. Thus the Raman scattering experiment is more suitable for the examination of the polarized spectra in wider region. And it enables us to make more complete mode assignments and to determine the mode symmetry and so on. Of course the modes of B_2 and E symmetries are both infrared and Raman active and so the data obtained by these two spectroscopic techniques together give more complete information about the vibrational specta.

In KDP it is thought that the hydrogens play a significant role in the process of ferroelectric transition. The change in the anharmonic motions of the hydrogens, proton tunneling and its ordering, at the phase transition may cause a significant change in the Raman spectra. So the measurements of the Raman spectra of KDP, DKDP and ADP as a function of temperature may lead us to a better understanding of the role of hydrogen motions in the phase transition.

2. Experiments

2-1 Sample Preparation

The dimension of the sample was typically 9×3×3 mm with faces parallel to the orthogonal principal axes x, y and z for tetragonal symmetry. The laser beam entered on a 3×3 mm surface. The single

crystals of KDP and ADP were bought from Nippon Denpa Kogyo Co. The final polishing was done with 0.1 μ alumina and ethanol. The sample of DKDP for the Raman measurements was cut from the same single crystal used for the infrared measurements. The crystal was cut using fiber wetted with heavy water. The final polishing was done using saturated solution of heavy water (D_2O) to minimize the rehydrogenation.

2-2 Optical System and Spectrometer

The excitation source for Raman scattering experiments was He-Ne laser. Its output power was about 50 mW at 6328 A. The general geometrical arrangement of the optical system is shown in Fig. 5-1 (a). The laser beam was reflected by the corner mirrors and entered the sample from a window on the bottom of the cryostat. The laser beam was focused on the sample by the collecting lens. As the crystals used were transparent, the beam was transmitted through sample and again reflected and focused on the sample by a concave mirror to improve signal to noise ratio. The scattered radiation was collected by another lens and focused onto the spectrometer slit. The collecting lens is mounted on the holder which has micrometer adjustable positioning. A rotatable polarizer was set in front of the spectrometer slit for the polarization studies. The optical arrangement for excitation and collection of scattered light is shown in Fig. 5-1 (b). The Raman lines observed in the present investigation were found to have spectral-width of 8 cm^{-1} with all three slits set at 300 μm and slit heights 10 mm. This setting was used for most of the scattering experiments.

The spectrometer used for the experiment was a Spex 1400 double monochromator. It consists of two identical 3/4-meter Czerny-Turner

spectrometers linked side by side. The gratings in the instrument were 600 line/mm blazed at 7500 A. The use of a double monochromator was essential to the present investigation for the following reason. In the grating spectrometer the primary source of stray light is the undiffracted light scattered by the grating. Raman lines are so weak in intensity and consequently masked by the stray light due to the Rayleigh line in the case of a single monochromator. The stray light in a double monochromator is much more reduced and it makes possible to measure the Raman lines. The Raman spectra in the present investigation are in the low-frequency region and it is desirable to measure the spectrum as close to the exciting line as possible. So it is necessary to reduce the stray light due to the Rayleigh line.

The photo-multiplier tube used was EMI 9558 A, which has a S-20 type photo-cathode. It was cooled below -20°C to reduce the noise due to the dark current. The lock-in detection system consisting of a preamplifier, a lock-in amplifier and a recorder was used. The incident laser beam was chopped by the sector at the frequency of 810 Hz.

2-3 Measurements

2-3-1 Polarized Measurements

For the Raman scattering measurement, the sample was set in the sample holder and illuminated by the laser as shown in Fig. 5-1 (b). The 90° scattering geometry was used and the experimental configurations, for example x(yx)y, were chosen according to the selection rule shown in Tables 5-1 and 5-2. The polarization directions of incident and scattered radiation, which were taken to be parallel to the laboratory coordinate X_L, Y_L, and Z_L, were determined by use of half-

wavelength plate and rotatable polarizer.

2-3-2 Temperature Control

The low temperature works were done by use of a specially constructed glass cryostat for liquid-nitrogen. A sample holder was mounted in the cryostat and a Teflon plate (d=2 mm) was put between the sample holder and the cooled bath as a thermal insulator. A heater was wound around the sample holder. The temperature of the sample holder was stabilized by adjusting the heater current using an electronic temperature controller. A chromel-alumel thermocouple with a diameter of 0.3 mm was used as a temperature sensor. The estimated accuracy of the temperature control is ±1 K, and stability is within ±0.1 degree in the temperature range from 80 K to 273 K.

The sample is set into the square well of the sample holder with silver paste. Good thermal contact between the sample and the sample holder was insured by the use of silver paste. The temperature sensor was set on the sample holder near the sample.

The high temperature furnace was used for the measurements in the temperature range from 295 K to 400 K. The sample temperature was also stabilized by the electronic temperature controller within ±0.1 degree at several temperatures between 295 K to 400 K.

2-4 Selection Rules and Polarized Measurements

It is known that the Raman scattering by the polar vibration is characterized by the wave-vector of the scattering phonon near the Brillouin zone center.[6] However a group theoretical analysis is carried out only for the limiting vibration with k=0 and predicts that the spectrum should depend only on the direction of polarization of incident

light and scattered one. In this view point, the selection rules for the polar vibration will be discussed below in connection with the phonon propagation direction.

In KDP the B_2 mode is both infrared and Raman active. It is polarized parallel to the z axis. According to the group character table, B_2 modes transform as α_{xy} Raman tensor component. When the measurement is done by the x(yx)y experimental configuration, the incident light travels along x axis and the scattered light travels along y axis. By the conservation of momentum a phonon is produced in xy plane with z polarization, since the xy component of tensors is measured. So this phonon has a propagation direction perpendicular to its polarization and is a transverse optical phonon (TO). If measured by the x(yx)z configuration, a phonon is produced in the xz plane with z polarization. This phonon is both transverse and longitudinal (LO). Poulet[7] has shown that in the polar crystal the longrange electric field due to the lattice polarization tends to make the energy of LO mode greater than that of TO mode. Therefore it is necessary to consider the phonon propagation direction when we measure the polar vibrational mode.

The selection rules for the polar vibrational mode are easily derived using the procedure of Poulet.[7] The results for KDP in D_{2d} are listed in Table 5-1. The Raman intensity is proportional to the square of Raman tensor component and also listed in the table. In KDP doubly degenerate E modes are both infrared and Raman active and polarized parallel to the x and y axes. In this case any experimental configuration for 90° scattering is found to give neither TO nor LO mode.

When the temperature is lowered through T_c the crystallographic

axes rotate 45° in the xy plane. The x', y' and z axes are taken to be parallel to these new crystallographic axes. The vibrational modes in this phase are characterized by the normal coordinate x', y' and z. In this case we obtain tensors which apply to the longitudinal and transverse phonons, and then these tensors are transformed to x, y and z coordinate. Experiments were done in x, y and z coordinate system. The results of selection rules in C_{2v} symmetry are shown in Table 5-2.

3. Results and Discussion

3-1 Mode Symmetries

Raman spectra for single crystals of KDP and DKDP were measured in the region up to 1100 cm^{-1} at several temperatures above and below T_c. The spectra were taken in the x(yy)z, x(zz)y, x(yx)y and x(yz)y configurations. The results are shown in Figs. 5-2(a)~(d) for KDP and Figs. 5-3(a)~(d) for DKDP respectively. Experiments on a single crystal of ADP in the antiferroelectric phase were impossible because ADP crystal shatters and becomes opaque at the transition. So the measurements were made only in the paraelectric phase. The results of ADP are shown in Figs. 5-4(a) and (b).

KDP

The polarized spectra were recorded at 295 K, 200 K, 130 K and 90 K. As seen in Fig. 5-2 polarizing characteristics in the spectra are clearly observed. Comparison of the results with group character table enables us to decide the mode symmetries. The observed bands in the paraelectric phase for $T>T_c$ are very broad and change only slightly with the temperature approaching T_c from above. When the temperature

is crossed through T_c, the marked changes in the spectra occur. Most of the bands become sharp and intense and some new bands appear. In the spectrum taken in the x(yz)y configuration most of the bands above T_c split at the transition temperature. Some other remarkable changes in the spectra at the transition temperature are as follows: in the x(yx)y spectrum the Rayleigh wing is observed above T_c, and it disappears drastically below T_c and a new band appears near 150 cm^{-1}; the broad background continuum is observed in the x(yz)y spectrum extending from Rayleigh line to 100 cm^{-1} above T_c and disappears below T_c; a similar feature appears in the x(yy)z spectrum from the exciting line to 180 cm^{-1} above T_c and disappears below T_c.

The Raman frequencies observed in the present measurements are listed in Table 5-3. The discussion about the mode symmetry will be made in the following.

The spectrum at 295 K are shown in Fig. 5-2 (a). According to the group character table shown in Table 2-2, A_1 mode transforms as α_{xx}, α_{yy} and α_{zz} Raman tensor components. Thus the strong bands in the x(yy)z and x(zz)y spectra can be assigned to A_1 symmetry and so the bands at 359 cm^{-1}, 918 cm^{-1} and a broad one at 520 cm^{-1} are assigned to A_1 symmetry.

The bands which appear only in the x(yy)z but not in the x(zz)y spectra should be assigned to B_1 symmetry. They transform as α_{xx} and α_{yy} Raman tensor components. The bands at 155 cm^{-1}, 394 cm^{-1}, 473 cm^{-1} can be assigned to B_1 symmetry.

The modes of B_2 symmetry transform as α_{xy} Raman tensor component and so the bands in the x(yx)y spectrum are assigned to B_2 symmetry.

The Rayleigh wing extending up to 150 cm^{-1} and the bands at 178 cm^{-1} and 394 cm^{-1} are B_2 modes. Also the modes in B_2 symmetry transform as P_z dipole moment, and so they are infrared active. The present Raman spectra are in good agreement with the far-infrared spectra shown in Chap. 3.

The modes of E symmetry transform as α_{yz} and α_{zx} Raman tensor components and P_y dipole moment. The bands in the x(yz)y spectrum are at 96 cm^{-1}, 116 cm^{-1}, 192 cm^{-1}, 533 cm^{-1} and 580 cm^{-1}. These bands are assigned to E symmetry. This spectrum taken in the x(yz)y configuration is compared with the far-infrared spectrum for E⊥C. In the infrared spectrum five bands are observed in the region below 300 cm^{-1}. They are at 86 cm^{-1}, 104 cm^{-1}, 122 cm^{-1}, 152 cm^{-1} and 206 cm^{-1} (Table 3-2). In the Raman spectrum the 104 cm^{-1} and 152 cm^{-1} bands are absent probably because they may be very weak.

In the ferroelectric phase the spectra were recorded at 90 K. The results are shown in Fig. 5-2 (d). As stated in Chap. 2 the crystallographic axes rotate 45° in the xy plane below the transition temperature. The non-zero Raman tensor components are characterized by the new normal coordinate (x', y', z). So the Raman tensor must be transformed into (x, y, z) coordinate in which experiments were done. Such a calculation was made in Sec. 2 and the results are shown in Table 5-2. The x(yy)z configuration gives $\alpha_{x'y'}$ and $(\alpha_{x'x'}+\alpha_{y'y'})$ Raman tensor components, and so the modes observed in the x(yy)z spectra belong to A_1 or A_2 symmetry. The x(zz)y and x(yx)y measurements give α_{zz} and $(\alpha_{x'x'}-\alpha_{y'y'})$ Raman tensor components respectively. The bands in the spectra taken at these configurations belong to A_1 symmetry. The bands in the x(yz)y spectra belong to B_1 or B_2 symmetry which transform as $\alpha_{y'z}$ or $\alpha_{zx'}$ Raman

tensor component. Furthermore when the temperature is crossed T_c the spectrum changes corresponding to the structural phase transition. The correlation of the modes from one phase to the other is as follows; in the x(yy)z spectrum, A_1 and B_1 modes for $T>T_c$ transform to A_1 and A_2 modes for $T<T_c$, respectively. Similarly we find; A_1 modes for $T>T_c$ transform to A_1 modes for $T<T_c$ in the x(zz)y spectrum, B_2 modes for $T>T_c$ to A_1 modes for $T<T_c$ in the x(yx)y spectrum and E modes for $T>T_c$ to B_1 and B_2 modes for $T<T_c$ in the x(yz)y spectrum. These correlations are naturally consistent with the correlation between the irreducible representations of D_{2d} symmetry and those of C_{2v} symmetry given in Table 2-3.

Now turn to the consideration about the spectra taken at 90 K. As stated above the strong bands in the spectra taken in the x(yy)z, x(zz)y, and x(yx)y configurations can be assigned to A_1 symmetry. In the x(yy)z spectrum, both A_1 and A_2 modes are included. According to the correlation table A_2 modes and B_1 modes for $T>T_c$ transform to A_2 modes below T_c. A_2 modes for $T>T_c$ are optically inactive. Therefore in the x(yy)z spectrum the bands which can be assigned to A_2 symmetry are as follows: the bands at 322 cm^{-1} and 574 cm^{-1} which are not observed above T_c, and the bands at 161 cm^{-1}, 394 cm^{-1} and 484 cm^{-1} which are assigned to B_1 modes above T_c. It is interesting to notice that in the x(yx)y spectrum, the Rayleigh wing disappears below T_c and a new band appears near 143 cm^{-1}. This band is also observed in the x(yy)z spectrum and is assigned to A_1 symmetry.

In the x(yz)y spectrum many new bands appear below T_c. This fact corresponds to the removal of degeneracy such as E modes for $T>T_c$ transform into B_1 and B_2 modes below T_c. But we cannot distinguish B_1 mode from B_2 mode because in the x(yz)y spectrum both B_1 and B_2

modes are included.

The results obtained here are summarized in Table 5-3. The mode frequencies and their mode symmetries are also listed.

DKDP

The spectra of DKDP are shown in Figs. 5-3 (a)~(d) at several temperatures above and below T_c. The spectra are, on the whole, similar to those of KDP and the mode symmetries are determined by the similar manner as in the case of KDP. The results are listed in Table 5-4. Comparison of the spectra with those of KDP leads us to know some deuteration effects. In the paraelectric phase the deuteration effects are pointed out as follows: In the spectrum of B_2 symmetry two bands appear around 200 cm^{-1}, while in KDP only one broad band is observed. These two bands in DKDP form a composite peak and its line shape changes drastically with temperature. The Rayleigh wing is also observed in DKDP but weak compared with that of KDP. The deuteration effects the shift of frequency of some bands; A_1 mode which goes from 917 cm^{-1} to 883 cm^{-1}, E mode which is shifted from 533 cm^{-1} to 516 cm^{-1} and so on. Some additional bands appear in DKDP. They are at 520 cm^{-1} in B_2 symmetry and 883 cm^{-1} and 970 cm^{-1} in E symmetry. The other additional bands are also found at 710 cm^{-1} in B_1 symmetry and at 970 cm^{-1} in A_1 symmetry.

When the temperature is lowered through T_c, the marked changes occur in the spectra. In the x(yy)z spectrum, a new, rather strong band appears at 1008 cm^{-1}, and a 970 cm^{-1} band above T_c splits into two bands at 963 cm^{-1} and 968 cm^{-1}. In the x(zz)y spectrum, a 970 cm^{-1} band above T_c splits into two bands at 968 cm^{-1} and 974 cm^{-1}. In the

x(yx)y spectrum, the Rayleigh wing disappears below T_c but no band is observed below 150 cm^{-1}. While, in KDP the Rayleigh wing disappears below T_c and a new band appears near 143 cm^{-1}.

ADP

In ADP the spectra were recorded at 295 K, 200 K and 152 K, i.e., only in the paraelectric phase. The results are shown in Table 5-5. These spectra are very similar to those of KDP, except the spectrum of E symmetry. The high-frequency bands above 300 cm^{-1} have almost the same frequency as that of KDP. The bands below 300 cm^{-1} have the frequency about 30 cm^{-1} higher than that of KDP. The bands above 300 cm^{-1} are attributed to the PO_4 internal modes as discussed later. The bands below 300 cm^{-1} are the lattice vibrational modes which shift harmonically to the higher frequency as K ion is substituted by NH_4 ion.

In the spectrum of E symmetry, the Rayleigh wing is also observed as in that of B_2 symmetry. Such a Rayleigh wing is not observed in the spectrum of E symmetry for KDP. The other bands of E symmetry for ADP are at 68 cm^{-1}, 121 cm^{-1}, 175 cm^{-1}, 192 cm^{-1} and 290 cm^{-1}, of which 175 cm^{-1} and 192 cm^{-1} bands form a composite peak. In KDP the corresponding spectrum shows the existence of several bands at 96 cm^{-1}, 116 cm^{-1} and 192 cm^{-1}. The lowest frequency band of ADP has fairly low-frequency compared with that of KDP. The 290 cm^{-1} band of ADP is not found in KDP nor in DKDP.

The polarized Raman spectra of KDP, DKDP and ADP are measured. The mode symmetries of the observed bands are determined. The changes of the spectra at the transition temperature are observed corresponding

to the structural phase transition.

The differences among the spectra of KDP, DKDP and ADP are observed. The remarkable differences between KDP and DKDP are observed in the spectra of B_2 symmetry in the region below 300 cm^{-1}. On the other hand the differences between ADP and KDP are observed in the spectra of E symmetry in the region below 300 cm^{-1}.

In these experiments, the measurements above 1100 cm^{-1} were tried but the results were not good enough for the quantitative analysis, because the scattering efficiencies in these crystals are very low, and the sensitivity of the photo-multiplier (S-20 type photo-cathode) decreases in the high-frequency region.

Further discussion about the present results will be done in the following sections.

3-2 Mode Assignments I: In the Region above 300 cm^{-1}

In Fig. 5-5 Raman lines of different substances at 295 K are shown for comparison. As seen in the figure the spectra are very similar to each other, except the low-frequency spectra in the x(yx)y and x(yz)y configurations. The different substituents shift certain modes more or less in the frequency. But their influence on the relative intensities is hardly observable. The spectra are separated into two regions. The low-frequency region below 300 cm^{-1} corresponds to the external vibrations of $[K-(H_2PO_4)]$ sublattice, and the region from 300 cm^{-1} to 1100 cm^{-1} corresponds to the internal vibrations of tightly bound PO_4 ion. In this section the author will discuss about the spectra in the region from 300 cm^{-1} to 1100 cm^{-1} comparing with the group theoretical analysis given in Chap. 2.

In Chap. 2 the author has discussed how the PO_4 ion behaves in the crystalline field. The present result confirms that the PO_4 ion behaves as an individual molecule in the crystal. The spectra can be interpreted as that the PO_4 tetrahedra are slightly deformed and have the symmetry of site group. This result is in consistent with that of Murphy et al.[8] and others.[9]

The possible interpretation of the observed spectra due to the PO_4 internal vibration is as follows. It is well known that free PO_4 ion has four distinct frequencies;[10] $\nu_1(A_1)=980\ cm^{-1}$, $\nu_2(E)=363\ cm^{-1}$, $\nu_3(F_2)=1083\ cm^{-1}$ and $\nu_4(F_2)=515\ cm^{-1}$. As seen in Fig. 5-5 the strong bands can be seen near $363\ cm^{-1}$, $515\ cm^{-1}$ and $980\ cm^{-1}$. These bands are the characteristic of the molecular vibrations of PO_4 ion modified slightly by the crystalline field. As the PO_4 tetrahedra are thought to be slightly deformed in the crystal, the $E(\nu_2)$ mode of free PO_4 ion at $363\ cm^{-1}$ splits into two bands at $359\ cm^{-1}$ and $393\ cm^{-1}$ in the crystal of KDP. Similarly the $F_2(\nu_4)$ mode of free PO_4 ions at $515\ cm^{-1}$ splits into three bands at $473\ cm^{-1}$, $533\ cm^{-1}$ and $580\ cm^{-1}$. The $A_1(\nu_1)$ mode at $980\ cm^{-1}$ is observed at $918\ cm^{-1}$. Now we consider the spectral decomposition of the modes of T_d symmetry into the symmetry species of the crystal symmetry D_{2d} and the site symmetry S_4. The results are shown in Tables 5-6 and 5-7. In the paraelectric phase $E(\nu_2)$ mode of free PO_4 ion appears in the α_{xy} spectrum at $394\ cm^{-1}$ but does not in the α_{yy} spectrum.* According to Table 5-6 $E(\nu_2)$ mode of PO_4 ion corresponds to the B symmetry species of S_4 group, but does not to B_1 symmetry species of D_{2d} group. Similarly the $473\ cm^{-1}$ band which is $F_2(\nu_4)$ mode

*Note: In the α_{yy} spectrum the weak band is observed at $393\ cm^{-1}$. However, reducing the angular aperture viewed from the monochromator, this band in the α_{yy} spectrum disappears.

of free PO_4 ion, appears in the α_{yy} spectrum but not in the α_{yx} spectrum. In other words $F_2(\nu_4)$ mode corresponds to the B symmetry species of S_4 group and not to B_2 symmetry species of D_{2d} group. The $A_1(\nu_1)$ mode of free PO_4 ion is observed in both α_{yy} and α_{zz} spectra, so this mode corresponds to the A symmetry species of S_4 group. Therefore the characteristic vibrational modes of free PO_4 ion are found to be decomposed to the modes of S_4 symmetry group. The S_4 symmetry group is the site group of D_{2d} symmetry where PO_4 ion lies in the crystal. The PO_4 ion thus seems to behave as individual molecule having S_4 symmetry.

In the ferroelectric phase the bands attributed to the PO_4 internal modes become sharp and intense, and new bands appear but overall feature of the spectra is almost unchanged as shown in Fig. 5-6. This fact suggests that the PO_4 ion also behaves as an individual molecule in the ferroelectric phase. But the site group is no longer S_4 and lower symmetry group. The site group below T_c seems to be C_2 group as discussed in Chap. 2. If this is the case the characteristic vibrational modes of PO_4 ion transform like A and B symmetry species of C_2 group as shown in Table 5-7, and the degeneracy is removed.

The spectra taken in the x(yy)z, x(zz)y and x(yx)y configurations give modes of A type symmetry and the x(yz)y spectrum shows the modes of B type symmetry. In the x(yz)y spectrum the splitting of the bands at the transition is expected to be observed, but such a splitting is not observed experimentally. This may be due to the fact that the spectra were recorded with relatively large spectral slit-width of about 8 cm^{-1} or more.

As seen in Fig. 5-5 some additional bands are observed in DKDP which are not found in KDP. They are 710 cm^{-1} band of B_1 symmetry and

970 cm^{-1} band of A_1 symmetry. These bands are O-D bending vibrations according to the previous infrared works.[11-13] The corresponding bands in KDP are in the high-frequency region which is out of the present experiments.

The spectra of ADP in the region from 300 cm^{-1} to 1100 cm^{-1} are almost the same as those of KDP. The crystal of ADP contains NH_4 tetrahedra but the internal vibrational modes of NH_4 group have very high frequency above 1600 cm^{-1} which is also out of the region of the present experiments.[10]

When the experimental results are compared with the group theoretical analysis, the behavior of PO_4 ion in the crystal becomes clear. The PO_4 ion behaves as an individual molecule in the crystal having S_4 symmetry above T_c and C_2 symmetry below T_c. The exact mode assignments are made and the results are shown in Tables 5-3, 5-4 and 5-5.

3-3 Mode Assignments II: In the Region below 300 cm^{-1}

KDP and DKDP

The spectra of KDP and DKDP in the low-frequency region below 300 cm^{-1} are shown in Fig. 5-7 for the x(yy)z configuration. A band is observed at 154 cm^{-1} for KDP above T_c and the corresponding band is observed also at 154 cm^{-1} for DKDP. These bands are B_1 mode. While the group theoretical analysis allows two B_1 modes which are translational vibrations of $[K-(H_2PO_4)]$ sublattice, only one band is observed. The other is missing probably because it is either very weak or very low frequency. Below T_c B_1 mode transforms to A_2 mode and is observed

at 161 cm^{-1} for KDP and 160 cm^{-1} for DKDP. In KDP a strong band is observed at 145 cm^{-1} at 90 K which is absent in DKDP. This band also appears in the x(yx)y spectrum and is assigned to A_1 symmetry species. Figure 5-8 shows the low-frequency spectrum in the x(yx)y configuration. The bands observed above T_c are B_2 modes, and below T_c they transform to A_1 modes. The Rayleigh wing is observed in KDP above T_c and also observed in DKDP but weak. This Rayleigh wing in KDP is due to the polarization fluctuation of the ferroelectric mode observed in the far-infrared measurement.[1, 14] Below T_c this wing in KDP disappears gradually and a new band appears, which has a 90 K peak at 143 cm^{-1}. This band is not found in the far-infrared spectrum as shown in Fig. 3-7. In DKDP the Rayleigh wing also disappears below T_c, but no mode is observed near 143 cm^{-1}. This 143 cm^{-1} band of KDP is largely effected by deuteration and may be an underdamped ferroelectric mode as suggested by Blinc et al.[15] The other band is observed near 200 cm^{-1} in KDP. This band has a 295 K peak at 178 cm^{-1}. Below T_c this band becomes sharp and shifts to higher frequency and has a 90 K peak at 208 cm^{-1}. This is the translational lattice mode as predicted by the group theoretical analysis. It is worth noticing that the group theoretical analysis predicts only one translational lattice mode above T_c, while two bands are observed in KDP above T_c. In DKDP the situation is somewhat different. The broad band is observed near 200 cm^{-1} above T_c. This broad band seems to consist of two bands, and the strong energy transfer occurs as the temperature approaches T_c. Such an energy transfer is observed in SbSI.[16] Below T_c the lower-frequency mode disappears and the higher-frequency one becomes sharp and intense. This band has a 90 K peak at 233 cm^{-1}. This 233 cm^{-1} band is the translational

lattice mode. Further, in the far-infrared spectrum two bands are observed around 200 cm^{-1} above T_c and below T_c these two bands split and become sharp. These two bands have 90 K peaks at 166 cm^{-1} and 228 cm^{-1}. While, in the Raman spectrum the band corresponding to the 166 cm^{-1} band is not found below T_c.

Figure 5-9 shows the spectra of KDP and DKDP for the x(yz)y configuration. In KDP the lattice modes are observed at 96 cm^{-1}, 116 cm^{-1} and 192 cm^{-1} at 295 K and in DKDP they are at 92 cm^{-1}, 113 cm^{-1} and 184 cm^{-1}. Thus the lattice modes of E symmetry are found to be hardly affected by deuteration. This fact suggests that there is no interaction between the lattice mode of E symmetry and the proton (deuteron) motion. According to the group theoretical analysis, five E modes are expected to be observed in both Raman and infrared spectra. But only three of them are found experimentally.

ADP

The low-frequency spectra of ADP are shown in Fig. 5-10 for the x(yx)y and x(yz)y configurations. The lattice mode of A_1 symmetry is at 184 cm^{-1} (not shown in the figure) and the lattice mode of B_2 symmetry is at 203 cm^{-1}. These frequencies are about 30 cm^{-1} higher than those of KDP. This fact is reasonably attributed to the harmonic shift due to the mass difference between K ion and NH_4 ion. As seen in Fig. 5-10 (a) the spectrum of E symmetry is quite different from that of KDP. The Rayleigh wing is also observed in the spectrum of E symmetry and this wing is due to the polarization fluctuation of the broad low-frequency mode observed in the far-infrared measurements.[1, 14)]

3-4 Phase Transition

3-4-1 Ferroelectric Mode

KDP

As seen in Fig. 5-8 (a) the broad Rayleigh wing is observed in KDP above T_c and it disappears below T_c. The present result is in good agreement with that of Kaminow et al.[3, 4] The imaginary part of complex susceptibility is derived from the Raman intensity $J(\omega)$ by use of eq. 1-6 which is rewritten here

$$J(\omega) = K(n(\omega) + 1)\ \chi''(\omega) \qquad (5\text{-}1)$$

where $n(\omega)$ is the Bose factor,

$$n(\omega) = [\exp\ (\frac{\hbar\omega}{K_B T}) - 1]^{-1}. \qquad (5\text{-}2)$$

The results are shown in Fig. 5-11. This is compared with the imaginary part ε'' of complex dielectric constant obtained by the far-infrared measurements[1, 14] shown in Fig. 3-7. Unfortunately, because of the experimental uncertainty in the region below 40 cm^{-1}, the peak is not observed in the figure. But the χ'' spectrum shows the existence of a low-frequency temperature dependent band above T_c which disappears or decreases in its width below T_c. This result is consistent with the result of the far-infrared measurement.

Kaminow et al.[3,4] fitted their Raman spectra by the simple-damped-harmonic oscillator function and exhibited the soft mode behavior. Wilson et al.[17] studied recently in more detail. These authors have neglected the strong coupling of the ferroelectric mode with the bands near 180 cm^{-1} in their analysis. Scott and his co-workers[18-20] observed strong anharmonic coupling between the ferroelectric mode and the lattice mode of B_2 symmetry in CsH_2AsO_4 and KH_2AsO_4 which are

isomorphous to KDP. The same anharmonic interaction would be necessary to interprete the low-frequency B_2 spectrum of KDP. As stated in Chap. 3 the far-infrared spectrum of B_2 symmetry could not be fitted by two uncoupled harmonic oscillators. This result suggests the necessity of coupled harmonic oscillator approach. The effect of strong coupling in KDP has been studied by She et al.[19] for B_2 mode and by Scott and Wilson[20] for E mode.

The imaginary part of the complex susceptibility $\chi''(\omega)$ for the coupled mode can be written in terms of the Green's function[18] and the mode strength P_i, P_j, as

$$\chi''(\omega) = \mathrm{Im}\left(\sum_{ij} P_i P_j G_{ij}(\omega)\right) \qquad (5\text{-}3)$$

where the Green's function satisfies the following coupled mode equation

$$\begin{bmatrix} \omega_a^2 - \omega^2 + i\omega\Gamma_a & \Delta^2 + i\omega\Gamma_{ab} \\ \Delta^2 + i\omega\Gamma_{ab} & \omega_b^2 - \omega^2 + i\omega\Gamma_b \end{bmatrix} \cdot \begin{bmatrix} G_{aa} & G_{ab} \\ G_{ab} & G_{bb} \end{bmatrix} = \begin{bmatrix} 1 & 0 \\ 0 & 1 \end{bmatrix}. \qquad (5\text{-}4)$$

Here we approximate Δ, Γ_a, Γ_b and Γ_{ab} as frequency independent constants. The Raman spectra may therefore be calculated by two coupled modes system in terms of seven parameters ω_a, ω_b, Γ_a, Γ_b, Δ, Γ_{ab} and P_a/P_b. The numbers of parameters are reduced when we diagonalize as $\Gamma_{ab}=0$.

The calculation was made and the parameters were obtained by the optimum fitting of eq. 5-1 to the observed spectrum, using expressions for $\chi''(\omega)$ and $G_{ij}(\omega)$ in eqs. 5-3 and 5-4. The parameters determined are listed in Table 5-8. Thus we could extract the correct temperature dependence of uncoupled ferroelectric mode. The square of characteristic frequency ω_a^2 and the temperature weighted inverse equivalent

relaxation time T/τ are shown in Fig. 5-12 where $\tau=\gamma_a/\omega_a^2$. The temperature dependence of ω_a^2 is approximately

$$\omega_a^2 \propto (T - T_c) / T.$$

This result is similar to the original work of Kaminow et al.[3, 4] but is not in agreement with the work of She et al.[19] The result obtained here is consistent with the prediction of the pseudospin tunneling mode model.[21] Also as seen in Table 5-8, the ferroelectric mode has a very large damping and relatively large mode strength P_a, which is strongly dependent on temperature. The large mode strength and its temperature dependence suggest that this mode contributes largely to the low-frequency dielectric constant.

The soft mode behavior of the ferroelectric mode of KDP becomes clear. But there is a large experimental uncertainty in the region below 40 cm^{-1} because the measurements were made with relatively large slit-width. It is necessary to measure the low-frequency spectrum more accurately to study the ferroelectric mode more completely.

As seen in Fig. 5-8 (a) the Rayleigh wing, ferroelectric mode, disappears gradually below T_c, and a new band appears and grows in intensity. This new band is not observed in DKDP. Blinc et al.[15] observed the same phenomenon in their Raman scattering measurements on KDP and DKDP. They explained this phenomenon as follows; the overdamped proton tunneling mode in the paraelectric phase becomes underdamped below the transition temperature.

The corresponding band is absent in the far-infrared spectrum as seen in Fig. 3-5. This fact means that the corresponding vibrational mode accounts largely for the change in the polarizability but does

not in the dipole moment. If this band is attributed to the proton tunneling mode, it must have very small dipole moment because the effective charge of the proton is very small, but it probably accounts largely for the change of the polarizability. Thus Blinc's proposal is reasonably consistent with the experimental results.

In the paraelectric phase the ferroelectric mode is observed in both Raman and infrared spectra. The temperature dependence of this mode is as that of collective tunneling mode model.[21] Further discussion will be done in Chap. 6.

DKDP

As seen in Fig. 5-8 (b) the Rayleigh wing is also observed in the spectrum of B_2 symmetry above T_c, and below T_c this Rayleigh wing disappears. The imaginary part $\chi''(\omega)$ of the complex susceptibility is derived from the Raman spectrum. The result is shown in Fig. 5-13. The χ'' spectrum shows the existence of a broad band above T_c which has no peak in this region. Below T_c this band disappears. The same results were obtained by Kaminow et al.[3, 4] As stated in Chap. 2 the far-infrared measurements on DKDP suggest the existence of a low-frequency mode below 20 cm^{-1}. The band observed in the $\chi''(\omega)$ spectrum is thought to be a higher-frequency tail of the low-frequency mode.

In KDP the Raman spectra due to the polarization fluctuation of the ferroelectric mode is observed in the spectrum of B_2 symmetry. The results are in good agreement with those of Kaminow et al.[3, 4] The characteristic frequency tends to be zero as the temperature approaches T_c from above. In DKDP the existence of such a mode is not

clearly observed experimentally. As pointed in Chap. 3 the corresponding mode must have the frequency below 20 cm^{-1}.

3-4-2 Tunneling Mode

In Chap. 2 the motions of four non-equivalent protons have been discussed. The collective proton tunneling modes transform as A_2, B_2 and E symmetry species. Recently Wilson et al.[17] examined the Raman spectra of KDP and found no mode which could be attributed to the collective tunneling mode. They also reported the possible evidence of proton ordering in the spectra of KDP. The similar spectra are obtained in the present work and in good agreement with theirs. As seen in Fig. 5-7 (a) the broad background continuum is observed in the x(yy)z spectrum (A_2 symmetry) above T_c and this continuum disappears below T_c. The similar feature is also observed in the x(yz)y spectrum (E symmetry). Wilson et at.[17] attributed these phenomena to the ordering of proton. They also pointed out the evidence of proton ordering in the x(yx)y spectrum (B_2 symmetry). As seen in Fig. 5-8 (a) the Rayleigh wing below T_c decreases gradually in intensity as the temperature is lowered. The present results of DKDP confirm their explanation. Figure 5-8 (b) shows the existence of the Rayleigh wing in the spectrum of DKDP. This Rayleigh wing below T_c decreases more rapidly than that of KDP. This phenomenon can be explained as follows. The deuteron has the smaller tunneling frequency than that of the proton and so the deuteron becomes ordered more rapidly than the proton does.

The other evidence of the proton ordering is also observed in the spectrum of higher-frequency region. As has been noted before the PO_4 bands above T_c are very broad. Below T_c these bands suddenly become sharp and intense. The broadening of the bands above T_c is thought to

be due to the coupling of the PO_4 internal vibration with the hydrogen low-frequency mode through anharmonicity. Blinc et al.[13] suggested the existence of the anharmonic low-frequency proton mode in a double minima potential well. The sharpening of the bands at the transition corresponds to the disappearance of the proton tunneling mode as the proton becomes ordered. In DKDP the corresponding bands above T_c are narrower than those of KDP. The deuteration effects the reduction of tunneling frequency and causes a disappearance of resonance condition. The similar interpretations were deducted by Wilson et al. in their Raman scattering measurements on KDP and by Levin et al.[12] in their infrared measurements on KDP and DKDP.

The broad PO_4 bands are also found in the spectra of ADP. ADP is also the hydrogen bonded crystal and the same phenomena is probable.

As discussed above the remarkable change in the spectral line shape at the transition can be reasonably attributed to the proton ordering. The anomalous line shapes in the paraelectric phase, such a broad linewidth of PO_4 bands and the background continuum, ~~is~~ are thought to be due to the coupling of the proton tunneling mode with the other vibrations, PO_4 internal and lattice vibration.

3-5 Antiferroelectric ADP

As seen in Fig. 5-10 x(yx)y spectrum (B_2 symmetry) is similar to that of KDP. But the x(yz)y spectrum (E symmetry) is quite different from that of KDP and shows the existence of a Rayleigh wing. The imaginary part of complex susceptibility was derived from the Raman scattering spectra. The results are shown in Fig. 5-14 and are in good

agreement with those obtained by the far-infrared measurements. The broad bands are observed in both spectra for B_2 and E symmetries but the one for E symmetry is fairly stronger than that for B_2 symmetry. The intensity of E mode increases drastically as the temperature is lowered to T_t and this mode is thought to give rise to the dominant contribution to the low-frequency dielectric constant. But the peak frequency hardly shifts with temperature. Therefore this broad low-frequency band observed here may have nothing to do with the antiferroelectric transition. The zone boundary mode will become unstable at the transition as discussed in Chap. 3. The origin of the low-frequency E mode is unknown yet. It is worth noticing that the frequencies of the lattice modes for E symmetry are quite different from those of KDP. The same phenomena are also observed in the far-infrared spectra. Further discussion will be done in Chap. 6.

4. Summary

The polarized Raman spectra of KDP and DKDP were measured in both phases as a function of temperature. The measurements on ADP were also done but only in the paraelectric phase. The frequencies and the symmetries of most of the observed bands were determined in both phases, and the correlation of the modes from one phase to the other was established. The experimental results being compared with the results of the group theoretical analysis, the correct mode assignments were also established. In all these substances PO_4 ion was found to behave as an individual molecule slightly deformed by the crystalline field, and the bands due to the internal vibrations of PO_4 ion were uniquely assigned.

In the low-frequency spectra the Rayleigh wing due to the polarization fluctuation of the ferroelectric mode was observed in KDP, and the soft mode behavior of the ferroelectric mode was confirmed. The deuteration caused the large changes in the spectrum of B_2 symmetry. The evidences of the proton (deuteron) ordering were also observed. In the antiferroelectric ADP the Raman scattering due to the polarization fluctuation of the low-frequency mode was observed in the spectrum of E symmetry. This result is consistent with that obtained by the far-infrared measurements.

References

1) T. Kawamura and A. Mitsuishi, Technology Reports of Osaka Univ. 23 (1973) 365.

2) T. Kawamura and A. Mitsuishi, To be submitted to Optics Commun.

3) I. P. Kaminow and T. C. Damen, Phys. Rev. Letters 20 (1968) 1105.

4) I. P. Kaminow, Light Scattering Spectra of Solids, ed. G. B. Wright (Springer, New York, 1969) p.675.

5) K. I. White, W. Taylor, R. S. Katiyar and S. M. Kay, Phys. Rev. Letters 33 A (1970) 175.

6) R. Loudon, Advan. Phys. 13 (1964) 423.

7) H. Poulet, Ann. Phys. (Paris) 10 (1955) 908.

8) G. M. Murphy, G. Weiner and J. J. Oberly, J. Chem. Phys. 22 (1954) 1322.

9) C. Y. She, T. W. Broberg and D. F. Edwards, Phys. Rev. B 4 (1971) 1580.

10) For example, G. Hertzberg, Infrared and Raman Spectra of Polyatomic Molecules (Van Nostrand, New York, 1954).

11) E. Wiener, S. Levin and I. Pelah, J. Chem. Phys. 52 (1970) 2881, and ibid. 52 (1970) 2891.

12) S. Levin, I. Pelah and E. Wiener, Phys. Stat. Sol. 58 (1973) 61.

13) R. Blinc and D. Hadzi, Mol. Phys. 1 (1958) 391, and J. Chem. Solids 13 (1960) 204.

14) T. Kawamura, A. Mitsuishi and H. Yoshinaga, J. Phys. Soc. Japan 28 (1970) 227.

15) R. Blinc and B. Zeks, Advan. Phys. 21 (1972) 693.

16) G. Harbeke, E. F. Steigmeier and R. K. Whener, Solid State Commun. 8 (1970) 1765.

17) C. W. Wilson and H. Z. Cummins, Light Scattering in Solids, ed. M. Balkanski (Flammarion, Paris, 1971) p. 420.

18) R. S. Katiyar, J. F. Ryan and J. F. Scott, Phys. Rev. B 4 (1971) 2635, and Light Scattering in Solids, ed. M. Balkanski (Flammarion, Paris, 1971) p. 436.

19) C. Y. She, T. W. Broberg and L. S. Wall and D. F. Edwards, Phys. Rev. B 6 (1972) 1847.

20) J. F. Scott and C. W. Wilson, Solid State Commun. 10 (1972) 597.

21) M. Tokunaga, Ferroelectricity 1 (1970) 195.

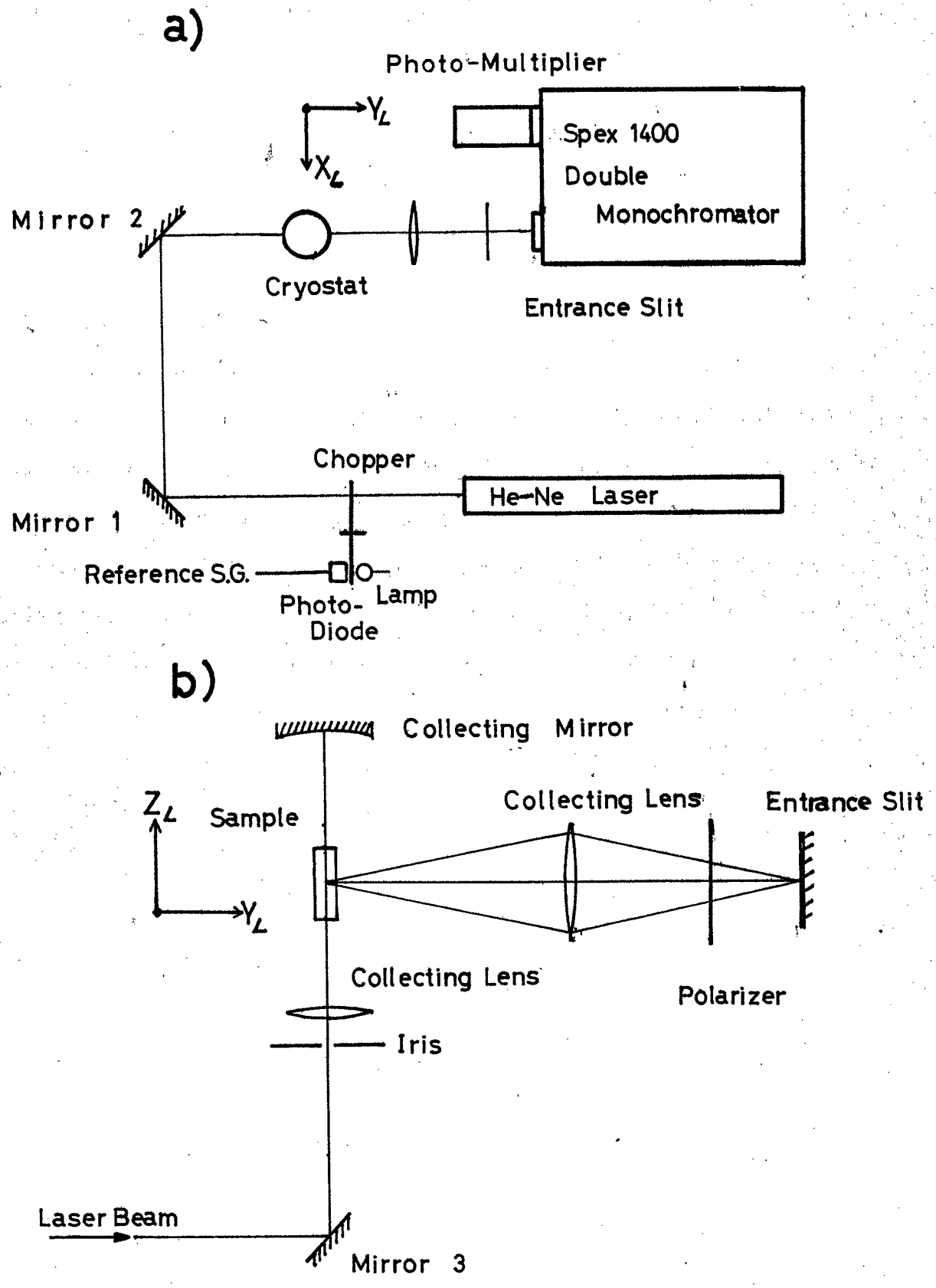

Fig. 5-1 a) Optical system of Raman scattering measurement.

b) Sample illumination system.

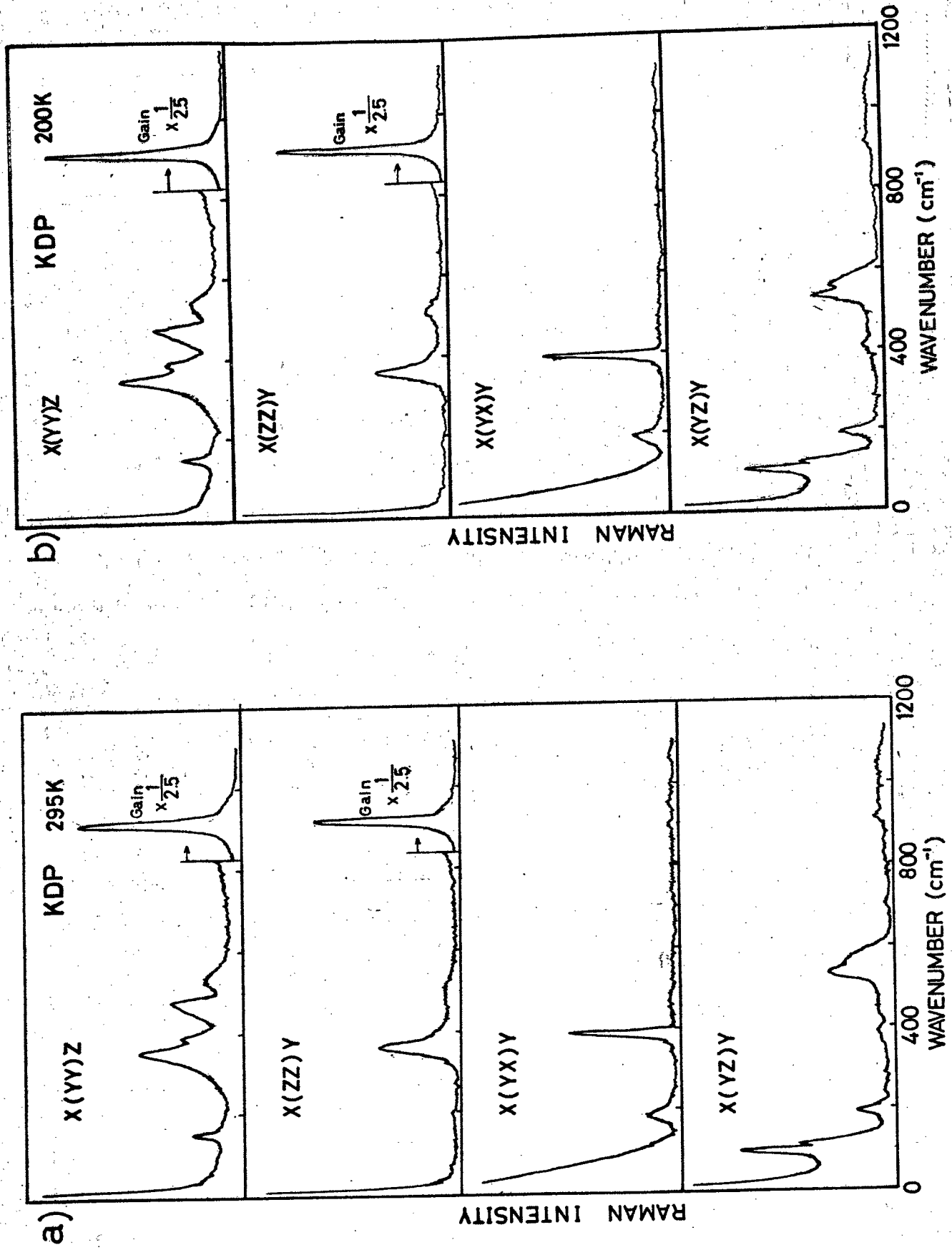

Fig. 5-2 1) Raman scattering spectra of KDP; a) at 295K, b) at 200K, c) at 130K and d) at 90K.

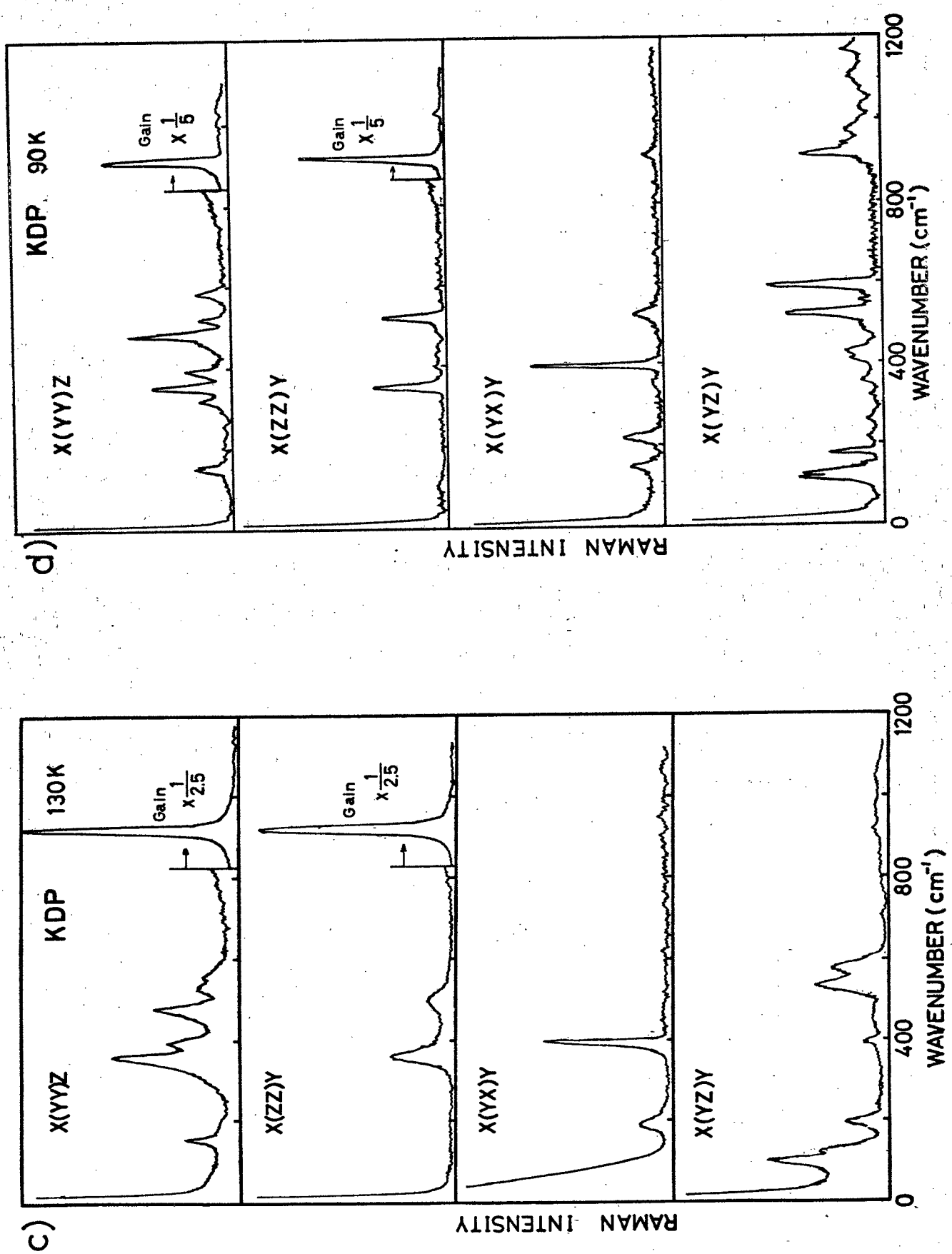

Fig. 5-2 2) Raman scattering spectra of KDP; a) at 295K, b) at 200K, c) at 130K and d) at 90K.

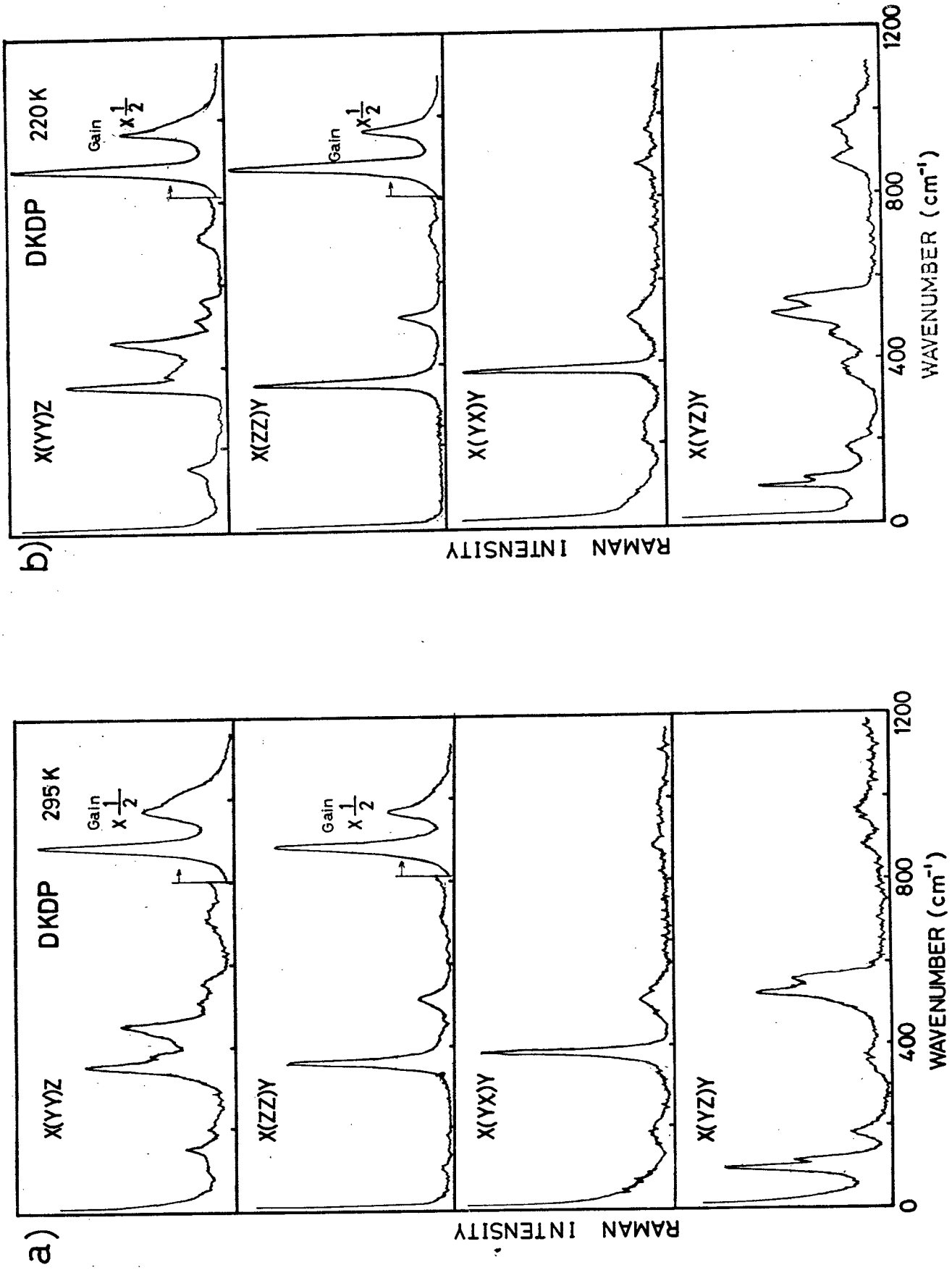

Fig. 5-3 1) Raman scattering spectra of DKDP; a) at 295K, b) at 220K, c) at 190K and d) at 90K.

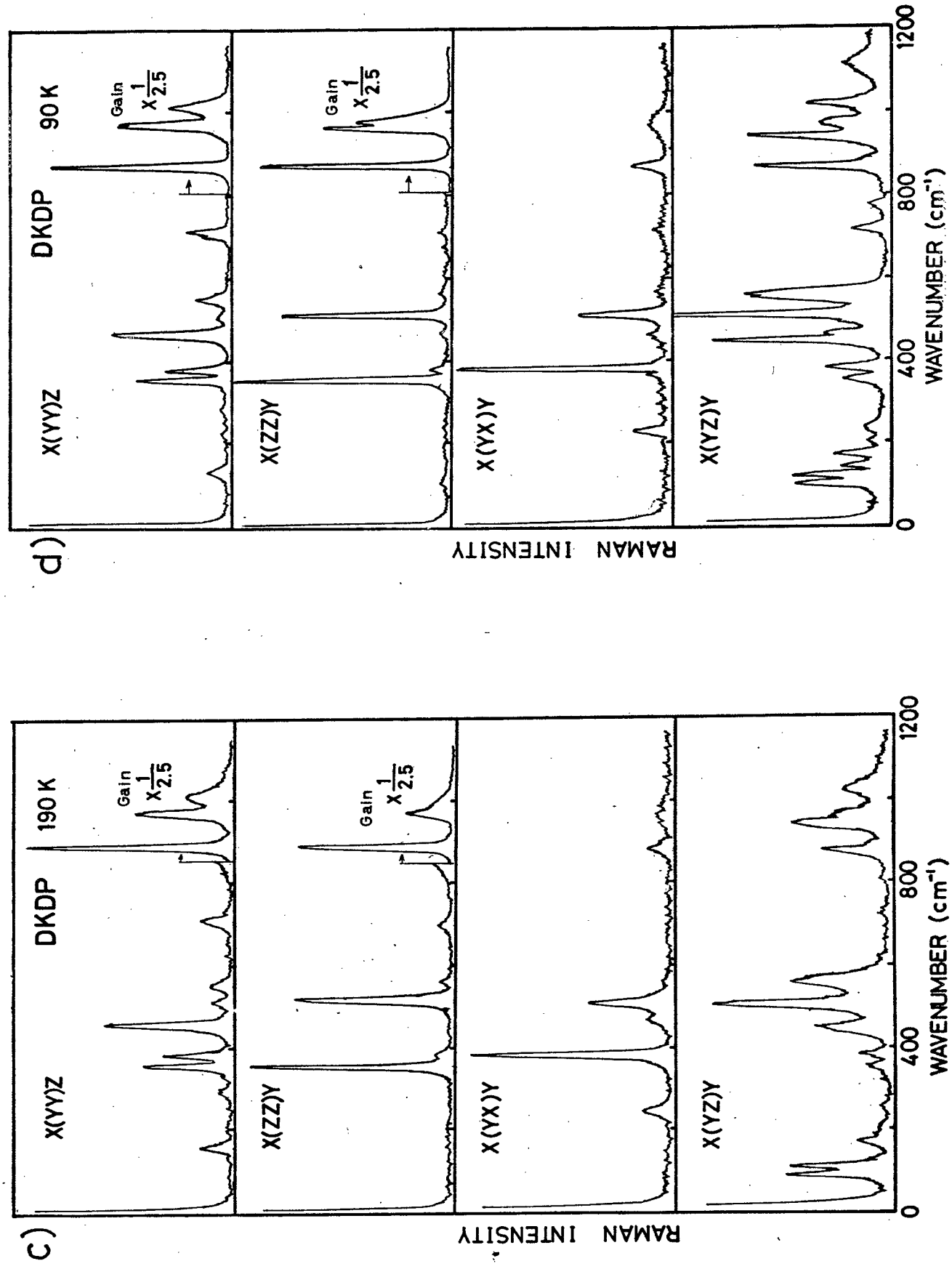

Fig. 5-3 2) Raman scattering spectra of DKDP; a) at 295K, b) at 220K, c) at 190K and d) at 90K.

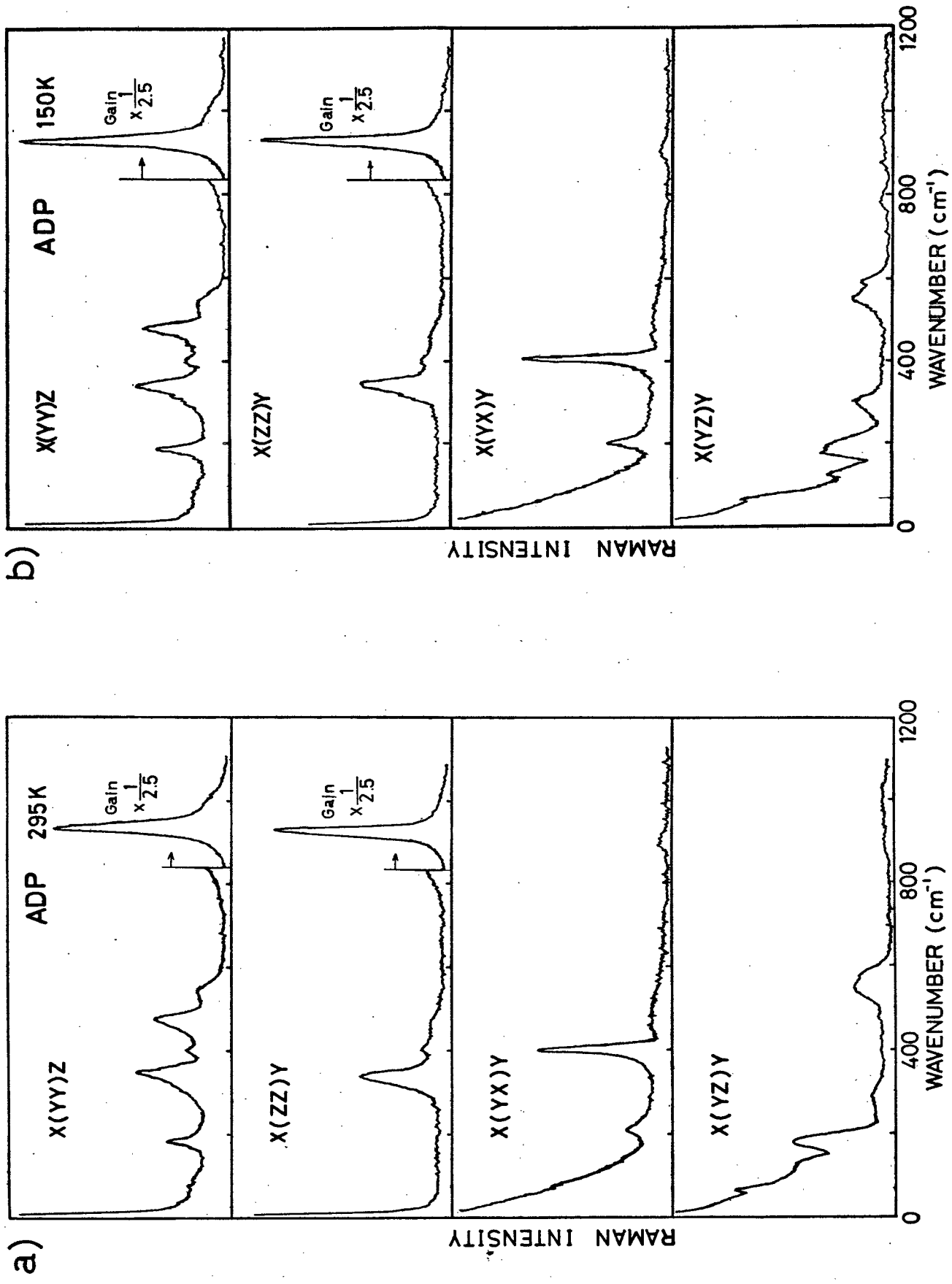

Fig. 5-4 Raman scattering spectra of ADP; a) at 295K and b) at 150K.

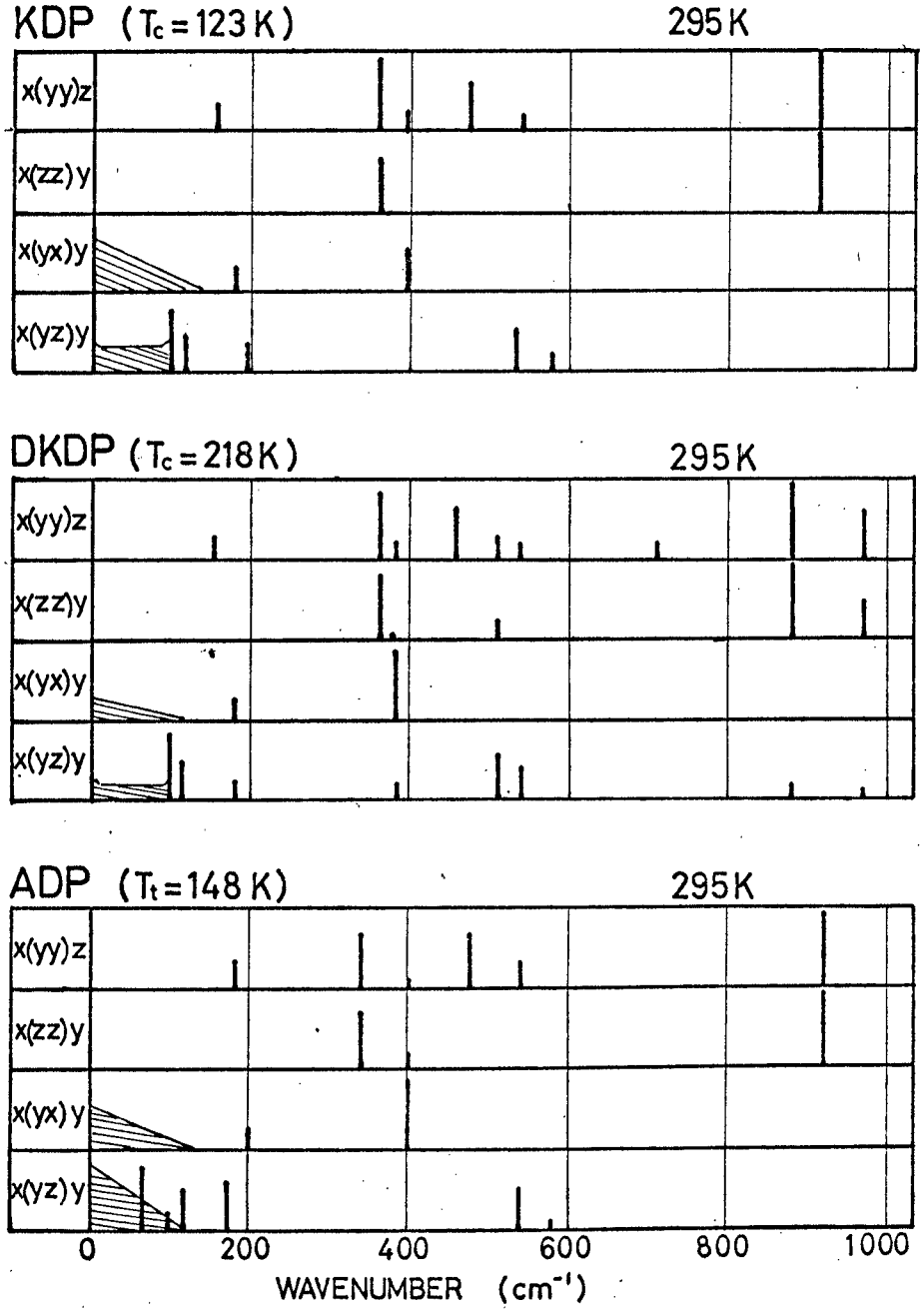

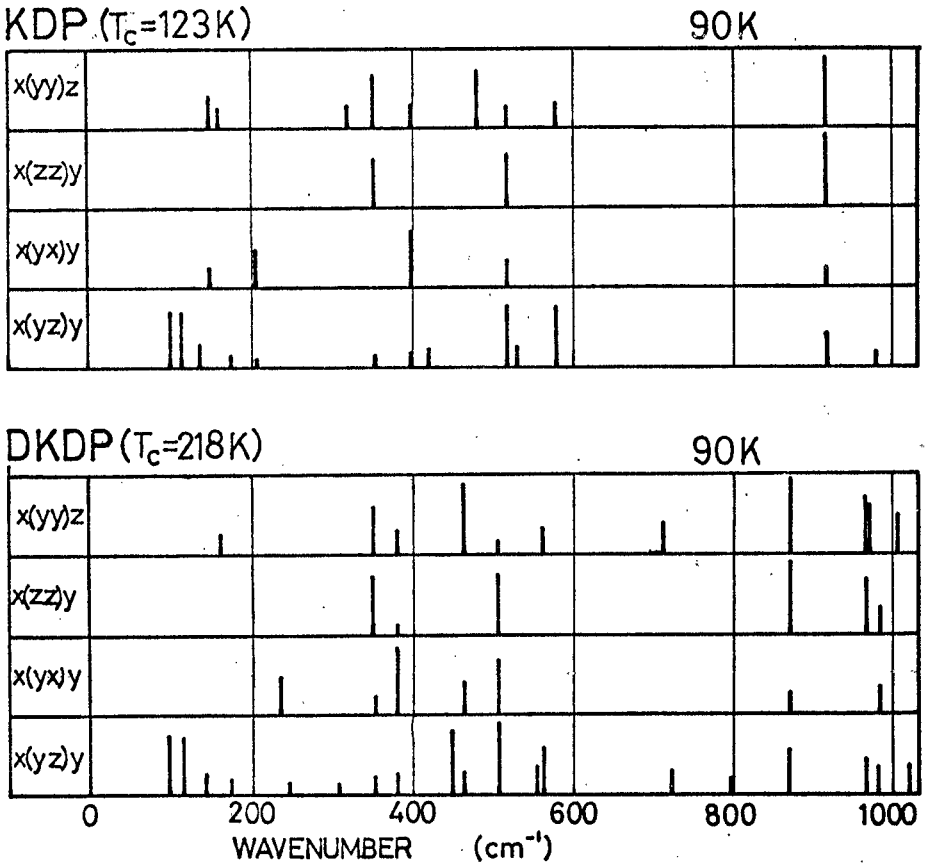

Fig. 5-6 Raman lines of KDP and DKDP at 90K.

← Fig. 5-5 Raman lines of KDP, DKDP and ADP at 295K.

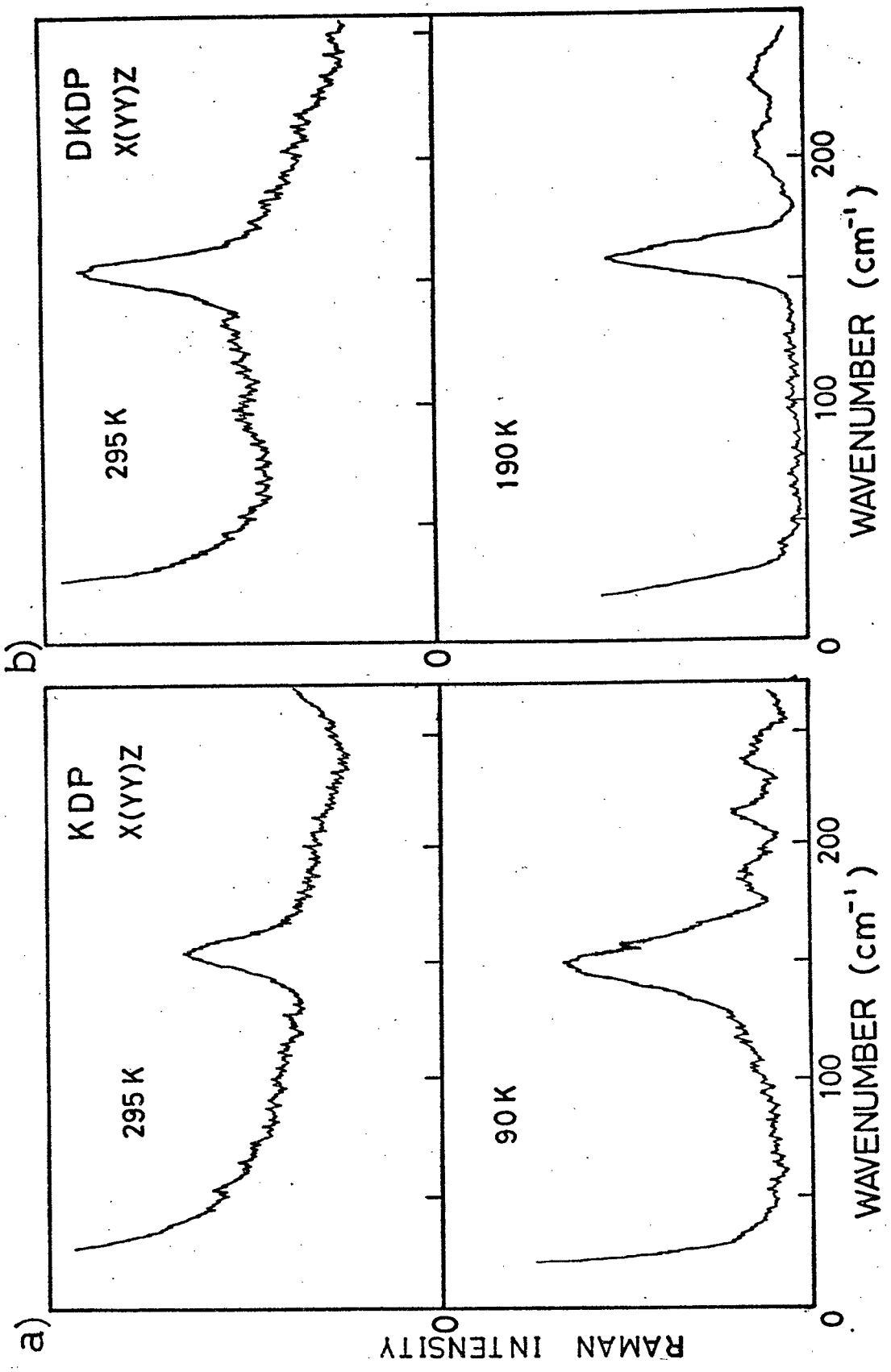

Fig. 5-7 a) Low-frequency spectrum of KDP at 295K and 90K in the x(yy)z configuration.

b) Low-frequency spectrum of DKDP at 295K and 190K in the x(yy)z configuration.

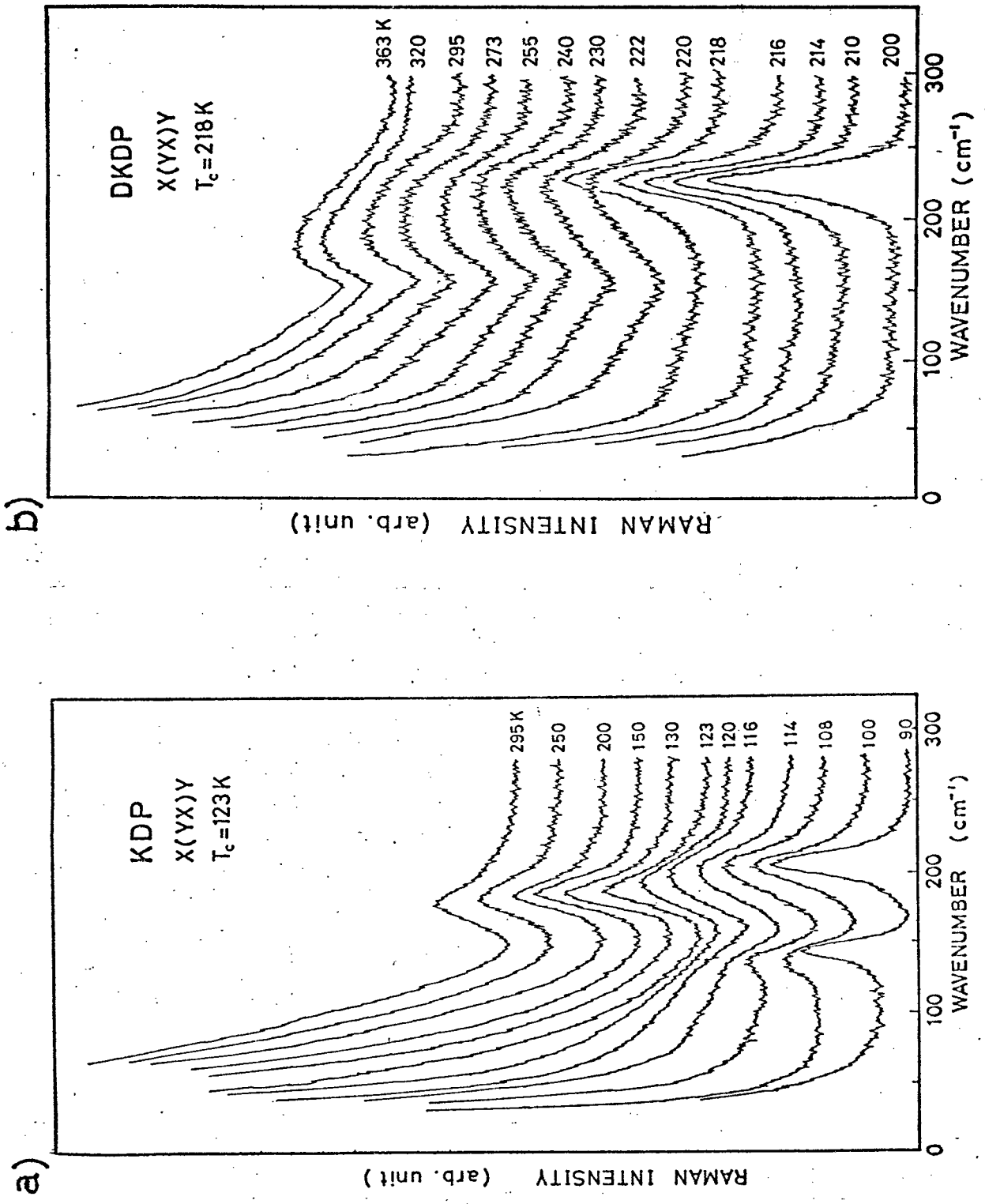

Fig. 5-8 a) Low-frequency spectrum of KDP at several temperatures in the x(yx)y configuration.

b) Low-frequency spectrum of DKDP at several temperatures in the x(yx)y configuration.

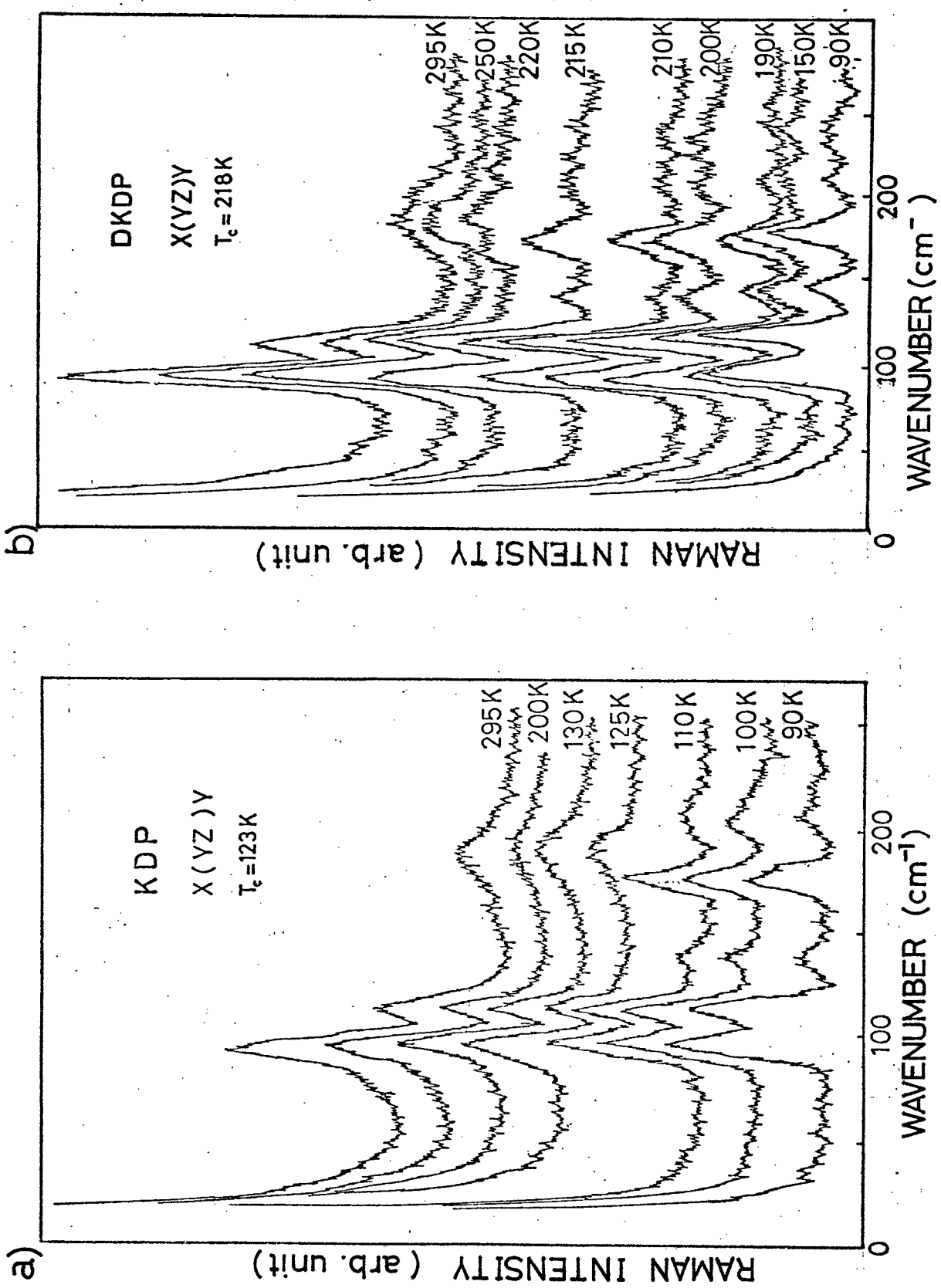

Fig. 5-9 a) Low-frequency spectrum of KDP at several temperatures in the x(yz)y configuration.

b) Low-frequency spectrum of DKDP at several temperatures in the x(yz)y configuration.

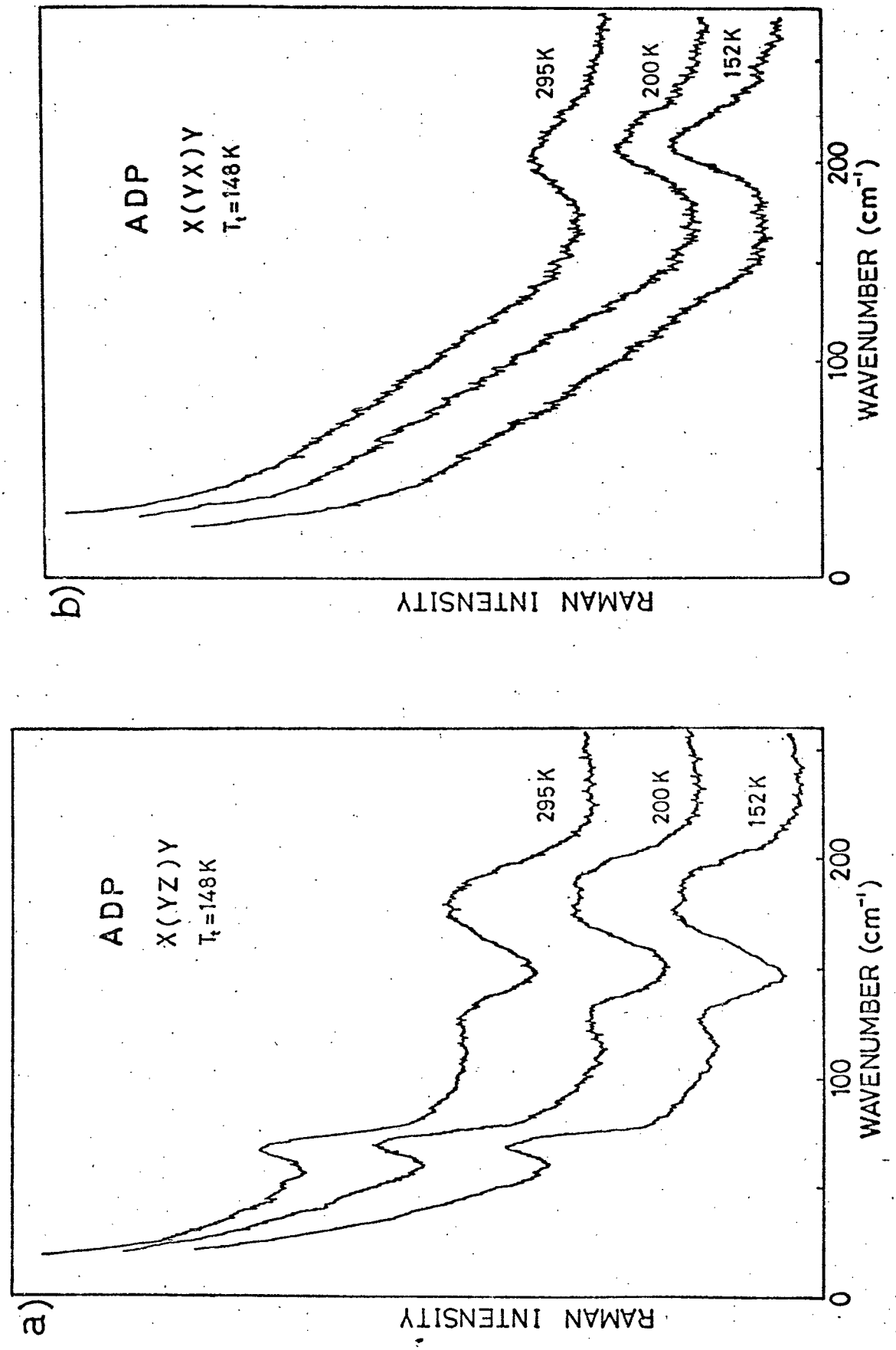

Fig. 5-10 a) Low frequency spectrum of ADP at several temperatures in the x(yz)y configuration.

b) Low-frequency spectrum of ADP at several temperatures in the x(yx)y configurations.

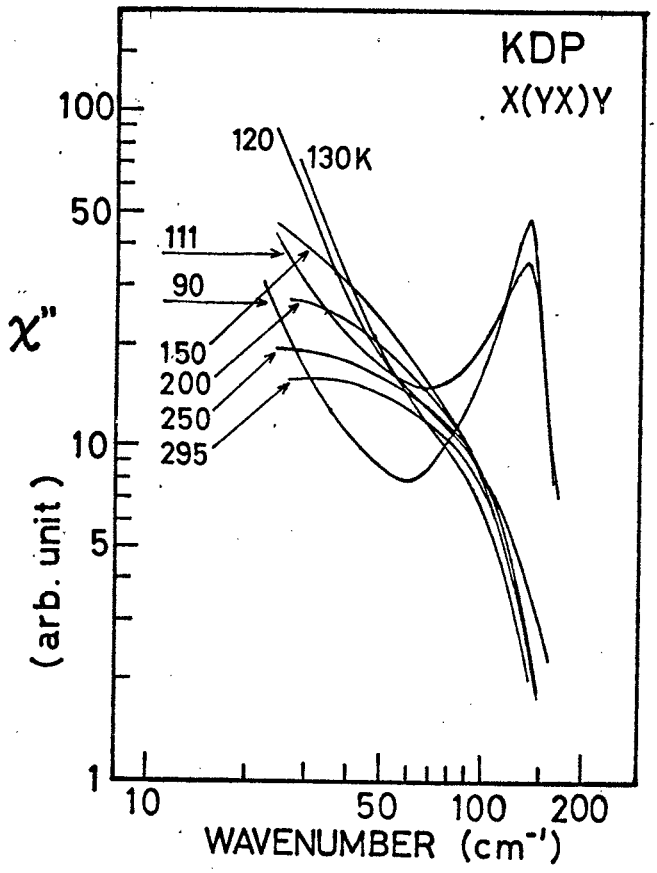

Fig. 5-11 Imaginary part of susceptibility of KDP obtained from the Raman scattering spectrum (Fig. 5-9(a)).

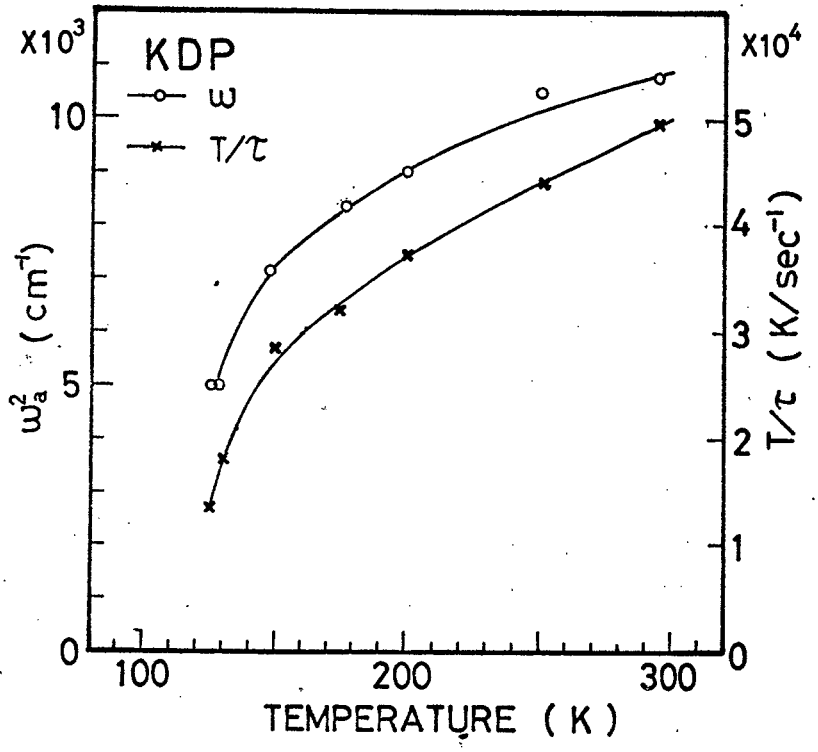

Fig. 5-12 Temperature dependence of the square of uncoupled mode frequency ω_a^2 and the temperature weighted inverse equivalent relaxation time T/τ above T_c in KDP.

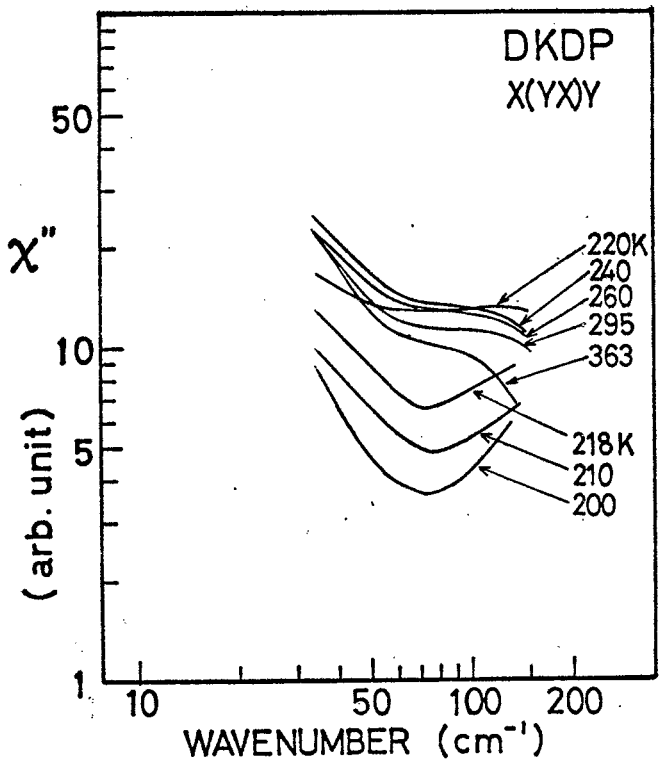

Fig. 5-13

Imaginary part of susceptibility for DKDP obtained from the Raman scattering spectrum (Fig. 5-9(b)).

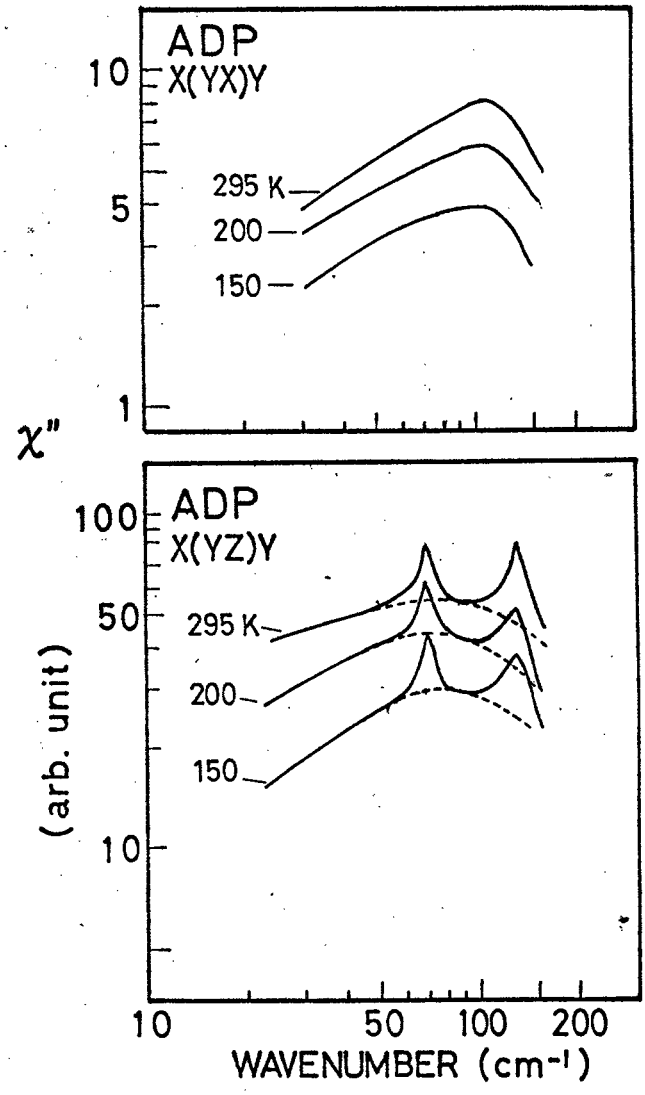

Fig. 5-14

Imaginary part of susceptibility for ADP obtained from the Raman scattering spectrum (Fig. 5-10).

Table 5-1

a) Raman Tensor for D_{2d} Symmetry

$$A_1:\begin{pmatrix} a & & \\ & a & \\ & & b \end{pmatrix} \qquad B_1:\begin{pmatrix} c & & \\ & -c & \\ & & \end{pmatrix} \qquad B_2:\begin{pmatrix} & d & \\ d & & \\ & & \end{pmatrix}$$

$$E(y):\begin{pmatrix} & & e \\ & & \\ e & & \end{pmatrix} \qquad E(x):\begin{pmatrix} & & \\ & & e \\ & e & \end{pmatrix}$$

b) Polarization Characteristic for D_{2d} Symmetry

Experimental Configuration	Raman Intensity	Charactor	θ
x(yy)z	a^2+c^2	A_1+B_2	
x(zz)y	b^2	A_1	
x(yx)y	d^2	$B_2(z)$: TO	90°
x(yx)z	d^2	$B_2(z)$: TO+LO	45°
x(yz)y	e^2	E(x), E(y): TO+LO	90°

Note: θ is the angle between the phonon wave vector and the z axis.

Table 5-2

a) Raman Tensor for C_{2v} Symmetry

$$A_1(z):\begin{pmatrix} a & & \\ & b & \\ & & c \end{pmatrix} \qquad A_2:\begin{pmatrix} & d & \\ d & & \\ & & \end{pmatrix}$$

$$B_1(x'):\begin{pmatrix} & & e \\ & & \\ e & & \end{pmatrix} \qquad B_2(y'):\begin{pmatrix} & & \\ & & f \\ & f & \end{pmatrix}$$

b) Polarization Characteristic for C_{2v} Symmetry

Experimental Configuration	Raman Intensity	Charactor	θ
x(yy)z	$d^2+(a+b)^2$	$A_1(z)$: TO+LO A_2	45°
x(zz)y	c^2	$A_1(z)$: TO	90°
x(yx)y	$(a-b)^2$	$A_1(z)$: TO	90°
x(yz)y	f^2+e^2	$B_1(x')$: LO $B_2(y')$: TO	90°

Note: 1) Crystallographic axes are parallel to the (x', y', z) coordinate.

Laboratory coordinate : (x , y, z)

2) θ is the angle between phonon wave vector and z axis.

Table 5-3

Raman Active Mode Frequencies in KH_2PO_4 (T_c=123K)

Raman Tensor Component	295K	200K	130K	Mode Assignment	90K	Mode Assignment
$T>T_c$ α_{yy}	154cm^{-1}	155cm^{-1}	156cm^{-1}	B_1 lattice mode	145cm^{-1}	A_1, lattice mode?
					161	A_2, lattice mode
					322	A_2, $\nu_2(PO_4)$
	359	358	358	A_1, $\nu_2(PO_4)$	355	A_1, $\nu_2(PO_4)$
$T<T_c$	393	395	394	B_1, $\nu_2(PO_4)$	394	B_1, A_1, $\nu_2(PO_4)$
	473	478	480	B_1, $\nu_4(PO_4)$	484	A_2, $\nu_4(PO_4)$
α_{xy}, $\alpha_{xx}+\alpha_{yy}$	520b	520b	520b	A_1, $\nu_4(PO_4)$	520	A_1, $\nu_4(PO_4)$
					574	A_2, $\nu_4(PO_4)$
	918	917	917	A_1, $\nu_1(PO_4)$	915	A_1, $\nu_1(PO_4)$
α_{zz}	360	360	359	A_1, $\nu_2(PO_4)$	355	A_1, $\nu_2(PO_4)$
	520bw	520bw	520bw	A_1, $\nu_4(PO_4)$	516	A_1, $\nu_4(PO_4)$
α_{zz}	916	917	918	A_1, $\nu_1(PO_4)$	916	A_1, $\nu_3(PO_4)$
α_{xy}	- Rayleigh wing(~160)-			B_2 lattice mode?	143	A_1, lattice mode?
	178	183	186	B_2 lattice mode	208	A_1, lattice mode
	394	395	395	B_2, $\nu_2(PO_4)$	395	A_1, $\nu_2(PO_4)$
					518	A_1, $\nu_4(PO_4)$
$\alpha_{xx}-\alpha_{yy}$					915w	A_1, $\nu_1(PO_4)$
α_{yz}	96	100	102	E, lattice mode	101	B_1,B_2,lattice mode
	116	119	120	E, lattice mode	115	B_1,B_2,lattice mode
					139w	B_1,B_2,lattice mode
$\alpha_{xz}+\alpha_{yz}$	192	195	194	E, lattice mode	177w	B_1,B_2,lattice mode
					209w	B_1,B_2,lattice mode
					257w	B_1,B_2,lattice mode
					355	B_1,B_2, $\nu_2(PO_4)$
	390w	390w	390w	E, $\nu_2(PO_4)$	393	B_1,B_2, $\nu_2(PO_4)$
					421	B_1,B_2, $\nu_2(PO_4)$
					518	B_1,B_2, $\nu_4(PO_4)$
	533	534	535	E, $\nu_4(PO_4)$	530w	B_1,B_2, $\nu_4(PO_4)$
	580s	580	581	E, $\nu_4(PO_4)$	582	B_1,B_2, $\nu_4(PO_4)$
					913	B_1,B_2, $\nu_1(PO_4)$
					976w	B_1,B_2, $\nu_3(PO_4)$

Table 5-4

Raman Active Mode Frequencies in KD_2PO_4 (T_c = 218K)

Raman Tensor Component	295K	220K	Mode Assignment	190K	90K	Mode Assignment
α_{yy} $T>T_c$	154cm^{-1}	154cm^{-1}	B_1, lattice mode	160cm^{-1}	164cm^{-1}	A_2, lattice mode
	360	360	A_1, $\nu_2(PO_4)$	358	354	A_1, $\nu_2(PO_4)$
	383w	384w	B_1, $\nu_2(PO_4)$	384	380	~~A_2~~, A_1 $\nu_2(PO_4)$
	458	457	B_1, $\nu_4(PO_4)$	458	462	A_2, $\nu_4(PO_4)$
$T<T_c$	510bw	513w	A_1, $\nu_4(PO_4)$	510	506	A_1, $\nu_4(PO_4)$
$\alpha_{xy}, \alpha_{xx}+\alpha_{yy}$	542	550	A_1, $\nu_4(PO_4)$	548	561	A_1, $\nu_4(PO_4)$
					670	A_2, ?
	710bw	710bw	B_1, γ(OD)	710	708	A_1, γ (OD)
	883	884	A_1, $\nu_1(PO_4)$	875	870	A_1, $\nu_1(PO_4)$
					963	A_1, δ (OD)
	970	970	A_1, δ (OD)	968	968	A_1, δ (OD)
				1008	1004	A_2, $\nu_3(PO_4)$
α_{zz} $T>T_c$	362	357	A_1, $\nu_2(PO_4)$	355	349	A_1, $\nu_2(PO_4)$
					380	A_1, $\nu_2(PO_4)$
α_{zz} $T<T_c$	519	515	A_1, $\nu_4(PO_4)$	510	506	A_1, $\nu_4(PO_4)$
	884	883	A_1, $\nu_1(PO_4)$	873	869	A_1, $\nu_1(PO_4)$
	967	967	A_1, δ (OD)	968	968	A_1, δ (OD)
	980s	980s	A_1, δ (OD)	980s	974	A_1, δ (OD)
α_{yx} $T>T_c$	Rayleigh wing(~150)		B_2, lattice mode?			
	192cm^{-1}	224cm^{-1}	B_2, lattice mode	227cm^{-1}	233cm^{-1}	A_1, lattice mode
					352	A_1, $\nu_2(PO_4)$
$T<T_c$	381	381	B_2, $\nu_2(PO_4)$	383	379	A_1, $\nu_2(PO_4)$
					464	A_1, $\nu_2(PO_4)$
$\alpha_{xx'}-\alpha_{yy'}$	510bw	510bw	B_2, $\nu_4(PO_4)$	510w	505	A_1, $\nu_4(PO_4)$
	880w	882w	B_2, $\nu_1(PO_4)$	874w	870	A_1, $\nu_1(PO_4)$
		965w	B_2, δ (OD)	974w	973	A_1, δ (OD)
α_{yz} $T>T_c$	92	94	E, lattice mode	94	95	B_1, B_2, lattice mode
	113	114	E, lattice mode	115	118	B_1, B_2, lattice mode
				142	144	B_1, B_2, lattice mode
	184	185	E, lattice mode	174	176	B_1, B_2, lattice mode
					209	B_1, B_2, lattice mode
$T<T_c$					245	B_1, B_2, lattice mode
$\alpha_{y'z}+\alpha_{zx'}$				353	352	B_1, B_2, $\nu_2(PO_4)$
	381w	382w	E, $\nu_2(PO_4)$	379	379	B_1, B_2, $\nu_2(PO_4)$
		458w	E, $\nu_4(PO_4)$	448w	447	B_1, B_2, $\nu_4(PO_4)$
				470s	470	B_1, B_2, $\nu_4(PO_4)$
	516	516	E, $\nu_4(PO_4)$	505	505	B_1, B_2, $\nu_4(PO_4)$
	546s	546s	E, $\nu_4(PO_4)$	553	551	B_1, B_2, $\nu_4(PO_4)$
				561	561	B_1, B_2, $\nu_4(PO_4)$
					722	B_1, B_2 ?
					793	B_1, B_2 ?
	880w	881w	E, $\nu_1(PO_4)$	871	870	B_1, B_2, $\nu_1(PO_4)$
				940	961	B_1, B_2 δ (OD)
	970w	970w	E, δ (OD)	970 s	970	B_1, B_2 δ (OD)
				1018	1018	B_1, B_2, $\nu_3(PO_4)$
					1103	B_1, B_2, $\nu_3(PO_4)$

Table 5-5

Raman Active Mode Frequencies in $NH_4H_2PO_4$ (T_t=148K)

Raman Tensor Component	295K	200K	152K	Mode Assignment
α_{yy}	182cm^{-1}	182cm^{-1}	181cm^{-1}	B_1, lattice mode
	340	341	341	A_1, $\nu_2(PO_4)$
	401	402	404	B_1, $\nu_2(PO_4)$
	481	483	483	B_1, $\nu_4(PO_4)$
	542b	544b	546b	A_1, $\nu_4(PO_4)$
	921	924	926	A_1, $\nu_1(PO_4)$
α_{zz}	341	344	344	A_1, $\nu_2(PO_4)$
	400bw	400bw	400bw	A_1, $\nu_2(PO_4)$
	921	924	926	A_1, $\nu_1(PO_4)$
α_{yx}	- Rayleigh Wing (~160) -			B_2, lattice mode?
	204	207	209	B_2, lattice mode
	401	402	404	B_2, $\nu_2(PO_4)$
α_{yz}	- Rayleigh Wing (~160) -			E, lattice mode?
	68	68	68	E, lattice mode
	121	125	128	E, lattice mode
	175	176	177	E, lattice mode
		189	190	E, lattice mode
	295w	298	299	E, lattice mode
	542	544	546	E, $\nu_4(PO_4)$
	580s	580s	590	E, $\nu_4(PO_4)$

Table 5-6

Spectral Decomposition of the PO_4 ion in the Crystal Field.

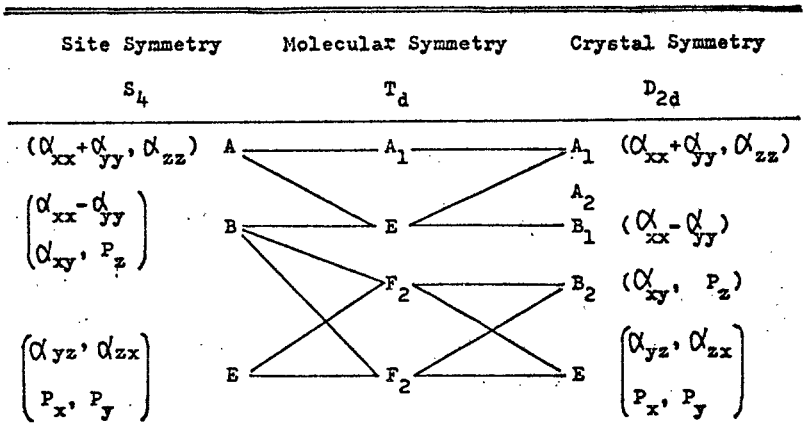

Table 5-7

Spectral Decomposition of the PO_4 ion in the Crystal Field.

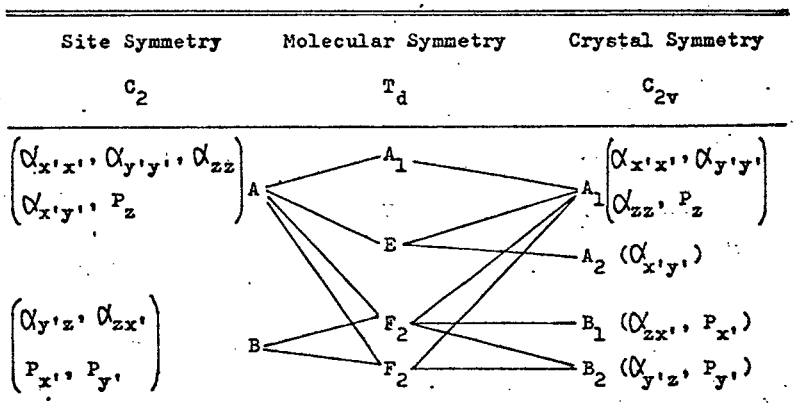

Table 5-8

The Parameters (cm^{-1}) in KDP

Temp. K	ω_a	P_a	Γ_a	ω_b	P_b	Γ_b	Δ
295	104	425	192	163	47	17.1	98
250	103	441	180	165	47	11.7	104
200	94	445	164	165	46	10.9	105
175	92	444	141	169	63	14.7	107
150	86	456	142	170	72	11.1	106
130	70	478	115	171	54	11.1	109
126	70	485	138	171	54	10.9	109

Chapter 6 Discussion and Conclusion

1. Discussion

1-1 Far-Infrared and Raman Spectra

In the paraelectric KDP, the modes of both B_2 and E symmetries are infrared and Raman active. Thus we can compare the results obtained by the infrared measurements with those by the Raman scattering. The results measured by two methods, on the whole, agree with each other. Some disagreements are pointed out in the following. For example, while five bands are observed in the far-infrared spectrum of E symmetry in the region below 300 cm^{-1}, only three bands are found in the Raman spectrum of E symmetry. Whereas it is the displacements of ions which participate in the infrared absorption, it is the displacements of the electron shells which participate in the Raman scattering. Therefore it is probable that a vibrational mode is observed in the infrared spectrum but not in the Raman spectrum even if this mode is allowed to be observed group-theoretically in both Raman and infrared spectra. The group theoretical analysis does not give any information for the infrared strength or the Raman strength.

1-2 Isotope Effects

The deuteration causes a reduction of the frequency of the tunneling motion and this effects the ferroelectric mode frequency and the relatively small line broadening of the PO_4 bands. The other effects are also observed in the spectra.

As stated in Chaps. 3 and 5, the deuteration effects on the spectra are as follows:

i) Some additional bands, which are not identified in KDP nor ADP, are observed in both far-infrared and Raman spectra above 300 cm^{-1}. These bands are attributed to the PO_4 ion internal modes.

ii) The additional band is also observed near 160 cm^{-1} in the spectrum of B_2 symmetry. In the paraelectric phase this band is observed in both far-infrared and Raman spectra. In the ferroelectric phase the corresponding band is observed only in the infrared spectrum but not in the Raman spectrum.

These facts indicate that the deuteration causes a significant distortion of lattice and PO_4 tetrahedra. If this is the case the selection rules for DKDP may differ from those for KDP. Skalyo et al.[1] have shown, in their neutron scattering experiments on DKDP, the existence of large distortional motions of oxygen tetrahedra and the deuterium atom movements along the c axis in the paraelectric phase. Thus deuteration results in the considerable distortion of the crystal structure as well as the reduction of tunneling frequency.

1-3 Ferroelectric Phase Transition

As discussed in Chap. 1, the hydrogen motion plays a significant role in the process of phase transition and is described theoretically as the proton tunneling mode.[2] The evidences of proton tunneling and its ordering are observed in the spectra as discussed in Chap. 5. The more important evidence of this mode is the ferroelectric mode.

The ferroelectric mode is observed in KDP in both far-infrared and Raman spectra. This mode is a polar one and is accompanied by the large polarization. Its frequency and intensity depend strongly on temperature. Such results are consistent with collective tunneling

mode model.[3] This model can be described in terms of a pseudospin Hamiltonian and following Tokunaga[3]

$$H = - \sum_i (2\Omega_T) X_i - \sum_{ij} J_{ij} Z_i Z_j \qquad (6\text{-}1)$$

where $Z_i = \pm\frac{1}{2}$ represents a dipole along the ferroelectric c axis, Ω_T is the tunneling frequency, J_{ij} represents the dipole-dipole and short range Coulomb interaction. The interaction term tends to align neighbouring dipoles and the tunneling term disturbs this inclination. The transition point is determined by balancing these two opposite inclinations. Tokunaga et al.[4] introduced $[K^+-(PO_4)^{-3}]$ dipoles as Z_i, where the motions of these dipoles instantaneously follow those of proton motions. This is a necessary deduction from the fact that the proton displacements are at right angles to the c axis. The dynamical properties of this model[3] indicate the displacive type behavior. The essential one is the proof of the existence of a collective proton mode with the temperature dependent frequency such as

$$\omega_o^2 \propto (T - T_c). \qquad (T>T_c) \qquad (6\text{-}2)$$

If the deuteron with its heavier mass is substituted for the proton, it reduces the frequency of tunneling motion. Therefore the interaction term in eq. 6-1 dominates the tunneling term and the Hamiltonian is reduced to the Ising spin system. In this case the order-disorder model is accepted and this model leads to a Debye susceptibility.

In the present work, the far-infrared measurements on DKDP suggest the existence of a low-frequency dispersion below 20 cm^{-1}. The Raman spectra of DKDP show the high-frequency tail in χ'' falling off more gradually than ω^{-1}. It may be a Debye type dispersion in the case of DKDP. Microwave measurements of Hill et al.[5] on DKDP show that χ_z''

has a Debye form with a 300 K peak at 1 cm^{-1}, which is beyond the range of the present experiments.

Kobayashi[6] proposed a coupled proton-phonon mode model in which the collective proton mode couples to the polar lattice mode of $[K\text{-}(PO_4)]$ sublattice as shown in Fig. 1-2. This polar mode produces a dipole moment along the c axis. The electric dipole moment of O-H-O bond interacts with the electric field created by the polar lattice mode. The frequency of the coupled mode is

$$\omega_+^2 \simeq \omega_{TO}^2$$

$$\omega_-^2 \simeq B(T - T_c) \qquad (T>T_c)$$

where ω_{TO} is the characteristic frequency of the polar lattice vibrational mode. Thus this model predicts two modes, one of which is like the soft mode of displacive type ferroelectrics.

It has been noted in the preceeding chapter that two bands are observed in both Raman and far-infrared spectra of B_2 symmetry in KDP in the paraelectric phase below 300 cm^{-1}. These bands are the ferroelectric mode and the band near 200 cm^{-1}. Below T_c the ferroelectric mode disappears and the other one near 200 cm^{-1} remains in both Raman and infrared spectra. On the other hand the group theoretical analysis predicts only one translational vibrational mode of $[K\text{-}(PO_4)]$ sublattice which belongs to B_2 symmetry species of D_{2d} group for $T>T_c$. The observed band around 200 cm^{-1} above T_c is the lattice vibrational mode predicted by the group theoretical analysis. The corresponding band is also observed in DKDP in both phases and in both Raman and infrared spectra.

Therefore the ferroelectric mode is not thought to be a lattice

vibrational mode in a usual sense, but a polarization fluctuation of $[K^{+}-(PO_4)^{-3}]$ dipole or a coupled proton-phonon mode. If the latter case, the ferroelectric mode can be assigned to ω_- mode and the band near 200 cm^{-1} to ω_+ mode.

The effect of deuteration on the ferroelectric mode is clearly observed. The deuteration with its heavier mass reduces the frequency of tunneling motion and causes a reduction of the frequency of the collective tunneling mode or the coupled proton-phonon mode. Thus the present results are consistent with the collective tunneling mode model[3] or the coupled proton-phonon mode model.[6] Below T_c the ferroelectric mode becomes unstable and the frozen out displacement of the ion produces a large spontaneous polarization along its c axis. Further study is necessary to identify which one is the correct mechanism of the ferroelectric phase transition in KDP. Cochran[7] proposed a lattice instability theory of KDP as the similar manner to that of displacive type ferroelectrics. If this is the case a lattice vibrational mode becomes unstable at the transition and frozen out displacements produce a large spontaneous polarization. The author believes that this model is not a correct model of KDP. The reason is as follows. While the present results show the existence of two bands below 200 cm^{-1}, the group theoretical analysis predicts only one lattice mode. The lattice instability theory doesn't predict such a phenomenon.

We can conclude that the essential excitation which causes the ferroelectric transition of KDP is the collective tunneling mode and the dipole system which produces a large spontaneous polarization along

its c axis is the $[K^{+}-(PO_4)^{-3}]$ dipole or frozen out displacements of B_2 mode, i.e., displacements of $[K-(PO_4)]$ sublattice. In wider sense the coupling of the collective tunneling mode to $[K-(PO_4)]$ sublattice motion is also essential to the ferroelectric phase transition.

1-4 Antiferroelectric ADP

The broad low-frequency band is observed in both far-infrared and Raman spectra of B_2 symmetry. And also a broad low-frequency band is observed in the spectra of E symmetry. When the temperature is lowered to T_t these bands become intense and shift to lower frequency. As discussed in Chap. 3 it seems that in the antiferroelectric ADP the zone boundary lattice vibrational mode becomes unstable[6-8] and the antiferroelectric phase transition occurs. So the mode observed here is thought to have nothing to do with the antiferroelectric phase transition.

The broad B_2 mode can be attributed to the ferroelectric mode as that of KDP. The broad E mode is not identified in KDP nor DKDP and its origin is rather unknown though, a possible explanation is as follows. As discussed in Chap. 2 the collective tunneling modes transform as A_2, B_2 and E symmetry species of D_{2d} group and can interact with the lattice vibrational mode of the same symmetry. Thus the broad E mode may be the collective tunneling mode or the coupled proton-phonon mode as similar manner to the ferroelectric mode of B_2 symmetry. If this is the case E type proton mode interacts with $[K^{+}-(PO_4)^{-3}]$ dipole along its a axis or the lattice vibrational mode of E symmetry. It is worth noticing that the spectrum of E symmetry is quite different from that of KDP or DKDP. This fact means that the lattice vibrational mode of E symmetry strongly interacts with the proton mode.

2. Conclusion

The polarized infrared and Raman spectra of ferroelectric KDP and DKDP have been measured in both paraelectric and ferroelectric phases as a function of temperature: those of ADP only in the paraelectric phase.

The frequencies and the symmetries of most of the observed bands have been determined in both phases. The correlation of the modes from one phase to the other is also established. The mode assignments of the observed bands have been made with the aid of the group theoretical analysis. The PO_4 ion in these crystals has been found to behave as an individual molecule slightly deformed by the crystalline field and the bands due to the internal vibrations of PO_4 have been determined.

The ferroelectric mode behavior has been observed in the spectrum of B_2 symmetry for KDP in the paraelectric phase. The data are consistent with the collective tunneling mode model or the coupled proton-phonon mode model. In DKDP the corresponding band has not been observed but the data have suggested the existence of a low-frequency dispersion below 20 cm^{-1} in the paraelectric phase. The deuteration effect on the ferroelectric mode behavior has also confirmed that the models of KDP based on the collective tunneling mode are appropriate.

The evidences of the proton tunneling and its ordering in KDP have been deduced from the abrupt change in the spectrum on crossing the transition temperature. These phenomena have been seen in the spectra indirectly through their coupling to the other crystalline vibrations and have been also demonstrated by the DKDP results.

It has been found that deuteration has resulted in the consider-

able distortion of the lattice and PO_4 ion as well as the low tunneling frequency for deuteron. It casues a change in the selection rules for infrared absorption and Raman scattering.

In the antiferroelectric ADP the low-frequency broad E mode has been found. This mode is able to be attributed to the E type collective tunneling mode or the coupled proton-phonon mode of E symmetry. It seems that the zone boundary lattice vibrational mode becomes unstable at the antiferroelectric phase transition and E mode has nothing to do with the phase transition.

Finally, it seems probable that the essential excitation which causes the ferroelectric phase transition in KDP is the collective tunneling mode and the dipole system which produces a large spontaneous polarization is the displacement of $[K\text{-}(PO_4)]$ sublattice.

References

1) J. Skalyo, Jr., B. C. Frazer and G. Shirane, Phys. Rev. B 1 (1970) 278.

2) R. Blinc, J. Phys. Chem. Solids 13 (1960) 204.

3) M. Tokunaga, Prog. Theor. Phys. 36 (1966) 857, and Ferroelectrics 1 (1970) 195.

4) M. Tokunaga and T. Matsubara, Prog. Theor. Phys. 35 (1966) 581.

5) R. M. Hill and S. K. Ichiki, Phys. Rev. 130 (1961) 150.

6) K. K. Kobayashi, J. Phys. Soc. Japan 24 (1968) 497.

7) W. Cochran, Advan. Phys. 9 (1960) 387, and ibid. 10 (1961) 401.

8) H. Meister, J. Skalyo, Jr., B. C. Frazer and G. Shirane, Phys. Rev. 184 (1969) 550.

論　文　目　録　　大阪大学

河　村　徹　郎

報告番号甲第163号

主論文　Optical Properties of KDP Type Crystals in the Low-Wavenumber Region

（KDP型結晶の低波数域における光学的性質）

（主論文のうち印刷公表したもの）

1. Far-Infrared Spectra of KH_2PO_4 and $NH_4H_2PO_4$

（KH_2PO_4 及び $NH_4H_2PO_4$ の遠赤外スペクトル）

Japanese Journal of Applied Physics, 7巻
昭和43年6月

1. Far-Infrared Spectra of KH_2PO_4 and $NH_4H_2PO_4$

（KH_2PO_4 及び $NH_4H_2PO_4$ の遠赤外スペクトル）

Journal of Physical Society of Japan, 28巻
昭和44年9月

1. An Observation of the Change in Cooled-KDP Temperature due to 337 μm Incident Radiation

（337 μm 入射光による冷却したKDPの温度変化の観測）

Journal of Physics D: Applied Physics, 5巻
昭和47年9月

1. Far-Infrared and Raman Spectra of KH_2PO_4 and $NH_4H_2PO_4$

（KH_2PO_4 及び $NH_4H_2PO_4$ の遠赤外及びラマンスペクトル）

大阪大学工学報告,
23巻, 昭和48年

(主論文のうち未公表のもの)

1.Far-Infrared and Raman Spectra of KD_2PO_4

(KD_2PO_4の遠赤外及びラマンスペクトル)

執筆中

Optics Communication

投稿予定